Drp1 and Opa1 reciprocally structure the inner mitochondrial membrane and electron transport chain in lung adenocarcinoma

Dane Sessions
Palo Alto, California

B.S. Biology, University of Michigan, Ann Arbor, 2014

A Dissertation presented to the Graduate Faculty of the University of Virginia in Candidacy for the Degree of Doctor of Philosophy

Department of Microbiology, Immunology, and Cancer Biology
University of Virginia
December 2022

Abstract

Cancer is the number two cause of US mortality after cardiovascular disease and lung cancer is the highest mortality form of cancer. Lung adenocarcinoma (LUAD) represents almost half of all lung cancer cases and has a current five-year survival rate of 24%. The high mortality is significantly driven by the fact that many LUAD cases are diagnosed at late stages after primary tumor cells have already metastasized to distant sites such as the brain. The standard of care for LUAD includes surgical resection, if possible, combined with traditional platinum-based chemotherapies (i.e. cisplatin), immunotherapy, and targeted molecular therapy, when possible (i.e. anti-EGFR antibodies). About half of LUAD tumors demonstrate activating driver mutations in genes of the mitogen-activated protein kinase (MAPK) pathway, such as *EGFR* (12%), *KRAS* (30%), and *BRAF* (7%), that normally transmits proliferation, survival, and growth signals from the cell surface to the nucleus.

Activating mutations in MAPK components confer metabolic changes to tumor cells compared to their normal tissue counterparts. In particular, *KRAS* mutations upregulate glycolytic metabolism to promote rapid cytoplasmic ATP synthesis and to generate biosynthetic precursor molecules required for nucleotide and lipid synthesis. Mitochondria are organelles that are the primary orchestrators of cellular metabolism and regulate intrinsic apoptosis, signaling molecule generation like reactive oxygen species, and buffer ions like calcium. Mitochondria are not static within the cell, but rather demonstrate complex fusion-fission dynamics regulated by large dynamin-related GTPases: Mfn1/2 and Opa1 are the direct effectors of fusion of the mitochondrial outer and inner membranes, respectively, and are functionally opposed by Drp1 that directly executes mitochondrial fission and reorganizes cristae during apoptosis. Opa1 is localized to the

mitochondrial inner membrane and intermembrane space and also functions to promote cristae morphology and oxidative phosphorylation capacity.

Oncogenic signaling regulates mitochondrial dynamics. In particular, our lab has demonstrated that oncogenic KRas promotes mitochondrial fission through Erk2-mediated phosphorylation of Drp1. Our group also established that Drp1 is required for *KRAS*-mutant pancreatic ductal adenocarcinoma (PDAC) and that depletion of Drp1 in this system inhibits tumor metabolism and development *in vitro* and *in vivo*. The goals of this dissertation are twofold: 1) to elucidate the requirements for mitochondrial dynamics machinery in *KRAS*-mutant LUAD, as tumors of different tissue origin are known to demonstrate differential metabolic signatures and dependencies, and 2) to understand how fusion and fission effectors interact with each other to promote mitochondrial function and drive tumorigenesis.

To approach these questions, we established *in vitro* and *in vivo* systems of mitochondrial dynamics perturbation in LUAD that inactivate mitochondrial fission through Drp1 depletion, fusion through Opa1 depletion, or both simultaneously. We find that contrary to PDAC, *KRAS*-mutant LUAD growth and development are insensitive to inactivation of mitochondrial fission. We also demonstrate that LUAD requires Opa1 to maintain electron transport chain (ETC) function to regenerate the electron carrying molecule NAD^+ required for oxidative biosynthesis and that Opa1 is only required when Drp1 is expressed and enzymatically active. We find that Opa1 depletion destroys ETC complex I assembly and function required to regenerate NAD^+, and that co-depletion with Drp1 rescues this phenotype. We propose a model in which steady-state Drp1-mediated fission reorganizes cristae in a manner deleterious to ETC function, and that Opa1 opposes fission by reestablishing cristae morphology to restore ETC assembly and function.

Acknowledgments

The work I performed for this dissertation was possible only with the support of many, and for that I am incredibly grateful. For brevity, this section highlights just a few of my appreciations, but is certainly not exhaustive.

I must start by thanking my wife, Julia. In the years the work for this dissertation was performed, we were fortunate to get married and to recently welcome our daughter, Sophia, to the world. Thank you for your *infallible* love and guidance through the uncertainty of my education. Thank you and Sophia for showing me what is truly important in this world. And thank you for listening to me talk about mitochondria at every opportunity.

To all my parents, thank you for putting up with my interminable schooling and I promise to get a job at some point. To my mom, Nina, thank you for allowing me to find my own way to medicine and science. To my dad, Dave, thank you for teaching me to never quit. To my dad, Kent, thank you for introducing me to mindfulness. To my mom, Manon, thank you for stability. To my father-in-law, Peter, thank you for showing me the trailhead to this tortuous path and guiding me along the way. To my mother-in-law, Kim, thank you for modeling unrestricted kindness. To my mother-in-law, Robin, thank you for always welcoming me. To Kristian, Blake, Steffen, Marit, Ivy, and Meredith, thank you all for the good times past and those yet to come.

I must also thank mentors who consistently invest in my personal and scientific development. Cari, thank you for taking a chance on me when you started your own research group. My time in your lab was transformative and I would not be here today without it. Marty, thank you for showing me it is possible to have an encyclopedic

knowledge of biology (including intricacies of folate metabolism), and for your patience during our conversations. Kwon, thank you for hands-on teaching me the fundamentals of mouse wizardry; everything in this dissertation relied on it. Dan, thank you for challenging me to consider the bigger picture. Heather, thank you for emphasizing the art of storytelling in science. Drew, thank you for your service as an approachable and engaged committee chair and educator.

Last, I must thank the Kashatus lab. I am forever grateful that the lab accepted me last-minute without hesitation (as far as I'm aware) as I transitioned from medical school to graduate school. For camaraderie, thank you to the other Kashatus lab graduate students that I was lucky enough to overlap with: Sarb, Saad, Salma, and Chris. Thank you, Jen, for making the lab a place I was (and am) excited to go to every day. It made all the difference. Last, but probably not least, thank you Dave for your *exceptional* mentorship. Thank you for allowing me the freedom to explore responsibly. Thank you for teaching me to consider the y-axis. Thank you for teaching me to use words sparingly and with intention. And thank you for making research fun.

Thank you to those mentioned above and those whom I did not have space to include. Your support has meant the world to me.

TABLE OF CONTENTS

LIST OF FIGURES AND TABLES

LIST OF ABBREVIATIONS

AdCre: adenovirus Cre
AdEV: adenovirus empty vector
AKB: alphaketobutyrate
BTIC: brain tumor-initiating cells
cnPAGE: clear native polyacrylamide gel electrophoresis
CP: complexome profiling
CSC: cancer stem cell
CT: computed tomography
CTG: Cell Titer-Glo
DHAP: dihydroxyacetone phosphate
DHO: dihydroorotate
EMT: epithelial-mesenchymal transition
ER: endoplasmic reticulum
ETC: electron transport chain
EV: empty vector
FFPE: formalin-fixed, paraffin-embedded
FL: floxed
G3PS: glycerol 3-phosphate shuttle
GEMM: genetically engineered mouse model
HPLM: human plasma-like medium
IBM: inner boundary membrane
IGA: in-gel activity
IHC: immunohistochemistry
IMM: inner mitochondrial membrane
IMS: intermembrane space
LSC: leukemic stem cell
MAPK: mitogen-activated protein kinase
MAS: malate-aspartate shuttle
MEF: mouse embryonic fibroblast
MICOS: mitochondrial contact site and cristae organizing system
MOMP: mitochondrial outer membrane permeabilization
mtDNA: mitochondrial DNA
MTS: mitochondrial targeting sequence
NSC: neural stem cell
OCR: oxygen consumption rate
OMM: outer mitochondrial membrane
OXPHOS: oxidative phosphorylation
OxSyn: oxidative biosynthesis
PAM: protoadjacent motif
PET: positron emission tomography
ROS: reactive oxygen species
RTK: receptor tyrosine kinase
SILAC: stable isotope labeling of amino acids
TEM: transmission electron microscopy
TKI: tyrosine kinase inhibitor
WT: wildtype

1 Chapter 1. Introduction

This introduction will provide the necessary background for my work studying mitochondrial function and fusion-fission dynamics in lung adenocarcinoma. In the first section, I will outline critical concepts of human lung adenocarcinoma including epidemiology, social burden, genetic driver mutations, treatment, and modeling. I will next introduce mitochondria with particular focus on their myriad functions and architecture, as well as how fusion-fission dynamics impact these facets. Some parts of this chapter are derived from a review article I published titled “Mitochondrial dynamics in cancer stem cells” in the peer-reviewed journal *Cell and Molecular Life Sciences*. Sessions DT, Kashatus DF. Mitochondrial dynamics in cancer stem cells. Cell Mol Life Sci. 2021 Apr;78(8):3803-3816. doi: 10.1007/s00018-021-03773-2. Epub 2021 Feb 13. PMID: 33580834.

1.1 Lung adenocarcinoma (LUAD)

1.1.1 Burden and epidemiology

Cancer is currently the second highest cause of United States mortality [1]. Lung and bronchus cancer is the highest mortality form of cancer and was the cause of death of 136,084 people in the US in 2020 with males and females demonstrating nearly equal numbers of deaths [2]. Lung and bronchus cancer is also currently the only form of cancer that falls in the top 10 global causes of death (currently number six) [3]. Lung cancer is broadly categorized into small cell lung carcinoma (15% of all lung tumors) and non-small cell lung carcinoma (NSCLC, 85% of all lung tumors) based on histologic characteristics from tumor biopsies. NSCLC is further subdivided into large cell carcinoma, squamous cell carcinoma, and lung adenocarcinoma (LUAD). Lung adenocarcinoma is the most common form of lung cancer and represents 40% of all lung cancer cases. Although LUAD

is the most-diagnosed lung malignancy in never-smokers, risk factors for the development of LUAD include inhalation of tobacco smoke (firsthand or secondhand) and exposure to other inhaled environmental pollutants like radon, asbestos, and silica. The incidence of LUAD has unfortunately remained fairly consistent over the past two decades, ranging between 20-25 people diagnosed per 100,000, although the five-year survival has increased from 20 percent to 25% in this same time period [4]. The greatest incidence is observed in those of age 65 and older. Ethnically, white and black populations demonstrate the highest incidence and Native Americans the lowest.

A strong driver of the high mortality of LUAD and lung cancer more broadly is the fact that many tumors are diagnosed at late stage. Diagnosis of LUAD occurs at the localized stage in 25.3% of cases, regional stage in 20.1% of cases, and unfortunately distant stage in 52.5% of cases, with 2.1% of cases being unstaged [4]. Metastatic spread of LUAD is very common, since most LUAD is diagnosed at late stage and occurs through both lymphatic and blood vessels. The most common sites of LUAD metastasis include other lobes of the lung on the ipsilateral and contralateral sides relative to the primary tumor, as well as the bones, brain, and liver. Hallmark symptoms of lung adenocarcinoma, or any primary lung malignancy, include cough, difficulty breathing, weight loss, chest pain, and recurrent pulmonary infection, but can also include symptoms from paraneoplastic syndromes including vasculitides, dermatoses, and others. Symptoms from metastatic disease reflect site of metastasis. Overall, lung adenocarcinoma is a disease of enormous morbidity and mortality in the US and worldwide.

1.1.2 Genetics

Cancer is predominantly a genetic disease in that mutations in genes of normal cells drive abnormal or dysregulated cell behavior that leads to tumor development and metastasis.

Gene mutations can have a variety of effects on gene products including: 1) gene deletion through chromosome arm loss, introduction of early stop codons, or frameshift mutations from insertions or deletions, 2) amplification of gene copy number, 3) point mutations that hyperactivate or inactivate functional domains or regulatory or interaction regions, and 4) chromosomal rearrangements leading to gene fusion products with altered regulatory sequences. Examination of individual human tumors using technologies like DNA sequencing (targeted or whole genome), fluorescence in-situ testing, and immunohistochemistry have revealed which mutations occur in specific types of cancer. Often, mutations in the same suite of genes are observed in tumors of a specific cancer type from different individuals. This provides rationale for studying how mutations in these genes drive cancer development and how targeting the products or cellular outcomes of these mutations may be of high value therapeutically.

Genes mutated in cancer can be broadly separated into two groups. Genes with mutations that result in hyperactive forms of gene products that normally drive cellular processes like survival, proliferation, and growth are called oncogenes. Genes that normally suppress cellular processes like survival, proliferation, and growth are tumor suppressor genes and are typically inactivated in tumors to allow dysregulated tumor growth. Many of the most-frequently observed oncogene drivers of human LUAD activate cell signaling cascades from cell surface membrane receptors through intracellular pathways including the mitogen-activated protein kinase (MAPK) or PI3K-Akt pathways to promote cellular proliferation, resistance to programmed cell death (apoptosis) and tissue invasion and metastasis [5]. This section will highlight a few of the most-frequently observed mutations, but is not an exhaustive list of all mutations found in human LUAD.

Mutations in the epidermal growth factor receptor (*EGFR),* which encodes a cell surface receptor tyrosine kinase (RTK), are found in about one-third of patients [6]. The product of *EGFR* binds extracellular ligand (EGF) that causes receptor dimerization, phosphorylation, and signaling through effectors of the MAPK or Akt pathway. The most frequent mutations in *EGFR* occur as small deletions (e.g. E746-A750, L747-E749/T751) or point mutations (e.g. T790M, L858R) in the tyrosine kinase domain which leads to constitutive EGFR activation and signaling of downstream effectors.

Another frequently-mutated oncogene in human LUAD is *KRAS*, which encodes a small GTPase intracellular effector of RTKs that transmits signals through both the MAPK and PI3K-Akt pathways and is mutated in about one-fourth of tumors. KRas (and other Ras family members HRas and NRas) undergoes conformational change upon binding GTP that permits association with other intracellular effectors of the MAPK and PI3K-Akt pathways to promote signal transmission. GTP hydrolysis to GDP is required to inactivate these associations and thus turn off the Ras-driven signal. The vast majority of alterations in this gene occur as inactivating point mutations in the G12 or G13 residues of the GTPase domain that lock Ras in its functional state. Mutations are also observed in the Q61 residue which inhibits the coordination of water required for GTP hydrolysis. *KRAS* mutations are also associated with a history of smoking. Activating point mutations in this gene, in particular the G12D mutation, are drivers of the models of LUAD used in the work described in this dissertation.

Other clinically-relevant oncogenes that drive human LUAD development include dysregulated variants of RTK-coding genes other than *EGFR* including *ALK, ROS1*, *MET*, and *RET.* These genes are typically dysregulated by chromosomal rearrangements and amplification. Additionally, human LUAD can be driven by mutations of intracellular

effectors of RTK signaling such as the kinase-encoding gene *BRAF* that hyperactivates the MAPK pathway, but not the PI3K-Akt pathway. *BRAF* mutations are most prevalent in melanoma (50% of tumors), but occur in about 2% of LUAD as well [5]. The most prevalent mutation in *BRAF* is a V600E point mutation that mimics phosphorylation in the kinase domain and hyperactivates BRAF-mediated signaling.

The most prevalent inactivating mutations of tumor suppressor genes occur in *TP53 (*about 50% of human LUAD tumors). *TP53* encodes the homotetramer-forming protein p53 [7] that functions as a master transcriptional regulator upon DNA-binding [8]. p53 regulates cell stress by activating cellular senescence, apoptosis, or cell cycle arrest. Mutations in *TP53* can inactivate its function through a variety of mechanisms including decreased expression, protein conformation alteration, and DNA binding alteration. Expression of TP53 is regulated by ubiquitin-mediated degradation through the E3 ubiquitin ligase MDM2 that demonstrates amplified expression in human LUAD. Inactivation of TP53 through homozygous deletion is uncommon in human cancer, but is useful in tumor modeling and is thus employed in tumor models described in this dissertation.

1.1.3 Treatment

Approach to treatment of human LUAD considers multiple factors including extent of disease (tumor stage), comorbidities (weight loss, poor lung function), and, recently, molecular characterization of individual tumors [9]. Imaging modalities including chest radiograph and computed tomography (CT) scan are critical tools for detection of lung malignancy. Tumors may be identified in early-stage asymptomatic individuals that undergo imaging for other purposes or in typically late-stage symptomatic patients with suspicion for lung malignancy. Patients with suspected late-stage malignancy undergo

further imaging to evaluate for presence of metastases using CT or positron emission tomography (PET) scans. Ultimately biopsy of suspected lesions for microscopic evaluation is required to confirm the diagnosis of lung cancer or LUAD specifically. Biopsy specimens also permit molecular characterization of individual tumors to guide personalized therapies, if such options are available.

One hallmark of care for LUAD caught at early stages is surgical resection of a lobe or entire lung and offers the highest likelihood of prolonged survival. Candidacy for surgical resection is dependent on comorbidities and pulmonary function, as the remaining lung tissue must be able to support life in the patient. If complete surgical resection is inappropriate or patients do not wish to undergo the procedure, alternatives include localized radiation therapy, radiofrequency ablation, and cryoablation. Surgery is also considered as a palliative but not curative measure in circumstances where tumor burden impacts airway patency.

Systemic cytotoxic chemotherapy is another mainstay of treatment for LUAD, especially because most patients are diagnosed at late stages of disease after the primary tumor has spread and thus are not candidates for surgical resection. Platinum-based chemotherapy agents like cisplatin and carboplatin are widely-used as neoadjuvant therapy to shrink tumors before surgical resection, adjuvant therapy to kill tumor cells remaining after surgery, and as therapy in patients who do not undergo surgical resection. Platinum-based agents kill tumor cells by introducing DNA damage through intra- and inter-strand crosslink formation that must be repaired by base-excision repair, nucleotide-excision repair, homologous recombination, or nonhomologous end joining, depending on the genetic lesion [10]. Due to the general cytotoxic mechanism of action of these

therapies, side effects of these include damage to kidneys, nerves, and the auditory system.

Advances in molecular characterization have brought about personalized therapy directed by mutations detected in individual tumors. Molecular characterization of tumors is typically performed on solid biopsy tissues, although advances in detecting abnormalities in circulating cell-free DNA from lysed tumor cells are making this a more attractive and less invasive technique. The driver mutations most-frequently observed in human LUAD are outlined above in the “Genetics” section. Identification of individual mutations allows clinicians to match patients with drugs that inhibit the specific products of mutant genes that drive their tumors. Patients with tumors that harbor mutations in *EGFR* are treated with EGFR tyrosine kinase inhibitors (TKIs). High response rates to TKI therapy has been associated with particular mutations in *EGFR,* specifically the L858R point mutation and deletions in exon 19. A recent clinical trial has identified that the third-generation EGFR TKI osimertinib is more efficacious at promoting progression-free survival and duration of response in untreated and advanced LUAD than earlier-generation TKIs gefitinib and erlotinib [11].

TKIs have been developed for RTKs other than *EGFR* that are frequently mutated in human LUAD and inhibitors are sometimes indicated for multiple mutated RTKs. Patients with *ALK*-mutant tumors may be treated with the TKIs crizotinib, ceritinib, alectinib, and others. Patients with *ROS1*-mutant tumors may be treated with crizotinib, entrectinib, or lorlatinib. Patients with *MET*-mutant tumors may be treated with capmatinib or tepotinib. Although many patients harbor tumors with RTK mutations for which RTK-targeted molecular therapy is available, patients with activating mutations in signaling pathway effectors may currently have fewer targeted options available. Patients with tumors

harboring *BRAF V600E* mutations may be treated with dual therapy consisting of dabrafenib that specifically inhibits the mutant *BRAF* protein as well as trametinib that inhibits the downstream effector MEK. Unfortunately, these agents are not typically efficacious in patients with tumors harboring non-V600E *BRAF* mutations.

Although one-fourth of human LUAD tumors harbor activating mutations in *KRAS*, very few Ras-targeted therapies exist. Historically, Ras itself has been very difficult to therapeutically target. Molecules that inhibited the covalent addition of hydrophobic moieties and membrane-localizing moieties to Ras have been developed [12], but ultimately were not efficacious due to the activity of alternative modification enzymes. Recently, inhibitors specific for the *KRAS* G12C mutation have been developed that irreversibly bind the C12 residue and interfere with nucleotide binding affinity and effector interaction [13]. Although potent inhibitors of the Ras effector kinases MEK and ERK have been developed, they have not yet demonstrated efficacy in treating human LUAD. In general, there is an enormous lack of targeted treatment options for *KRAS*-mutant tumors.

The final broad treatment avenue for LUAD is use of immune checkpoint inhibitors to bolster the immune response to tumors. Tumor cells may express cell surface molecules including PD-L1 that inactivate tumor-recognizing lymphocytes by binding lymphocyte surface receptors like PD-1 and CTLA-4. Antibody inhibitors of these receptors like pembrolizumab (anti-PD-1) and ipilimumab (anti-CTLA-4), or antibodies against their tumor surface antigens like PD-L1 (atezolizumab) block lymphocyte inactivation and thus increase immune response to tumor cells. Tumor biopsies are screened for expression of PD-L1 to inform clinicians how to best utilize immunotherapies. PD-L1 low-expressing tumors are typically treated with pembrolizumab plus carboplatin whereas PD-L1 high-expressing tumors may be treated with pembrolizumab monotherapy [14].

In general, the approach and sequence of treatment is tailored to the many factors regarding patient preferences, tumor spread, and molecular characterization. Even with the treatment arsenal outlined above, the mortality of LUAD remains immense and thus requires continued focus on understanding LUAD biology and development of novel treatment regimens.

1.1.4 Tumor modeling

Tumor modeling is critical to gain insights into the basic biology of tumor development and progression and to assess the efficacy of novel treatment avenues. Many tumor models have been developed with important distinguishing characteristics including species of tumor cell and/or host, timing of tumor initiation, mechanism of mutation introduction, environment (co-culture with other cells or surfaces on which cells are cultured), and more. Each model has advantages and disadvantages and thus model selection must be tailored to the biological questions being asked and often multiple models are utilized to ensure results are generalizable and robust.

Cells or tissues used in cancer modeling come from many sources and species. Many human- and mouse-derived cancer cell lines are commercially available through sources like the American Type Culture Collection (ATCC) that distribute cell lines and provide information regarding their use, genetics, and patient history (if from a human). Examples of commercially-available human lung adenocarcinoma cell lines are A549, H1975, and H1650 cells. Use of human cell lines is advantageous in that they offer an opportunity to make biological discoveries in the same species that scientists and clinicians seek to treat clinically; however, many widely-used human tumor cell lines were established many years ago and genetically and phenotypically drift away from their original human tumor

cells as time passes and the cells replicate outside of their original host. Alternatives to these widely available resources are patient- or mouse-derived tumor samples, which are technically the same as cell lines except that they are freshly isolated from human or mouse sources and thus have likely experienced less drift. These samples are probably more representative of the original tumor and thus findings from them are more relevant, though they are often laborious to generate due to required coordination with surgeons or mouse sacrifice.

The simplest tumor model systems involve culture of cell lines or primary tumor cells *in vitro* in liquid media that provide the salts, nutrients, pH buffering, and growth factors necessary to keep cells alive and growing. These cells are often housed in flat-bottom plastic dishes onto which many types of tumor cells will adhere (lung cancer cells, pancreatic cancer cells, etc.), although some cell types will remain suspended in cell culture media (e.g. leukemia cells). These simple systems offer many advantages including ease of cell density manipulation, cell harvest, and accumulation of vast amounts of cellular material. Additionally, cells suspended or attached in two-dimensional culture are highly accessible to drugs placed in media and to vectors of genetic manipulation such as transfected DNA and RNA as well as viral transduction. Modification of cellular behavior through chemical action or genetic or epigenetic manipulation is paramount to understanding how cells and the genes that encode their components function, so these qualities of cell culture models are highly desirable. Two-dimensional adherent culture conditions are also optimized for intracellular imaging, as cells can spread out, which eases visualization of intracellular components like organelles.

Recently, there has been intense interest in developing cell culture systems that better recapitulate the complex native environment of tumors. These efforts recognize that

although culturing a single cell type on two-dimensional plastic surfaces with enormous amounts of nutrients available may maximize rates of cell replication and survival, it does not accurately reflect the cellular heterogeneity, attachment substrate rigidity, and nutritional and oxygen availability that tumor cells must navigate in human hosts. To bridge this gap, many multicellular culture models have been developed that co-culture tumor cells with fibroblasts, endothelial cells, and other cell types to better mimic cell-cell interactions that can have profound effects on transcriptional states [15]. These models may allow free mixing of different cell types in the same chamber, or may physically separate cells by a barrier through which cells can send cellular projections or secreted factors to facilitate interaction. Additionally, cells may be cultured in or on two-dimensional or three-dimensional substrates other than plastic, such as the polysaccharide agar [16] or protein matrices [17] to better approximate cancer cell behaviors and recapitulate the extracellular matrix within which tumor cells are embedded in humans. Recently, spheroid culture models have been established in which cells that are normally adherent are cultured in dishes onto which they cannot adhere, which facilitates cellular aggregation and compaction into sphere-like structures that better recapitulation cellular behaviors *in vivo* [18]. Third, optimization of media components and concentrations can better recapitulate the nutrition and growth factors available to cultured cells which is known to have significant effects on cellular metabolism [19].

Although *in vitro* cell culture models are useful as exquisitely controlled systems, they are unable to fully capture the complexity of the tumor microenvironment present *in vivo,* including the vasculature that supplies nutrients and oxygen and carries away wastes, extracellular matrix composition, and infiltration of immune cells and fibroblasts. The most commonly used live animal model of cancer biology is the mouse (*Mus musculus*) due to its relatively recent shared ancestry with humans, small size and ease of handling, rapid

achievement of sexual maturity, and high litter frequency, although other organisms like zebrafish (*Danio rerio)* are used as well.

The simplest mouse models of cancer biology involve the transplantation of previously-established tumor cell lines into mice. Immunodeficient mice are used frequently for this technique because they lack the immune cell compartments that would normally recognize the transplanted cells as foreign and eliminate them. These mice are therefore critical for the transplantation of human cells or mouse cells from distant ancestry into mice. In particular, transplantation of recently-derived or harvested tumor cells from human patients into mice serve as powerful models of cancer biology called patient-derived xenografts. Immune-competent mice are valuable tools when transplanting tumor cells from mice with recent shared ancestry to the recipient mouse because the immune cell compartment is present and thus can better recapitulate an anti-tumor immune response that may be present in humans. Immune-competent models have been of particular importance in recent years for those studying the interaction between immunity and cancer, and have yielded the insights that drive immunotherapy today.

Subcutaneous transplantation of tumor cells has been used widely due to the accessibility of the subcutaneous space for tumor cell injection; however, recent work has highlighted how subcutaneous administration of tumor cells may not recapitulate the tumor microenvironment native to the type of tumor cells being used. As an alternative, orthotopic transplantation studies seed tumor cells into the organ or space from which the cells were derived (i.e. lung cancer cells injected into the lung) to better recapitulate the microenvironment and this has been shown to have dramatic effects on critical aspects of tumor biology like metabolism.

In vivo transplantation studies offer a variety of approaches and permit genetic manipulation of cell lines before transplantation, but may not faithfully recapitulate tumor initiation and development as tumor cell lines used in these models were derived from previously-established tumors. To best model initiation and development, tumors should develop from the cells native to the mice within a particular study. As tumorigenesis is driven by genetic mutation, introduction of mutations into mice is essential to initiate this process. Lung cancer in particular can be initiated in mice through exposure of mouse lungs to tobacco smoke or alternative carcinogens like methyl-nitrosurea and urethane. This approach recapitulates the widespread DNA damage caused by carcinogens like tobacco smoke [20] that initiates lung tumorigenesis in humans, but generates so many mutations that studying the effects of any specific mutations is difficult.

An alternative approach to generate tumors *de novo* in mice is to use genetically-engineered mouse models (GEMMs) in which mouse tissues are primed to form tumors by inserting specific DNA sequences around genetic elements or genes that drive tumor formation upon sequence-specific deletion. One of the most widely-used GEMM systems is Cre-lox recombination that inserts loxP DNA sequences around genetic elements of interest that are recombined and deleted by the action of the protein Cre. Expression of Cre can be localized by tissue-specific promoters or with viral vectors that introduce Cre only to cells that are infected. Lung adenocarcinoma GEMMs frequently utilize Cre-lox recombination to activate an oncogenic allele of *KRAS* or *EGFR* and to inactivate *TP53* [21]. These models generate disease that closely resembles human lung adenocarcinoma and permits study of LUAD biology in the context of known driver mutations, although genomic heterogeneity still arises during tumor development [22].

Ultimately, a mixture of *in vitro* and *in vivo* tumor models is utilized to explore cancer biology. When evidence of biological phenomena accumulates across multiple systems, it generates strong support for mechanisms of disease compared to the use of solely tissue culture models, for instance. Work outlined in this dissertation relies heavily on cell culture-based tumor models as well as a GEMM of *KRAS*-driven LUAD. In fact, cell lines in this dissertation were established from the GEMM and utilized for further mechanistic evaluation in cell culture, demonstrating how different model systems can be intricately linked.

1.2 Mitochondrial Function, Structure, and Dynamics

Mitochondria contain two phospholipid bilayer membranes and perform critical cellular functions including orchestration of metabolism, regulation of intrinsic apoptosis, and buffering of ions like calcium. Mitochondrial form is intimately linked with function and is regulated under homeostatic and pathologic conditions. This section will provide an overview of mitochondrial function, structure, and fusion-fission dynamics.

1.2.1 Overview of mitochondrial function

1.2.1.1 Metabolism

Mitochondria are frequently thought of as the powerhouses of cells, as they are principal sites of synthesis of ATP, the energy currency that drives many cellular chemical reactions; however, mitochondria coordinate critical facets of cell metabolism other than ATP synthesis including regulation of glycolysis, lipids, amino acids, nucleotide precursors, one-carbon metabolism, and heme synthesis. Tumors demonstrate metabolic signatures distinct from those of the surrounding normal tissue. The hallmark metabolic signature of cancer cells is the Warburg effect, in which cells preferentially utilize glycolysis to synthesize ATP and lactate from glucose under aerobic conditions in which normal

tissues typically synthesize most ATP through mitochondrial oxidative phosphorylation. Mutant Ras activates highly glycolytic metabolism [23–25] that promotes tumorigenesis through generation of glycolytic intermediates that are siphoned off to other pathways including the pentose phosphate and lipid synthesis pathways. Under conditions in which nutrients are abundant, cells are also able to synthesize ATP faster, though less efficiently, through glycolysis compared to oxidative phosphorylation. Pyruvate, the end product of glycolytic breakdown of glucose, is the central node molecule of the lactate or oxidative phosphorylation pathway split. To promote glycolysis and tumor cell stemness, tumors can downregulate pyruvate dehydrogenase (PDH), which converts pyruvate into acetyl-CoA for mitochondrial oxidation [26]. Tumor cells also upregulate less-efficient variants of glycolytic enzymes to allow buildup of glycolytic intermediates [27].

Although tumor cells often upregulate glycolysis, mitochondrial metabolism is essential for KRas-mutant tumor cells [28]. Through the citric acid cycle, mitochondria generate molecules that are precursors for amino acid, lipid, and nucleotide synthesis and reduce the electron acceptor molecules NAD^+ and succinate [29–31]. The reduced forms of these molecules, NADH and $FADH_2$ are then oxidized by the mitochondrial electron transport chain so they can again serve as electron acceptors in the citric acid cycle. Inhibition of electron carrier oxidation by the mitochondrial electron transport chain stalls the citric acid cycle and its synthesis of key molecules like the amino acid aspartate. This in turn inhibits cellular growth and proliferation as cells require amino acids like aspartate for protein synthesis and nucleotide synthesis [32].

Lipids assemble into cellular membranes, serve as energy storage and signaling molecules, and are incorporated into proteins as posttranslational modifications. Lipid metabolism is dysregulated in many ways in tumor cells to meet demands of highly

proliferative cell states. Lipids can be synthesized *de novo* in the cytoplasm from mitochondria-generated citrate or taken up from the extracellular environment. Mutant KRas alters expression of lipid homeostasis genes including fatty acid synthase (*FASN), SREBP1*, and *SCD* in lung adenocarcinoma to promote *de novo* fatty acid synthesis and inhibition of FASN inhibits tumor growth [33]. Ras activation of PI3K and mTOR signaling mediates these lipogenesis transcriptional changes [34]. Additionally, inhibition of ACLY, the enzyme that converts mitochondria-derived citrate to acetyl-coA for lipogenesis, inhibits lung tumor growth [35]. These studies demonstrate that lung tumor development requires *de novo* lipid synthesis and that KRas is able to induce this metabolic change.

Although we are gaining an appreciation for metabolic changes observed in tumors, it is also apparent that there is significant metabolic heterogeneity in human lung cancer cell lines [36] and in primary human lung tumors *in vivo* [37]. Additionally, cell-of-origin can significantly affect metabolic profiles, as demonstrated between PDAC and LUAD tumors initiated with the same driver mutations [38] [39]. Further, phenotypes observed in *in vitro* studies are not always recapitulated *in vivo.* For instance, KRas-mutant lung tumors require pyruvate carboxylase and pyruvate dehydrogenase *in vivo*, but are much less reliant on glutaminase than cells cultured *in vitro* [40]. This highlights the need for further *in vivo* studies of tumor metabolism that may better inform how to target tumor metabolism as therapy in humans.

1.2.1.2 Apoptosis

Mitochondria are primary regulators of the programmed cell death pathway apoptosis. Apoptosis can be stimulated extrinsically by ligands such as FasL binding to cell surface receptors like Fas, or can be stimulated intrinsically by internal cell cues like extensive DNA damage. Both pathways eventually lead to widespread activation of caspases that

cleave intracellular proteins, fragment DNA, and cause cell death; however, intrinsic apoptosis requires mitochondria as mediators of apoptosis following intrinsic apoptotic stimuli, whereas extrinsic apoptosis is capable of activating caspases independent of mitochondria. Mitochondria potentiate intrinsic apoptosis through mitochondrial outer membrane permeabilization (MOMP) and release of the ETC protein cytochrome C from the inner membrane into the cytoplasm. In the cytoplasm, cytochrome C associates with APAF1 and caspase 9 to form the apoptosome that activates executioner caspases 3 and 7. MOMP is primarily achieved through the oligomerization of two proteins, BAK and BAX, that form pores in the mitochondrial outer membrane. In healthy cells, these two proteins are sequestered by antiapoptotic proteins including BCL-2, BCL-X_L, and MCL1. Other proapoptotic proteins including BIM, BID, PUMA, and NOXA, activate apoptosis through either inhibition of the antiapoptotic proteins or stimulation of BAX and BAK. Intrinsic apoptosis also causes changes to mitochondrial structure including substantial mitochondrial fragmentation and restructuring of cristae.

In general, cells must evade apoptosis for tumors to develop. This is often achieved through regulation of apoptosis effectors. TP53, the cell stress sensor and master tumor suppressor gene mutated in about half of human lung adenocarcinoma, promotes cell death by upregulating expression of proapoptotic factors PUMA [41] and NOXA [42] and by directly perturbing mitochondrial membranes [43, 44]. Inactivation or deletion of TP53 therefore renders cells less sensitive to cellular stresses and less likely to undergo apoptosis.

1.2.1.3 Calcium Buffering

Calcium is a cation integral to cell signaling and enzyme function, and mitochondria uptake calcium from the cytosol to buffer cytosolic calcium concentrations [45]. Intramitochondrial

calcium is critical to many mitochondrial functions including ATP synthesis by oxidative phosphorylation [46, 47], and protects against cell death by reducing the concentration of cytosolic calcium [48]. Cytosolic calcium flows through the mitochondrial outer membrane through voltage-dependent anion channels (VDACs) and moves into the mitochondrial matrix through the mitochondrial calcium uniporter (MCU) [49, 50]. The flow of calcium into the mitochondrial matrix is promoted by the mitochondrial inner membrane potential generated by ETC complexes I, III, and IV pumping hydrogen ions from the matrix into the intermembrane space and is inhibited under conditions that dissipate this potential such as treatment with FCCP [51]. Calcium is also transferred to mitochondria via contact with the endoplasmic reticulum [52] and promotes tumor cell proliferation and inhibits tumor cell death [53]. ER-mitochondria transfer relies on organelle contact sites that are regulated by mitochondrial dynamics machinery including Mitofusin 2 [54], which will be described in further detail later in this introduction. In general, mitochondria regulate calcium concentrations in other cellular compartments and participate in calcium-mediated cell signaling networks.

1.2.2 Overview of mitochondrial structure

1.2.2.1 Membranes and spaces

Mitochondria are double-membraned organelles whose internal architecture generates many different compartments including the outer membrane, intermembrane space, inner membrane, cristae, and matrix. The outer membrane is highly permeable to ions, contains protein transporters for larger molecules, and displays receptors for fission, fusion, and autophagic degradation of mitochondria. The narrow intermembrane space (IMS) contains the ETC and apoptosis protein cytochrome C and accumulates protons as ETC complexes I, III, and IV pump hydrogen ions from the matrix into the IMS, generating the proton gradient that drives synthesis of ATP in the mitochondrial matrix. The mitochondrial inner

membrane demonstrates intricate folds called cristae and houses many molecular transporters as well as ETC complexes I, III, IV, and V. Lastly, the matrix is the innermost mitochondrial chamber and contains many enzymes required for oxidation of pyruvate and fats, nucleotide synthesis, heme synthesis, and more. The matrix also houses mitochondrial DNA packaged with proteins into structures called nucleoids.

1.2.2.2 Mitochondrial DNA

Although most proteins that make up mitochondria are encoded by the nuclear genome, mitochondria contain their own 16-kilobase protein-coding circular genome (mtDNA) within the mitochondrial matrix, with often hundreds-to-thousands fold higher copy number than the cell's nuclear genome. Mitochondrial DNA is packaged into nucleoids with nuclear-encoded proteins that regulate mtDNA replication and transcription such as mitochondrial transcription factor A (TFAM) [55, 56], mitochondrial helicase Twinkle, mitochondrial RNA polymerase (POLRMT), DNA polymerase γ, and single-strand binding protein (SSBP1) [57]. The mitochondrial genome encodes 13 proteins that are subunits of respiratory complexes I, III, IV, or V, in addition to 2 mitochondrial rRNAs and 22 mitochondrial tRNAs. The mitochondrial genome is organized such that protein- and rRNA-coding genes are punctuated by tRNA-coding genes [58]. The entire genome is transcribed into a polycistronic transcript that is cleaved by RNAses to generate individual RNAs. Individual mitochondrial-encoded mRNAs are similar to nuclear-encoded mRNAs in that 3' polyadenylation stabilizes transcripts, but differ from nuclear-encoded mRNAs in that they lack a 5' 7-methylguanylate cap and do not require 5' untranslated regions (UTRs) for translation. Although expression of mtDNA-encoded genes does not conform to the cell cycle, mtDNA transcription is regulated by nuclear genes [59] and nuclear gene transcription is regulated by the activity of mtDNA-encoded genes [60, 61].

1.2.2.3 Electron transport chain

The mitochondrial electron transport chain is made up of five multi-subunit and inner membrane-bound protein complexes plus the two soluble electron carriers hemeprotein cytochrome C and the coenzyme ubiquinone (Figure 1-1). The ETC couples the oxidation of electron-carrying molecules like NADH, succinate, and dihydroorotate (DHO), to pumping of protons from the mitochondrial matrix into the intermembrane space that generates the proton motive force for mitochondrial ATP synthesis. Electrons enter the ETC from numerous sources: NADH offloads electrons at complex I, succinate offloads electrons at complex II, and DHO offloads electrons at the IMM-localized enzyme dihydroorotate dehydrogenase (DHODH). From these initial acceptor complexes or enzymes, electrons are transferred to the coenzyme ubiquinone, which reduces it to ubiquinol. Ubiquinol then reduces complex III and is reoxidized to uibiquinone. Complex III electrons then flow through cytochrome C to complex IV that reduces molecular oxygen to form water. Four protons are pumped across the IMM as electrons move through complex I or complex III, and two protons are pumped by complex IV. The proton gradient across the IMM powers the synthesis of ATP by ATP synthase in which four protons flow from the intermembrane space into the matrix for every ATP molecule synthesized from ADP and inorganic phosphate. Electron flow through the ETC can be inhibited by many mechanisms including insufficient supply of electron carrying molecules, insufficient ETC component assembly, function or abundance, insufficient oxygen to siphon electrons out of the ETC, and hyperpolarization of the IMM by insufficient ATP synthase activity. Reoxidation of each component of the ETC is required for the ETC to permit continuing electron flux and thus inhibition of electron flux at any specific site will also inhibit function of components upstream that rely on electron offloading into the ETC.

Four of the five ETC protein complexes (I, III, IV, and V) are assembled from a mixture of subunits encoded by nuclear or mitochondrial genomes. To accommodate ETC complex assembly, mitochondrial and nuclear gene expression are coordinated. Individual complexes I, III, and IV associate to form supercomplexes that are believed to increase respiratory efficiency [62], although this notion has been recently challenged [63]. Although the exact mechanisms still lack clarity, assembly of ETC complexes is regulated by cristae morphology and vice versa. For instance, dimerization of ATP synthase monomers induces membrane curvature and contributes to cristae morphology [64–66] and inhibition of cristae structure inhibits ETC supercomplex formation [67]. The exact mechanisms by which inner membrane structure and ETC assembly and function interact remain to be elucidated.

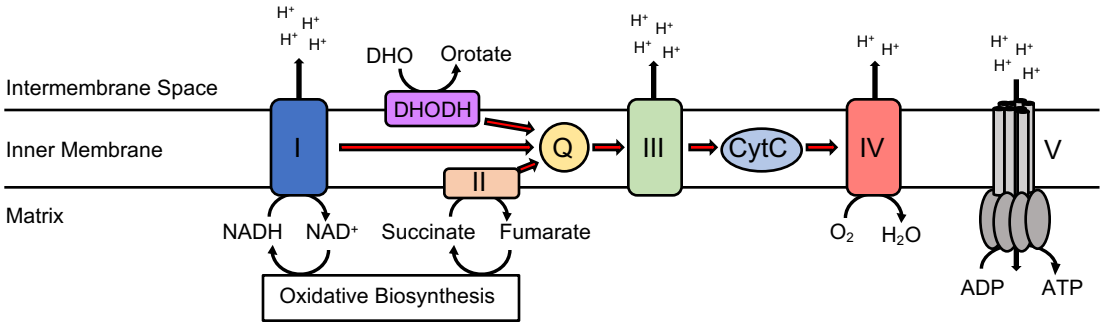

Figure 1-1. Schematic of the mitochondrial electron transport chain

Electrons are deposited into the ETC at multiple sites: complex I (blue) oxidizes NADH to NAD^+, complex II (orange) oxidizes succinate to fumarate, and DHODH (purple) oxidizes dihydroorotate (DHO) to orotate. Oxidation of NADH regenerates NAD^+ electron carriers required for oxidative biosynthesis. Oxidation of succinate to fumarate is a critical step in the Krebs cycle. Oxidation of DHO generates orotate required for *de novo* pyrimidine synthesis. Electron flow (red arrows) from complex I, complex II, or DHODH converges on the IMM-soluble electron carrier ubiquinone (Q, yellow) and then flows through complex III (green) to cytochrome C (light blue) and finally to complex IV (red). Complex IV reduces molecular oxygen, the final electron carrier, to form water. Electron flow through complex I, III, and IV is coupled to proton pumping from the mitochondrial matrix to the intermembrane space to generate the proton gradient. Protons flow back into the matrix through ATP synthase (grey) and drive the synthesis of 1 ATP per 4 protons. Disruption of electron flow including, and distal to, ubiquinone inhibits oxidation of electron-donor molecules. The coupling of proton pumping to electron flow results in inhibition of electron flux as the proton gradient increases, for instance under conditions of ATP synthase inhibition that normally relieves the proton gradient pressure.

1.2.1 Overview of mitochondrial dynamics

Mitochondria undergo continuous cycles of fusion and fission. Acute changes in fusion and fission can have dramatic effects on the shape and size of mitochondria. In particular, highly fused mitochondrial morphology is promoted under conditions of low nutrient availability and is associated with increased OXPHOS efficiency [68], and widespread fragmentation is observed in cells undergoing apoptosis [69].Chronic fusion-fission cycling acts as a quality control mechanism for preserving mitochondrial integrity by mixing mitochondrial contents [70] and eliminating defective mitochondria by mitophagy, the mitochondria-specific autophagy pathway [71, 72]. This section will introduce the fundamentals of mitochondrial fusion-fission dynamics and the mechanisms by which these dynamics are regulated by oncogenic signaling.

1.2.1.1 Mitochondrial fission machinery

Fission is generally initiated upon mitochondrial membrane constriction by endoplasmic reticulum contacts [73]. Next, the large cytoplasmic GTPase dynamin-related protein 1, or Drp1, is recruited to mitochondria where it oligomerizes and spiralizes on the outer mitochondrial membrane and constricts upon GTP hydrolysis to cleave a mitochondrion into two [74]. Binding of Drp1 to the mitochondrial outer membrane is accomplished through interaction of Drp1 with OMM receptors Mff [75, 76], Fis1 [77, 78], MiD49, and MiD51 [79]. Currently, there is conflicting evidence on whether other proteins such as dynamin 2 are required to completely sever mitochondria, but the role of Drp1 in this process is paramount [80–82].

Drp1 possesses multiple amino acid residues that are post-translationally modified and regulate fission. Phosphorylation of serine 616 (S616) by Erk [83, 84] and CDK1 [85] activate fission and couple Drp1 activity to cellular proliferation and growth and cell cycle

progression. Conversely, phosphorylation at S637 by PKA decreases fission activity of Drp1 [86]. Drp1 also possesses numerous lysine residues that are SUMOylated and stimulate fission [87, 88].

Multiple important cellular processes involve mitochondrial fission. For instance, apoptosis is associated with widespread and severe mitochondrial fragmentation [89]. The canonical mitochondrial OMM pore-forming and apoptosis proteins BAX and BAK promote Drp1 localization to mitochondria [90] and Drp1 inhibition delays, but does not completely prevent, apoptosis [91, 92]. Drp1 also potentiates BAX/BAK-independent apoptosis [69]. Cristae are remodeled during apoptosis to allow cytochrome C escape from the cristae intermembrane space and into cytoplasm where it forms the apoptosome with APAF1 and caspase-9. Drp1 and its OMM receptors MiD49/51 facilitate apoptotic cristae remodeling [93] and Drp1 inhibition inhibits cytochrome C release [92], indicating that fission induces structural changes in the outer and inner mitochondrial membranes. Activation of mitochondrial fission during apoptosis is coordinated with inhibition of mitochondrial fusion, demonstrating how the opposing arms of fusion and fission are often oppositely regulated to execute cellular functions [94].

Fission is also critical to organelle quality control through dispersion of mtDNA-containing nucleoids [95] and through clearance of dysfunctional mitochondria through the mitochondrial autophagy, mitophagy. Mitophagy facilitates mitochondrial quality control in a Drp1-dependent manner to purge cells of dysfunctional segments of mitochondria to maintain energy balance and mitochondrial function [96–98]. Interestingly, Drp1-dependent mitophagy also acts as a mechanism of avoiding apoptosis during embryonic development, demonstrating how multiple fission-dependent cellular processes can be oppositely coordinated [99].

1.2.1.2 Mitochondrial fusion machinery

Mitochondrial fusion requires three large GTPases. Outer mitochondrial membrane fusion is accomplished by the actions of outer membrane-bound mitofusin 1 (Mfn1) and mitofusin 2 (Mfn2) [100]. These proteins form both heterodimers and homodimers that then hydrolyze GTP to bring together and fuse the outer membranes of two mitochondria [101]. Mitofusins also tether mitochondria to peroxisomes [102] and the endoplasmic reticulum [103], demonstrating that these proteins broadly promote physical association of mitochondria with other mitochondria and other organelles. Mfn1 and Mfn2 demonstrate some functional redundancy in that both must generally be ablated to completely inhibit mitochondrial fusion [101].

Fusion of inner mitochondrial membranes requires the action of optic atrophy 1 (Opa1) that lines the inner mitochondrial membrane facing the intermembrane space [104]. Differential splicing of Opa1 RNA transcripts produces 8 separate mRNA species [105] encoding proteins that differ in potential sites for, and efficiency of, proteolytic cleavage. The domains present in Opa1 from amino terminus to carboxy terminus are: mitochondrial targeting sequence (MTS), an IMM-embedded transmembrane domain, two distinct cleavage sites, a coiled-coil domain, a GTPase domain, a middle domain, and a GTPase effector domain. Opa1 is cleaved from a fusion-promoting long form (L-Opa1) into a fission-promoting short form (S-Opa1) by proteases including PARL [106, 107], YME1L, and OMA1, with the ratio between the long and short forms dictating Opa1 action and mitochondrial morphology [108–110]. Ultimately, although the long-only isoform of Opa1 appears to promote much of endogenous Opa1 function, a mixture of long and short isoforms, is required to promote full function [111, 112].

Opa1 is critical to preservation of mitochondrial DNA [113, 114]. Although it is still unclear exactly how Opa1 acts in this manner, mtDNA-encasing nucleoids physically interact with IMM-embedded regions of Opa1 [114], suggesting that Opa1 may act as an IMM anchor for nucleoids to promote mtDNA transcription and replication. Opa1 may also promote mtDNA maintenance through mitochondrial fusion. This is possible since simultaneous deletion of Mfn1 and Mfn2 required for complete inhibition of fusion causes a substantial reduction in mtDNA, whereas deletion of either Mfn1 or Mfn2 alone has little or no effect [115].

Another essential function of Opa1 is its preservation of cristae structural fidelity. Opa1 deletion, or inactivation of its GTPase domain, causes severe cristae dysmorphism and reduction in ETC function [111, 116]. The sufficiency of long and short Opa1 isoforms in restoration of cristae fidelity following Opa1 deletion is controversial. Some reports indicate that cells with either long-only or short-only isoforms of Opa1 are capable of restoring cristae structure and ETC function [111], but others demonstrate that the short-only isoforms are insufficient [117]. Cristae morphology is also regulated by ATP synthase dimers and by the mitochondrial contact sites and cristae organizing system (MICOS). V-shaped dimerization and row formation of membrane-embedded ATP synthase induces membrane curvature [64–66]. Mammalian MICOS is comprised of 7 proteins that demonstrate different effects on cristae morphology when disrupted [118, 119]. Opa1 physically interacts with the core MICOS component MIC60 [120] and acts upstream of MIC60 in regulation of cristae morphology [121]. In all, the exact mechanisms by which cristae are generated and regulated by Opa1, Drp1, MICOS, and ATP synthase remain to be elucidated.

1.2.1.3 Oncogenic signaling and mitochondrial dynamics

A primary function of mitochondria is to allow cells to adjust to cues originating from both extracellular and intracellular environments. To accomplish this, mitochondria must be sensitive to changes in signaling pathway activity through alterations in metabolism and morphology which then feed back to modulate activity of other signaling pathways.

The Ras-MAPK axis is perhaps the most well-annotated pathway with regard to its effects on mitochondrial dynamics with evidence that spans many cellular model systems. Multiple groups, including our own, identified that ERK directly phosphorylates Drp1 on serine 616 to potentiate Drp1-mediated mitochondrial fission [83, 84]. Since ERK activation lies downstream of Ras, RAF, and MEK activity, increased flux through any part of this cascade increases Drp1 fission activity and decreases mitochondrial size. ERK-mediated phosphorylation of Drp1 has been demonstrated by our group and others to be required for MAPK-mediated tumorigenesis in multiple cancer types including KRas-mutant pancreatic ductal adenocarcinoma [83] and BRAF-mutant melanoma [84], as well as for nuclear reprogramming of MEFs into epithelial-like colonies through overexpression of pluripotency factors [122]. Moreover, ERK kinase directly phosphorylates T562 of MFN1, decreasing its ability to tether mitochondria together and therefore preventing mitochondrial fusion [123].

The PI3K-AKT pathway also acts as a pro-mitochondrial fission pathway. Independent of AKT, PI3K upregulates expression of the mitochondrial protein MTP18 that promotes mitochondrial fission and cellular proliferation in prostate cancer [124]. In neurons, AKT directly phosphorylates Drp1 S616 and increases mitochondrial fission [125].

MYC is a transcription factor proto-oncogene that has been extensively studied across multiple cancer types and promotes cell proliferation and growth. The effects of MYC on mitochondrial dynamics are variable depending on cellular context, but in Burkitt lymphoma, MYC directly occupies the Drp1 promoter to increase Drp1 transcription and mitochondrial fission [126]. A pro-fragmentation function of MYC has also been reported in mouse embryonic fibroblasts where c-Myc overexpression alone increases Drp1 S616 phosphorylation and localization to mitochondria [127]. Conversely, in breast mammary epithelia, c-Myc is an important driver of mitochondrial fusion through PLD6 activity and inhibition of YAP/TAZ function which is crucial in maintenance of stemness phenotypes [128].

Mitochondrial fission is also promoted by activation of the cellular stress sensor AMP-activated protein kinase (AMPK). In studies of U2OS osteosarcoma cells, AMPK expression is required for mitochondrial fragmentation following treatment with of mitochondrial ETC inhibitors antimycin A and rotenone [129] and chemical activation of AMPK promotes mitochondrial fission by direct phosphorylation at S155 and S172 of Mff.

Signaling pathway strength, including that of AMPK, can be regulated by mitochondrial dynamics. In glioblastoma Drp1 knockdown decreases oxygen consumption rate and increases cell stress, activating AMPK [130]. These reports exemplify how mitochondrial function is altered by incoming signals and how mitochondria then affect signaling strength of pathways that are sensitive to mitochondrial outputs.

1.2.2 Mitochondrial dynamics in cancer stem cells

This section will highlight the ways in which cancer stem cells (CSCs) regulate mitochondrial function through mitochondrial dynamics. This discussion highlights how

specific populations of cells within a tissue may demonstrate mitochondrial dynamics that differ from the surrounding majority tissue and the potential consequences of these differences on tumor biology and therapy.

1.2.2.1 Introduction

Recent research in cancer biology has reshaped the way that the cellular makeup and physiology of many solid and liquid tumors are understood by offering a hierarchical model of tumor organization to better explain cancer outcomes in both the laboratory and clinic. This interpretation, termed the cancer stem cell model, has been reviewed extensively elsewhere states that for numerous tumors, there exists substantial cellular heterogeneity established from a minority of long-lived stem cells that slowly and asymmetrically divide to self-replicate and give rise to daughter cells [131, 132]. Daughter cells have impressive short-term proliferative capacity to form the bulk of tumors and to differentiate into more mature cell types, but lack significant tumor-initiating capability. Experimental evidence for this model of cancer has so-far been most robust in studies of glioblastoma [133, 134], leukemia [135, 136], breast [137, 138], lung [139, 140], and colorectal cancers [141]. Cancer stem cells are also known to be inherently resistant to conventional chemo-therapeutic regimens and are believed to be the source of relapse after clinical remission. Therefore, increased understanding and appreciation for cancer stem cell biology are paramount to the development of new therapeutic regimens that aim to destroy this population of cells and to eradicate tumors in a manner that minimizes risk of future relapse.

Cancer stem cells often represent a minority of cells within a tumor, thus identification and isolation of these cells away from non-CSCs is crucial for efforts aimed at characterizing their biology. Identification of these populations relies on the expression of cell surface

markers that suggest stemness based on either their expression in non-cancer stem cells or coexpression with stemness markers in cancer cell subpopulations. Single surface epitope expression is often used for these means, but combinations of gene expression are also frequently employed in different systems. For example, CD133 positivity is used extensively to mark cancer stem cells in colon [142], lung [143], and brain [144] CSCs, whereas a CD24−CD44+ population is often purified as breast cancer stem cells [138]. Stemness is also frequently measured by functional behaviors such as capacity of cells to form tumor spheres, colony formation, limiting dilution assays, and serial transplantation assay performance.

Traditional chemotherapeutic regimens capitalize on destroying vastly proliferative cells, and can be successful in shrinking primary tumors. Unfortunately, these tumors often relapse, potentially due to CSC quiescence-driven therapeutic evasion and continued proliferation of daughter cells that repopulate tumors. This process is similar to the regrowth of epithelia in the body after initial insult, where basal somatic stem cells are tasked with regeneration of the cellular differentiation hierarchy that makes up that particular tissue. These intrinsic properties permit survival of CSCs which then resume the process of tumor expansion; however, it is becoming increasingly clear that external signals from the tumor microenvironment also drive cancer stem cell phenotypes and must be considered as well [145]. Similar to non-cancer stem cells, it appears that cancer stem cell phenotypes can be markedly plastic and informed by signals from the niche they inhabit. For instance, ablation of LGR5+ colorectal cancer stem cells promotes migration of differentiated daughter into the CSC niche in which they dedifferentiate into LGR5+ CSCs to drive further tumor growth [141, 146]. In contrast, ablation of glioma cancer stem cells does not result in restoration of CSCs by differentiated progeny [133]. This phenomenon may be tissue-specific and makes consideration of the tumor

microenvironment on cancer stem cell physiology and therapeutic development imperative.

Each of the cellular behaviors that distinguish CSCs from the tumor bulk and surrounding non-transformed stroma have been intimately linked with altered mitochondrial function. Because mitochondrial dynamics regulate mitochondrial function, it is unsurprising that CSCs demonstrate unique dynamics signatures.

1.2.2.2 Mitochondrial dynamics in CSC metabolism

Reorganization of mitochondrial structure through mitochondrial fusion and fission is associated with a host of functional outcomes in non-transformed stem cells as well as cancer stem cells. A variety of metabolic phenotypes are associated with mitochondrial morphologies that are highly dependent on tissue type and differentiation status. Classically, immature cell types such as embryonic stem cells and many tumor cells demonstrate highly fragmented mitochondria that rely on aerobic glycolysis for energy production [147, 148]. Elevated rates of aerobic glycolysis produces anabolic intermediates that fuel cell growth and proliferation through increased synthesis of nucleotides and lipids [149]. Additionally, metabolic phenotypes coordinated by mitochondria have been well-described to affect cellular identity reprogramming through modulation of chromatin accessibility [150, 151].

Mitochondria orchestrate gene expression through synthesis of metabolites that form retrograde signals by acting as cofactors and substrates for gene expression-modifying enzymes. The majority of research on mitochondrial intermediate-driven gene expression changes has focused on production of acetyl-CoA [152, 153], alpha-ketoglutarate [154], succinate [155], and reactive oxygen species [156, 157]. Included within this group of

enzymes are the Ten-eleven translocation (TET) and PHD families of DNA and histone demethylases, respectively, which are both activated by high levels of alpha-ketoglutarate and inhibited by succinate and fumarate [158]. Additionally, Jumonji domain-containing histone demethylase activity is regulated by alpha-ketoglutarate. Acetyl-CoA synthesized in the cytoplasm from mitochondrial-derived citrate is the substrate for acetylation of histones, DNA, and cytosolic enzymes. Alterations in levels of reactive oxygen species synthesized within mitochondria can both directly modify enzymes such as p38 MAPK [159] and DUSP6 [160], and activate antioxidant programs such as the NRF2 pathway that modulate gene expression through direct binding of ROS-sensitive transcription factors [161]. Additionally, mitochondrial content affects mitochondrial capacity to buffer cytosolic calcium, which modulates activity of calcium-sensitive cellular signaling such as that mediated by Calcineurin [162]. Retrograde signaling pathways interact in networks in which one mitochondrial metabolite influences activation of another mitochondrial retrograde signaling program, such as mitochondrial ROS activation of calcineurin signaling [163].

Mitochondrial retrograde signaling is regulated by mitochondrial dynamics and affects cellular metabolism. In mouse embryonic cortex development, neural stem cell (NSC) mitochondrial morphology exhibits a transient fragmentation phase critical to differentiation [164]. Highly-glycolytic NSCs with elongated mitochondria differentiate into neural progenitors that exhibit increased oxidative phosphorylation and fragmented mitochondrial morphology. Neural progenitors then differentiate into neurons as their mitochondria revert to fused network morphology. Genetic inhibition of Drp1 inhibits the conversion of neural stem cells into the more-differentiated progenitor cells *in vivo*, indicating decreased differentiation potential and increased self-renewal. Conversely, inhibition of Mfn1/2 or Opa1 decreases self-renewal *in vivo* and *in vitro*.

Studies in mouse embryonic fibroblasts (MEFs) demonstrate highly-fused mitochondrial networks with abundant cristae that are converted into fragmented and cristae-poor populations upon reprograming into induced pluripotent stem cells (iPSCs) [165]. This morphological change is coupled with a departure from oxidative phosphorylation-predominant metabolism in differentiated MEFs into a highly glycolytic metabolism in iPSCs. Increases in glycolytic gene expression profiles precede activation of pluripotency genes, adding a temporal relationship between engagement of glycolytic metabolism and nuclear reprogramming. These reports demonstrate that mitochondrial dynamics are intimately linked with metabolic phenotypes that inform differentiation status and plasticity and highlight how different tissue types display varying dependencies on both mitochondrial morphology and metabolism to support stem versus more differentiated cellular phenotypes. This is a critical concept to justify future investigations of the influence that mitochondrial dynamics holds on metabolism of different populations of stem cells throughout the body.

Focusing on stem cells in the context of cancer, metastatic and hormone treatment-refractory prostate cancer cells upregulate Mff compared to primary tumor and normal prostate counterparts [166]. Mff knockdown decreases *in vitro* cancer stem cell sphere formation and inhibits *in vivo* tumor growth. Mff knockdown also inhibits respiratory capacity of tumor stem cells in tumor sphere assays, but not in adherent cells representative of the tumor bulk. This indicates that even within a tumor, the stem-like cell populations can exhibit differential metabolic dependencies on mitochondrial dynamics machinery from the more differentiated non-stem tumor bulk.

Findings in prostate cancer stem cells are supported by studies in a patient-derived xenograph model of glioblastoma in which brain tumor-initiating cells (BTICs) display a significantly more-fragmented mitochondrial morphology compared to the more-differentiated non-BTIC tumor cells [130]. Although expression of Drp1 is comparable between BTIC and non-BTIC cells, activating phospho-S616 is increased, and inactivating phospho-S637 is decreased, in BTIC versus non- BTIC. Additionally, overexpression of phosphomimetic S616 and phospho-dead S637 Drp1 in differentiated non-BTICs decreases expression of glioblastoma differentiation markers GFAP and MAP2 and increases expression of stemness markers such as NES, NANOG, SSEA-1 (FUT4), and Oct4, among others. Metabolically, knockdown of Drp1 in BTIC decreases oxygen consumption and inhibits *in vitro* and *in vivo* tumor growth.

Two publications in the last six years have shed light on the relationship between mitochondrial morphology, metabolism, and cancer stem cell identity in acute myeloid leukemia. Leukemic stem cells (LSCs) are metabolically dormant compared to non-LSCs and exhibit lower levels of oxidative phosphorylation, glycolysis, and ATP [167]. AMPK activation in LSCs drives a highly-fragmented mitochondrial morphology phenotype mediated by upregulation of Fis1 [168]. Knockdown of Fis1 in primary AML inactivates the myeloid anti-differentiation gene GSK3 and promotes cellular differentiation. These studies highlight the importance of mitochondrial dynamics in driving mitochondrial function and cell identity.

1.2.2.3 Mitochondrial dynamics in CSC metastasis

Cancer stem cells are well-equipped to make the epithelial-to-mesenchymal transition (EMT) and transit from the tissue of origin to site of metastasis through unique and numerous mitochondrial processes [169]. Induction of EMT drives highly glycolytic

metabolism [170–172] dependent on mitochondrial dynamics, as Mfn1 knockdown promotes fragmented mitochondrial morphology, increases expression of glycolysis genes, and increases cancer cell migration and metastasis [173]. Gene expression changes in EMT are regulated by signaling networks such as AMPK and coupled with mitochondrial trafficking to the cellular leading edge that fuels local reactions around structures involved in cellular motility such as focal adhesions [174, 175]. Additionally, MYC directly binds to the promoters of Drp1 and mitochondrial trafficking genes including RHOT1, RHOT2, and TRAK2 to promote mitochondrial fission and motility within cells [126]. Cells with decreased mitochondrial fragmentation and trafficking demonstrate significantly impaired focal adhesion dynamics, cellular motility, and invasion capacity. Overexpression of Opa1 or dominant-negative Drp1 inhibits persistent cell migration by inhibiting the anterior localization of mitochondria between the nucleus and leading edge of migrating breast cancer cells [176]. These studies demonstrate how mitochondrial dynamics promote intracellular motility of mitochondria that sustains reorganization and function of molecular structures that propel cancer cells movement, as is required for metastasis.

1.2.2.4 Mitochondrial dynamics in CSC therapeutic resistance

Mitochondrial dynamics generally drive therapeutic resistance through upregulation of mitochondrial function in CSCs compared to non-CSCs. PDAC cells that survive complete $KRas^{G12D}$ ablation express CSC markers CD133 and CD44h, upregulate mitochondrial biogenesis transcription factor PGC1A, and increase mitochondrial mass [177]. These cells also demonstrate increased dependency on oxygen consumption and decreased glycolytic flux. Primary AML stem cells also demonstrate an increase in mitochondrial respiration, upregulation of anti-apoptotic protein BCL-2, and resistance to the standard AML chemotherapy agent daunorubicin [167].

1.3 Dissertation overview and significance

The Kashatus lab has historically focused on better understanding the roles and regulation of mitochondrial fission in the context of cancer. In the years leading up to the start of the project described by this dissertation, the lab published two important papers that demonstrated that Drp1 is directly phosphorylated and activated by Erk downstream of hyperactive Ras or MAPK signaling and that activation of mitochondrial fission is required for Ras-mediated tumorigenesis, with a particular focus on KRas-mutant PDAC. Inhibition of mitochondrial fission has two generally separable manifestations. Acutely, Drp1 inhibition causes complete tubulation of the mitochondrial network. KRas-mutant tumor cells display highly fragmented mitochondrial morphology, so the departure from this phenotype to a completely fused network may have morphology-dependent consequences on mitochondrial function. Chronically, inhibition of mitochondrial fission inhibits the continuous cycles of fusion and fission that regulate organelle quality control. Fusion permits mixing of inner mitochondrial contents including proteins and mtDNA, whereas fission allows isolation and degradation of dysfunctional segments of mitochondria by mitophagy. To distinguish between the two potential mechanisms of tumor inhibition by inactivation of Drp1-mediated mitochondrial fission, the lab reasoned that simultaneous inhibition of mitochondrial fusion and fission may restore morphology and thus morphology-dependent function, but would leave fusion-fission cycling inactivated. If metrics of tumorigenesis or mitochondrial function that are inhibited by Drp1 inhibition are restored under fusion-fission inhibition, that would suggest that Drp1 inhibition acts through changes to mitochondrial morphology-dependent functions and not through inhibition of overall cycling.

My project began as an attempt to identify which function of Drp1 is critical to tumorigenesis and to assess whether KRas-mutant tumors other than PDAC demonstrate

similar sensitivity to disruption of mitochondrial dynamics. The work in this thesis clarifies the consequences of inhibiting mitochondrial dynamics in KRas-mutant lung adenocarcinoma and proposes a novel mechanism of acute interaction between Drp1 and Opa1 in shaping the mitochondrial inner membrane and ETC function. This work has expanded the state of knowledge of mitochondrial dynamics in cancer as well as the Kashatus lab's technical capabilities during the pursuit of that knowledge. Many additional questions have been raised by this work, as outlined in Chapter 3 of this dissertation, and will require further investigation.

2 Chapter 2. Opa1 and Drp1 reciprocally regulate cristae morphology, electron transport chain function, and NAD^+ regeneration in KRas-mutant lung adenocarcinoma

This chapter is derived from the publication:

Sessions DT, Kim KB, Kashatus JA, Churchill N, Park KS, Mayo MW, Sesaki H, Kashatus DF. Opa1 and Drp1 reciprocally regulate cristae morphology, ETC function, and NAD^+ regeneration in KRas-mutant lung adenocarcinoma. Cell Rep. 2022 Dec 13;41(11):111818. doi: 10.1016/j.celrep.2022.111818. PMID: 36516772.

2.1 Introduction

Approximately one-third of all human tumors harbor mutations in *RAS* GTPases. Activating *RAS* mutations rewire cellular metabolism [23–25] and promote cell survival and proliferation. Mitochondria regulate many processes disrupted in cancer, including ATP synthesis, redox homeostasis and apoptosis. Mitochondria undergo cycles of fusion and fission regulated by four large dynamin related GTPases. Drp1 (*DNM1L*) executes

mitochondrial fission whereas Mfn1/2 and Opa1 execute fusion of mitochondrial outer and inner membranes, respectively. The fission and fusion GTPases also remodel the mitochondrial outer and inner membranes. For example, Drp1 remodels cristae during apoptosis [93] and Opa1 is critical to maintain cristae fidelity [67] to support oxidative phosphorylation (OXPHOS) [111, 178, 179] and resistance to apoptosis [116, 180] through sequestration of cytochrome C [181].

Oncogenic signaling impacts mitochondrial shape by regulating mitochondrial dynamics machinery. Oncogenic KRas activates mitochondrial fission through Erk2-mediated phosphorylation of Drp1 [83, 84] and inhibition of mitochondrial fission inhibits KRas-driven glycolytic flux, cellular transformation, and pancreatic tumor (PDAC) growth [182]. To determine if mitochondrial fission contributes to tumor growth in other Ras-driven malignancies, we explored the effects of mitochondrial dynamics disruption in KRas-driven lung adenocarcinoma (LUAD). Lung adenocarcinoma has the highest mortality of human cancers and 30% of LUAD tumors harbor oncogenic *KRAS* mutations; however, the role of mitochondrial dynamics in this malignancy is poorly defined compared to other KRas-driven tumors. As observed in PDAC and melanoma, Drp1 is phosphorylated downstream of Ras signaling in LUAD and regulates LUAD metabolism [183, 184]. However, while some studies find elevated Drp1 expression in tumors and a pro-tumorigenic role [183–185], others demonstrate decreased tumor Drp1 expression and anti-tumor roles [186].

Tissue of origin influences metabolism of tumors with identical driver mutations [39, 187]. Since PDAC and LUAD exhibit distinct metabolic phenotypes [37, 188–192], we explored whether LUAD demonstrates unique sensitivities to dynamics disruption. Surprisingly, deletion of Opa1, but not Drp1, inhibits *in vitro* colony formation and ETC function of KRas-driven LUAD cells, and blocks lung tumor development in a $Kras^{LSL\text{-}G12D/+}$; $Trp53^{FL/FL}$ (KP)

genetically-engineered mouse model (GEMM). Further, Drp1 deletion rescues the effects of Opa1 deletion on *in vitro* colony formation and ETC function, but not *in vivo* tumor growth. Mechanistically, Opa1 deletion impacts colony formation and tumor growth through disruption of cristae morphology and inhibition of ETC assembly and function. Consistent with recent work [29, 31, 193], the critical ETC function disrupted by Opa1 deletion is not mitochondrial ATP synthesis, but rather complex I-mediated NAD^+ regeneration. Collectively, these data suggest that Opa1-dependent cristae remodeling is critical to complex I-mediated NAD^+ regeneration in proliferative cells with substantial mitochondrial fission activity.

2.2 Materials and Methods

KPDO genetically-engineered mouse model (GEMM) of lung adenocarcinoma:

This is a fixed endpoint study assessing tumor burden and retention of mitochondrial dynamics gene expression in KP, KPD, KPO, and KPDO mice ten weeks after intratracheal adenovirus-Cre administration. The experimental unit for analysis of tumor burden is the mouse and the sample size is 15 mice per group. The experimental unit for retention of Drp1 and/or Opa1 expression is the individual tumor nodule (IHC, n=60 per group) or individual GEMM-derived tumor cell line (immunoblot and PCR, sample size variable based on number of independent tumor cell lines generated per mouse genotype). The only inclusion criterion was desired genotype of mice as determined by PCR. All mice that satisfied genotype requirements were enrolled until the sample size within a given group was satisfied. Four KPDO mice past the desired sample size (chronologically the last four) were mistakenly enrolled and infected with adenovirus-Cre. These mice were excluded from tissue harvest for tumor burden analysis to maintain equal group sample sizes, but were used to generate GEMM-derived tumor cell lines in the same manner as mice used as intended for tumor burden analysis. No randomization was

employed as mice were generated and enrolled based solely on genotype. Mice from both sexes were used in each of the four groups as generated, and the number of each sex is as follows (male, female): KP (9,6), KPD (6,9), KPO (13,2), KPDO (7,8). KP (*Kras*$^{LSL\text{-}G12D/+}$; *Trp53*$^{FL/FL}$) mice were supplied by Dr. Kwon Park. *Opa1*$^{FL/FL}$ (O) mice [194] were provided by Dr. Hiromi Sesaki. KP mice were mated with *Opa1*$^{FL/FL}$ and *Dnm1l*$^{FL/FL}$ (D) [195] to generate heterozygous KPO and KPD genotypes. KPD and KPO were mated to generate heterozygous KPDO mice. Breeders for all conditions were descendants from KPDO heterozygotes to maintain recent shared ancestry. KPD, KPO, and KPDO mice were generated by breeding parents heterozygous for floxed *Dnm1l* and/or *Opa1* alleles such that KP controls were generated in the same litters. Male and female mice of desired genotypes were generated from multiple breeder pairs per condition. Primer sequences used for mouse genotyping can be found in table S1. Intratracheal adenovirus-Cre infections were performed as previously described. [21]. Briefly, at ten weeks of age, enrollee mice were anesthetized with 250 mg/kg Avertin and intratracheally infected with $2.5x10^7$ PFU Adeno-Cre (Baylor Viral Vector Core). Mice were weighed and monitored twice per week for symptoms of disease including weight loss, hyperpnea, and piloerection for ten weeks. At ten weeks post-infection, mice were sacrificed by Avertin anesthetic overdose and exsanguination and lungs were harvested for fixation and/or tumor cell line isolation. At sacrifice, lungs were perfused intratracheally with ice cold 10% neutral buffered formalin. Mice from which tumor cell lines were derived had the right middle lobe ligated, removed, minced, and seeded into culture medium before perfusion. Perfused lungs were dissociated from the thorax and fixed in tubes containing formalin at 4C. Fixed lungs were paraffin embedded and sectioned to 5 um thick by the University of Virginia Research Histology Core. Hematoxylin and eosin staining and immunohistochemistry were performed by the University of Virginia Biorepository and Tissue Research Facility. All animal studies were performed in accordance with the University of Virginia Institutional

Animal Care and Use Committee. The following parameters were assessed: tumor burden per mouse (measured by tumor surface area versus total lung area on H&E-stained FFPE sections), individual tumor Opa1/Drp1 expression by IHC on FFPE sections, and Opa1/Drp1 expression in GEMM-derived tumor cell lines by immunoblot and PCR. GEMM tumor burden analysis**:** hematoxylin- and eosin-stained (H&E) lung sections were scanned at high resolution on Aperio ScanScope to generate digital images. Tumor burden was calculated using QuPath software [196] as percent tumor area (tumor surface area/total lung area). Total lung area, excluding exterior connective tissue, and tumor area were traced using the wand tool. Total lung area per sample was calculated as the sum of the area of each individual lobe per sample. Total tumor area per sample was calculated as the sum of the area of individual tumors present per sample. Representative whole-lung H&E images were pixel-downsized 10x from original and imported into FIJI. GEMM IHC analysis: IHC lung sections were scanned at high resolution on Aperio ScanScope to generate digital images. IHC DAB intensity was analyzed using QuPath [196] on 20 individual tumors per slide on 3 Drp1- or Opa1-stained slides per genotype assessed (60 total per genotype). All lobes present on slides were sampled. Each tumor had mean DAB intensity measured. $Drp1^{-/-}$;$Opa1^{-/-}$ MEFs were analyzed by removing background first to exclude space between cells and then had mean DAB intensity measured. Statistical analysis of tumor burden and Drp1 IHC intensity was performed by Kruskal-Wallis one-way analysis of variance followed by Dunn's multiple comparisons test using Prism v7 software. Descriptive statistics of tumor burden results by genotype (mean$\pm$SD): KP (13.43$\pm$7.92), KPD (8.37$\pm$6.13), KPO (3.68$\pm$2.86), KPDO (2.36$\pm$1.89). DS, KP, and KK performed anesthesia and intratracheal infection for all mice. DS monitored mice throughout study and performed sacrifice, tissue harvest, and data analysis.

Table 2-1. KPDO Mouse Genotyping Primers (5'-3')

Kras F1: CTAGCCACCATGGCTTGAGT
Kras F2: ATGTCTTTCCCCAGCACAGT
Kras R: TCCGAATTCAGTGACTACAGATG
Trp53 F: CACAAAAACAGGTTAAACCCAG
Trp53 R: AGCACATAGGAGGCAGAGAC
Dnm1l F: ACCAAAGTAAGGAATAGCTGTTG
Dnm1l R: ATGCGCTGATAATACTATCAACC
Opa1 F: TTAAGACACCCCAAGAGCTTGC
Opa1 R: CCAGCTTAGATCCCATTTGTTGACAG
Opa1 Recombined (Δ) F: CCATCTGTGTAGTGAACTTACTG
Opa1 Recombined (Δ) R: TGACGAGGCGTCCGAAGAACGGATCCAAGC

KPY40 and KP(D,O,DO) Tumor Cell Line Generation:

At sacrifice, right middle lobes were aseptically harvested, mechanically minced with a razor blade, trypsin-digested, and plated into 10-cm plates in high-glucose DMEM supplemented with 10% FBS and 1% penicillin/streptomycin. Tumor cells were purified from other cell types initially present in plates by natural selection for cells with oncogenic *Kras* and *Trp53* deletion over successive passages. Purification of tumor cells from non-tumor cells was confirmed by PCR amplification demonstrating recombined *Kras* and *Trp53* alleles, and the absence of $Kras^{LSL\text{-}G12D}$ and $Trp53^{FL}$ alleles present in non-tumor cells. AdEV- and AdCre-infected cells were used 3-7 days post-infection unless otherwise stated.

Cell Culture:

Human A549 and mouse LUAD cells were cultured in high-glucose DMEM (Life Technologies #11965-092) supplemented with 10% FBS and 1% penicillin/streptomycin ("full DMEM") at 37C in a 5% CO2 humidified incubator. For indicated uridine-containing media experiments, full DMEM was supplemented with 0.1 mg/mL uridine (Fisher Scientific).

Mouse Embryonic Fibroblast Cell Line Generation:

MEFs were prepared as previously described [197]. Briefly, *Trp53*$^{FL/FL}$ (P) mice or *Kras*$^{LSL\text{-}G12D/+}$; *Trp53*$^{FL/FL}$;*Dnm1l*$^{FL/FL}$;*Opa1*$^{FL/FL}$ (KPDO) mice were mated. At 13.5-14.5 days post-fertilization, pregnant females were euthanized by CO_2 asphyxiation and cervical dislocation and uterine horns were isolated. Individual embryos were placed in separate dishes and had head and red organs removed with scalpel and forceps. The remaining tissue was minced and enzymatically digested with trypsin at 37C for 10 minutes and placed into cell culture in full DMEM. Cell genotype was verified by PCR. Cells were immortalized by *in vitro* Adeno-Cre infection that facilitated homozygous recombination and deletion of the *Trp53* alleles. P MEFs were used for mitochondrial morphology imaging under MYLS22 treatment. KPDO MEFs were used to validate and optimize Drp1 and Opa1 IHC staining for use on GEMM lung sections.

Colony Formation Assay:

100 cells were seeded per well in triplicate in 12-well plates and grown for 1 week in full DMEM. After one week, cells were rinsed once in PBS and fixed in 10% formalin for 20 minutes at room temperature. Formalin was aspirated and cells were stained with 0.5 mL per well of 0.5% crystal violet solution (0.5g crystal violet, 20 mL methanol, 80 mL H20) for 10 minutes at room temperature. Crystal violet solution was removed and cells were

rinsed in H_20 twice for 10 minutes on a shaker before drying and imaging. Colony number was quantified using FIJI.

CellTiterGlo (CTG) Cell Viability Assay:

500 cells were seeded in 50 uL full DMEM in white-walled 96-well plates in technical duplicates or triplicates per independent experiment. The next day, media was changed to 50uL fresh DMEM with indicated compounds. 48 hours later, 50 uL CTG reagent (Promega) was added to each well and incubated for 15 minutes at room temperature before luminescence measurement. Individual wells of drug-treated (non-DMSO) cells were normalized to the mean of the DMSO-treated wells within an individual experiment. Statistical analysis was performed on the mean of normalized values from individual experiments within treatment groups such that the sample size of each treatment group was equal to the number of independent experiments.

Seahorse Mitochondrial Stress Test:

20-25,000 cells were seeded in 80 uL full DMEM per well and placed at room temperature for one hour to adhere before being placed in 37C incubator for another two hours. Assay media was made using Seahorse DMEM supplemented to a final concentration of 25 mM glucose and 4 mM glutamine and pH was adjusted to 7.4 after warming to 37C. Inhibitors were diluted in assay media at the following concentrations: 10x oligomycin (15 uM), 10x CCCP (20 uM), 10x antimycin A/rotenone (10 uM each). Before loading cells, all wells had seeding media aspirated and replenished with 180 uL Seahorse media. Reserve oxygen consumption rate was calculated by subtracting the average resting OCR from the average CCCP-treated OCR. Basal mitochondrial oxygen consumption rate was calculated by subtracting the antimycin A/rotenone-treated OCR from the resting OCR. No normalization was utilized as cells were seeded right before assay start to avoid effects

of differential proliferation. All cells within the same cell line were seeded at identical densities.

NAD/NADH-Glo Assay:

50,000 cells were seeded per well in 6-well plates in 2 mL full DMEM. After 24 hours, cells were rinsed in PBS, trypsinized, and counted. 5000 cells per condition were assayed per well in white-walled 96-well plates using the Promega NAD/NADH-Glo kit. Cells of independent experiments were seeded and assayed on separate days.

Cell Accumulation Assay:

10,000 cells were seeded in 6-well wells in full DMEM in two plates per independent experiment for day 2 and day 4 cell counts. 24 hours after seeding, media was replaced to fresh DMEM with DMSO or indicated compounds (oligomycin = $2x10\text{-}^{15}$ moles/cell [10 nM], CCCP = $5x10^{-14}$ moles/cell [250 nM], rotenone = $5x10^{-14}$ moles/cell [250 nM]). Cells were trypsinized, harvested, and counted using a hemacytometer on day 2 and day 4. Cells of independent experiments were seeded and assayed on separate days.

Mitochondrial Isolation:

Mitochondrial isolation was performed as previously described [198]. Cells were cultured in 15 cm plates in full DMEM to full confluence and then trypsinized, harvested, and rinsed once in PBS. The cell pellet was resuspended in 900 uL RSB Hypo Buffer and placed on ice for 15 minutes to allow cells to swell. Cells were transferred to a 5 mL Dounce homogenizer and homogenized with 20 strokes. Cells were transferred to a new 1.5 mL Eppendorf and 600 uL 2.5X MS homogenization buffer was added and mixed. Cells were centrifuged at 1300g for 5 min at 4C and the supernatant containing the mitochondrial fraction was transferred to a new tube. The mitochondrial fraction was centrifuged and

transferred two more times to remove remaining nuclei or cells. Mitochondria were pelleted by centrifugation at 15000g for 15 minutes, rinsed in 1 mL of 1X MS homogenization buffer, and pelleted again at 15000g for 15 minutes. Mitochondria were resuspended in buffer (150 mM sodium acetate, 30 mM HEPES, 1 mM EDTA, 12% glycerol (w/v), pH 7.5) at 2 ug protein/uL for further analysis. An aliquot of each lysate was reserved for immunoblot analysis of equal gel loading. Cells of independent experiments were seeded, harvested, and fractionated on separate days.

Mitochondrial Native PAGE and ETC Complex I In-Gel Activity (IGA) Assay:

High resolution clear native (hrCN) PAGE was performed as previously described [199]. Briefly, isolated mitochondria were solubilized with 2 ug dodecyl maltoside per ug protein on ice for 30 minutes. Solubilized mitochondria were centrifuged at 17,000xg for 10 minutes at 4C. 25 ug solubilized mitochondria was mixed with 1 uL loading buffer (50% glycerol, 0.1% ponceau S) per 10 uL sample. 4-10% acrylamide gradient gels were cast by hand by laying down 1 mL layers at concentrations including and between 4% and 10%. Gels were run at 4C for 1 hour at 100V and then 1 hour at 200V. After electrophoresis, gels for complex I activity assay were placed in complex I IGA buffer (5 mM Tris pH 7.4, 2.5 mg/mL MTT, 0.1 mg/mL NADH) on a shaker for 15 minutes at room temperature. After 15 minutes, buffer was removed, and gel was incubated in 10% acetic acid for 15 minutes on a shaker and then imaged. Complex I IGA band intensities were quantified using FIJI. After gel electrophoresis, gels for Coomassie stain were placed in 0.025% Coomassie G250 in 10% acetic acid at room temperature for 1 hour. Gels were then rinsed overnight in 10% acetic acid in containers with Kimwipes and imaged.

Mitochondrial DNA Measurement:

Measurement of the ratio of mitochondrial to nuclear DNA was performed as previously described [200]. Cells were cultured in 10-cm dishes and harvested by trypsinization. Cell pellets were lysed in 600 uL buffer (100 mM NaCl, 10 mM EDTA, 0.5% SDS, 20 mM Tris-HCl pH 7.4, 200 ug/mL proteinase K) at 55C for 3 hrs. DNA was precipitated with 250 uL 7.5M ammonium acetate and 600 uL 70% isopropanol and centrifuged at 4C for 10 minutes at 15,000g. The pellet was rinsed with 70% ethanol and centrifuged again and DNA was resuspended in TE buffer. DNA concentration was measured on a NanoDrop and DNA was diluted to 10 ng/uL for qPCR. qPCR was performed in triplicate for each sample and each primer set in 96-well plates with each well containing 10 uL 2x SYBR green qPCR mix, 8 uL of 10 ng/uL DNA, and 2 uL of 10 uM combined forward and reverse primers. The qPCR program run was 95C (5 min), 45 cycles of 95C (10s), 60C (10s), and 72C (20s), then a melting curve. Copy numbers of mitochondrial:nuclear DNA were calculated by the $\Delta\Delta$Ct method as #copies mtDNA = 2*2^(Ct(HK2)-Ct(ND1 or 16S)). Student's T-test was used for statistical analysis.

Table 2-2. Mouse mtDNA:nDNA Analysis qPCR Primers (5'-3')

Hk2 F: GCCAGCCTCTCCTGATTTTAGTGT
Hk2 R: GGGAACACAAAAGACCTCTTCTGG
mt-Nd1 F: CTAGCAGAAACAAACCGGGC
mt-Nd1 R: CCGGCTGCGTATTCTACGTT
mt-Rnr2 (16S) F: CCGCAAGGGAAAGATGAAAGAC
mt-Rnr2 (16S) R: TCGTTTGGTTTCGGGGTTTC

Transmission Electron Microscopy:

Cultured cells were harvested by trypsinization, rinsed in PBS, and pelleted. Cell pellets were fixed in 1 mL of 4% formaldehyde 0.1M sodium cacodylate at 4C for 1-3 days. Fixative was removed and pellets were rinsed twice in 1 mL 0.1M sodium cacodylate. After the second rinse, cells were placed in osmium tetroxide in 0.1M sodium cacodylate for 45 minutes at room temperature shaking in the dark. Cell pellets were then rinsed once in 0.1M sodium cacodylate and dehydrated by successive 10-minute incubations in 30%, 50%, 70%, 95%, and 100% ethanol. Dehydrated samples were embedded in increasing concentrations (25%, 50%, 75%, 100%) of resin and placed in the oven. Embedded samples were then sectioned and stained with uranyl acetate and lead. Samples were imaged at 30k magnification. Images were analyzed in a randomized and blinded fashion.

Mitotracker Red CMXRos Staining and Imaging:

Cells were seeded on coverslips in 6-well plates at 100,000 cells per well in full DMEM and adhered overnight. To stain, media was replaced with fresh full DMEM + 100 nM Mitotracker Red CMXRos for 45 minutes in a 37C incubator. After staining, media was aspirated and replaced with fresh DMEM for stain washout and cells were placed back in incubator for 60 minutes. Cells were rinsed once in PBS and fixed in 4% formaldehyde in PBS for 15 minutes at RT in the dark. Fixative was removed and nuclei were stained with DAPI-containing PBS for 10 minutes on a shaker in the dark at room temperature. Cells were rinsed twice with PBS on a shaker for 5 minutes each before mounting on slides in Prolong Gold. Slides were imaged on a Zeiss LSM710 and images were exported to TIFFs using ZEN Black software.

Mitotracker Green FM Staining and Imaging:

20,000 cells were seeded on glass-bottom dishes (Greiner Bio-One CELLview) dishes in full DMEM. The next day, cells were incubated in 150 nM Mitotracker Green FM in full DMEM for 1 hour in a 37C incubator. After incubation, cells were rinsed once in PBS and then placed in live-cell imaging DMEM (25 mM glucose, 4 mM glutamine, 1% FBS, no phenol red). Cells were immediately imaged using a Zeiss LSM900 with Airyscan. Crop area was set to 2x and scan speed was set to 4-9 μs per pixel in Zen Blue software.

Plasmid Construction and Viral Transduction Cell Line Generation:

Drp1 Plasmids: Mouse Drp1 was PCR amplified from pcDNA3.1 mDrp1 (Addgene #34706) and cloned into pLenti BlastR or pCW57.1 using InFusion cloning. Drp1 mutants were generated using InFusion cloning.

CRISPR: plentiCRISPRv2 was digested with BsmBI and annealed sgRNA oligos were ligated with T4 ligase. For double CRISPR cells, the puromycin resistance transgene from plentiCRISPRv2 was swapped for a neomycin resistance transgene to generate plentiCRISPRv2 NeoR and sgRNAs were cloned in using the same protocol. Lentivirus was generated in 293T cells by calcium phosphate cotransfection with psPAX2, pCMV-VSV-g, and plentiCRISPRv2 vectors. Media was removed from 293T cells 24 and 48 hours after transfection, filtered through 0.45 um PES filters, and applied to target cells with polybrene (5 ug/mL). Infected cells were selected in full DMEM with puromycin (3 ug/mL for mouse cells, 1 ug/mL for A549) or neomycin (1 mg/mL mouse and A549).

Table 2-3. CRISPR sgRNA Sequences (5'-3')

sgCTR: GTATTACTGATATTGGTGGG
Mouse *Opa1* sg1: GCGCCTGCGAGAGCTCGACA
Mouse *Opa1*/Human *Opa1* sg4: AAATGTAGCCAGTCCAAGCA
Human *Opa1* sg3: TCAGTGGAAAGATATGATAC
Mouse *Dnm1l* sg1: GCACAAATAAAGCAGGACGG
Mouse *Dnm1l* sg2: AATCGTGTTACAATACTCTG
Mouse *Mfn1* sg: GCTCAAGGTTGTAAGTCCGT
Mouse *Mfn2* sg: CCGAGGCAGACGCATCCCAG

Immunoblotting:

Cell pellets were lysed on ice in RIPA buffer with protease/phosphatase inhibitor cocktail (Roche). Protein concentration was determined by BioRad Protein Assay (BioRad) and 20 ug protein was resolved by SDS-PAGE in 10% acrylamide gels, transferred to PVDF membrane (Millipore), blocked in 5% fat-free milk, and probed with indicated antibodies.

TMRE Flow Cytometry:

500,000 cells were seeded in 10 mL full DMEM in 10-cm plates and adhered overnight. The next day, media was changed to full DMEM with DMSO, oligomycin, or CCCP at equimolar amounts per cell as the cellular accumulation experiment using these same compounds (oligomycin = $2x10^{-15}$ moles/cell [100 nM], CCCP = $5x10^{-14}$ moles/cell [2.5 uM]) and incubated for one hour at 37C. Cells were trypsinized, counted, and 250,000 per treatment were incubated in 500 uL PBS + 4 mM glutamine + 25 mM glucose + 100 nM TMRE for 30 minutes at 37C before analysis by flow cytometry on an Attune NxT flow

cytometer. Data were analyzed in FCS Express. TMRE intensity was determined in cells gated solely on the live cell population as determined by SSC x FSC.

Data Representation and Statistical Analysis:

Statistical analysis and data presentation were performed using GraphPad Prism v7. All dispersion and precision measures, statistical tests used and significance are indicated in individual figure panels and legends. When applicable, normalization before statistical analysis is described in the methods section for that particular assay (e.g. CTG assays of cell viability). When variation between groups was unambiguously unequal, non-parametric statistical testing was used (e.g. GEMM tumor burden analysis).

2.3 Results

2.3.1 Opa1 inhibition prevents KRas-mutant LUAD colony formation and is Drp1-dependent

Mitochondrial shape is maintained through a balance of fission and fusion. Persistent Ras-MAPK signaling hyperactivates mitochondrial fission through Erk2-mediated phosphorylation of Drp1 to promote tumorigenesis [83, 84, 182]. We hypothesized that KRas-mutant LUAD may be sensitive to unopposed MAPK-stimulated fission following inhibition of mitochondrial fusion. We used CRISPR-mediated Opa1 deletion to inactivate mitochondrial fusion in KPY40 lung tumor cells derived from a KP GEMM. To avoid adaptation to chronic Opa1 deletion, we used mixed-population cells within a week of viral transduction and observed robust depletion of Opa1 expression (Figure 2-1A). To assess the effects of acutely inhibiting Opa1 on individual cell growth and survival, we performed colony formation assays and found Opa1 depletion significantly inhibits LUAD colony formation (Figure 2-1B). We also confirmed this effect in mixed-population human *KRAS*-

mutant A549 LUAD cells (Figures 2.1C and 2.1D). Next, we pharmacologically inhibited Opa1 using MYLS22 [201] and validated inhibition of mitochondrial fusion in KPY40, A549, and mouse embryonic fibroblasts by examining mitochondrial morphology. DMSO-treated cells demonstrate mixed mitochondrial morphology whereas MYLS22-treated cells demonstrate fragmented morphology (Figures 2.1E, 2.2A, and 2.2B) similar to that observed by others upon Opa1 deletion [111, 116]. To assess whether pharmacological inhibition of Opa1 affects colony formation, we treated KPY40 cells with DMSO or MYLS22. MYLS22-treated cells demonstrate decreased colony formation at doses of 25 uM and 50 uM (Figure 2-1F). Together, these data demonstrate that genetic or pharmacologic inhibition of Opa1 decreases KRas-mutant LUAD colony formation.

To determine whether the effects of Opa1 inhibition are mediated by unopposed mitochondrial fission, we examined KPY40 colony formation following Drp1 deletion, Opa1 deletion, or both. We again used CRISPR to inactivate Drp1 first and Opa1 second. We observe complete Drp1 deletion and robust depletion of Opa1 in mixed-population cells, but no effect on mitochondrial markers SDHA and VDAC, indicating that acute deletion of Drp1 and/or Opa1 does not alter mitochondrial abundance (Figure 2-1G). Notably, inactivation of mitochondrial fission by Drp1 deletion does not affect colony formation in these cells (Figures 2.1H and 2.1I). This was surprising given that Drp1 deletion inhibits KP PDAC growth. Further, inactivation of mitochondrial fission completely rescues the effects of Opa1 knockout on colony formation. These results indicate that mitochondrial fission mediates the effects of Opa1 knockout on *in vitro* LUAD colony formation and suggest a functional link between Drp1 and Opa1.

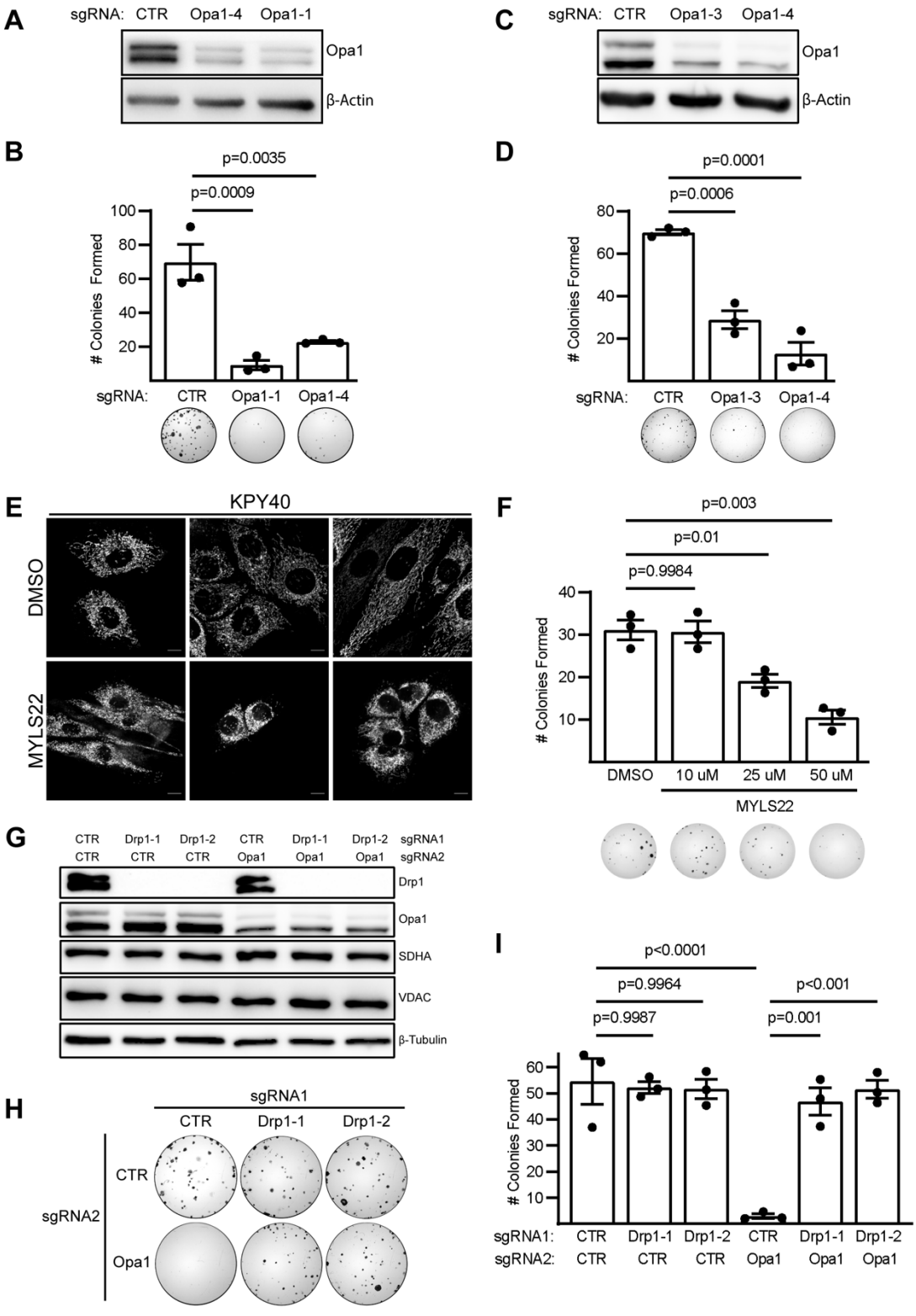
A
sgRNA: CTR Opa1-4 Opa1-1
Opa1
β-Actin
C
sgRNA: CTR Opa1-3 Opa1-4
Opa1
β-Actin
B
p=0.0035
p=0.0009
# Colonies Formed
sgRNA: CTR Opa1-1 Opa1-4
D
p=0.0001
p=0.0006
# Colonies Formed
sgRNA: CTR Opa1-3 Opa1-4
E
KPY40
DMSO
MYLS22
F
p=0.003
p=0.01
p=0.9984
# Colonies Formed
DMSO 10 uM 25 uM 50 uM
MYLS22
G
CTR Drp1-1 Drp1-2 CTR Drp1-1 Drp1-2 sgRNA1
CTR CTR CTR Opa1 Opa1 Opa1 sgRNA2
Drp1
Opa1
SDHA
VDAC
β-Tubulin
H
sgRNA1
CTR Drp1-1 Drp1-2
sgRNA2
CTR
Opa1
I
p<0.0001
p=0.9964
p=0.9987
p<0.001
p=0.001
# Colonies Formed
sgRNA1: CTR Drp1-1 Drp1-2 CTR Drp1-1 Drp1-2
sgRNA2: CTR CTR CTR Opa1 Opa1 Opa1

Figure 2-1. Opa1 inhibition prevents KRas-mutant LUAD colony formation in a Drp1-dependent manner

A. Immunoblot of Opa1 in KPY40 CRISPR cells.

B. Colony formation in KPY40 CRISPR cells with quantification. n=3 independent experiments. Mean±SD. One-way ANOVA + Dunnett's multiple comparisons test.

C. Immunoblot of Opa1 in A549 CRISPR cells.

D. Colony formation in A549 CRISPR cells with quantification. n=3 independent experiments. Mean±SD. One-way ANOVA + Dunnett's multiple comparisons test.

E. Mitotracker Green-stained KPY40 tumor cells treated with DMSO or 50uM MYLS22 for 72 hours. Scale = 10μm.

F. Representative colony formation in MYLS22-treated KPY40 cells with quantification. n=3 independent experiments. Mean±SD. One-way ANOVA + Sidak's multiple comparisons test.

G. Immunoblot of SDHA, VDAC, Drp1, and Opa1 in KPY40 CRISPR cells.

H. Colony formation in KPY40 double-CRISPR cells.

I. Quantification of KPY40 double-CRISPR colony formation. n=3 independent experiments. Mean±SD. One-way ANOVA + Sidak's multiple comparisons test.

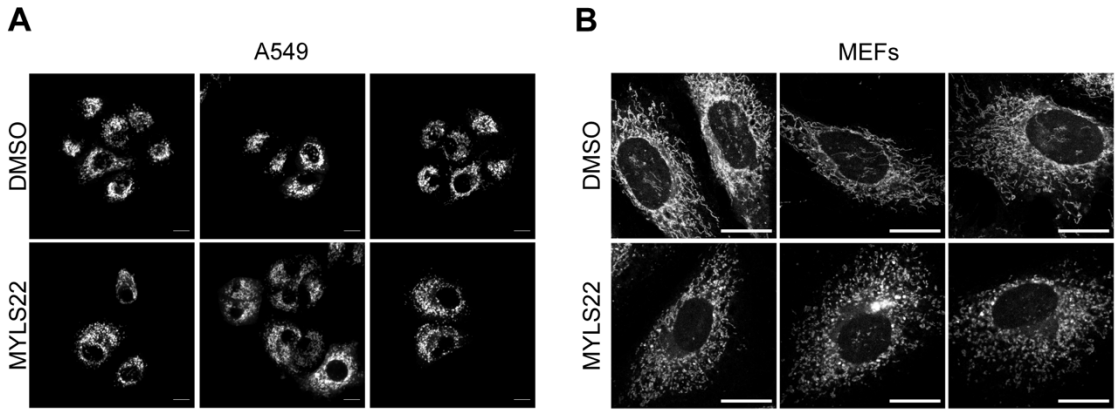

Figure 2-2. Cells treated with Opa1 inhibitor MYLS22 demonstrate fragmented mitochondrial morphology

A. Human A549 LUAD cells treated with DMSO or 50 uM MYLS22 for 72 hours and stained with Mitotracker Green. Scale bar = 10 μm.

B. MEFs treated with DMSO or 50 uM MYLS22 for 72 hours and stained with Mitotracker Red. Scale bar = 20 μm.

2.3.2 Deletion of Opa1, but not Drp1, inhibits KP LUAD development *in vivo*

To test whether deletion of Drp1, Opa1, or both affects spontaneous KP LUAD development *in vivo*, we generated *Kras*$^{LSL\text{-}G12D/+}$; *Trp53*$^{FL/FL}$ (KP) mice expressing wildtype Drp1 *(Dnm1l)* and Opa1 (*Opa1)*, or with homozygous floxed alleles of *Dnm1l* (KPD), *Opa1* (KPO), or both (KPDO) (Figure 2-3A). We initiated tumor formation and mitochondrial dynamics gene deletion by intratracheal administration of Adenovirus-Cre (AdCre) and allowed tumors to develop for 10 weeks (Figure 2-3B). Contrary to what is observed in KRas-driven PDAC [182], LUAD tumor burden in KPD mice is not significantly different from that of KP (Figure 2-3C); however, tumor burden in KPO mice is significantly less than in KP. Surprisingly, simultaneous deletion of Opa1 and Drp1 does not rescue tumor development. Hematoxylin- and eosin-stained lung sections demonstrate that all mice develop tumors with similar histological morphology (Figure 2-3D). Together, these data suggest that Drp1 is dispensable, but Opa1 is required, for KP LUAD development, and that deletion of Drp1 is insufficient to rescue Opa1 deletion-mediated decrease in tumor development *in vivo*.

Recombination of floxed alleles by AdCre in the KP LUAD model is incompletely efficient [202]. As a result, unrecombined alleles of genes that play a pro-tumorigenic role can be selected for during tumor development. The degree to which developed tumors retain floxed alleles provides insight to whether their gene products are required for tumor development. For example, there is a strong selective pressure to retain Drp1 expression in a PDAC GEMM with genetics identical to the LUAD model used here [182].

We took two approaches to determine whether individual tumors that form in KPD, KPO, and KPDO mice completely recombine mitochondrial dynamics alleles. First, we performed immunohistochemistry (IHC) on lung sections using antibodies targeting Drp1

or Opa1. Second, we isolated independent tumor cell lines from mice to assess the presence of Drp1 and Opa1 by immunoblot and PCR. Complete recombination of floxed *Kras* and *Trp53* alleles confirms pure tumor cell lines lacking stromal contamination (Figure 2-5A). KPD and KPDO mice exhibit decreased Drp1 IHC intensity in individual tumors compared to KP (Figures 2.4A and 2.4B) while KPO and KPDO tumors exhibit no significant decrease in Opa1 levels (Figures 2.4C and 2.4D). Consistent with this, six of seven individually derived KPD tumor cell lines exhibit no detectable Drp1 by immunoblot (Figure 2-4E) while all seven independently derived KPO tumor cell lines retain lower, but detectable, expression of Opa1 (Figure 2-4F). Interestingly, six of nine KPDO cell lines demonstrate complete deletion of Opa1 *in vivo,* but only in cells that exhibit complete deletion of Drp1 (Figure 2-4G). Three additional KPDO cell lines retain expression of Opa1 with or without retained Drp1 expression. Consistent with these data, we detect a single floxed *Opa1* allele by PCR in six of seven KPO cell lines and two floxed alleles in the other (Figure 2-4H), indicating that a single copy of *Opa1* is sufficient for tumor development. In KPDO mice, six of nine tumor lines harbor homozygous recombined $Opa1^{\Delta}$ alleles while the others retain one or both $Opa1^{FL}$ alleles (Figure 2-4I). Together, these data suggest that mitochondrial fission is dispensable for KP LUAD development *in vivo*, and that Opa1 is essential in tumor cells with intact mitochondrial fission. Further, inactivation of mitochondrial fission permits Opa1-null tumor cell line isolation but not *in vivo* tumor development.

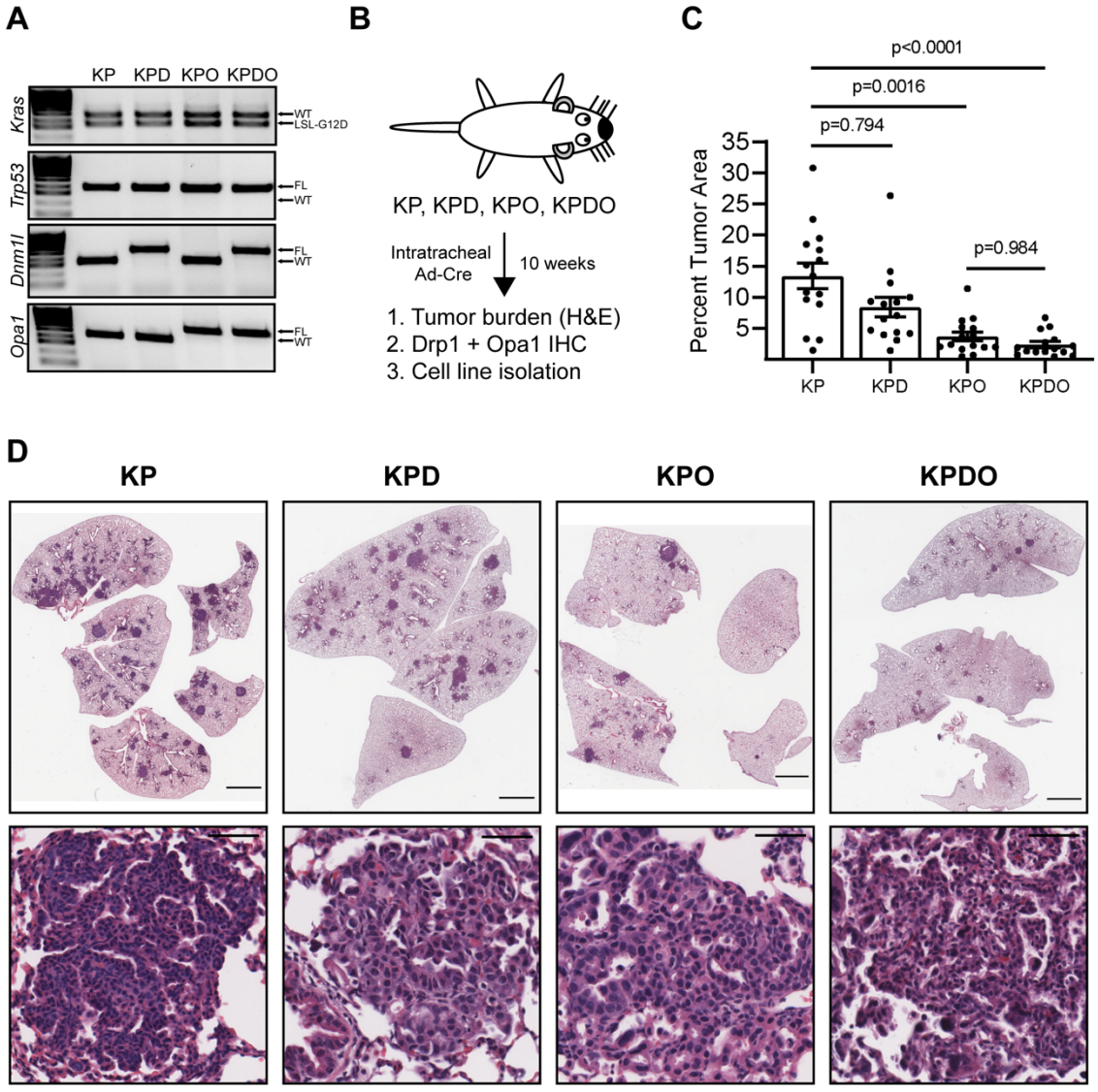

Figure 2-3. Deletion of Opa1, but not Drp1, inhibits KP LUAD development *in vivo*

A. PCR of *Kras, Trp53, Dnm1l,* and *Opa1* alleles in GEMM-enrolled mice

B. GEMM schematic and endpoints.

C. Tumor burden in individual GEMM mice. n=15 mice per genotype. Mean±SD. Kruskal-Wallis test + Dunn's multiple comparisons test.

D. Representative H&E-stained lungs and tumors in indicated genotypes. Scale = 2000 μm (lung), 50 μm (tumors).

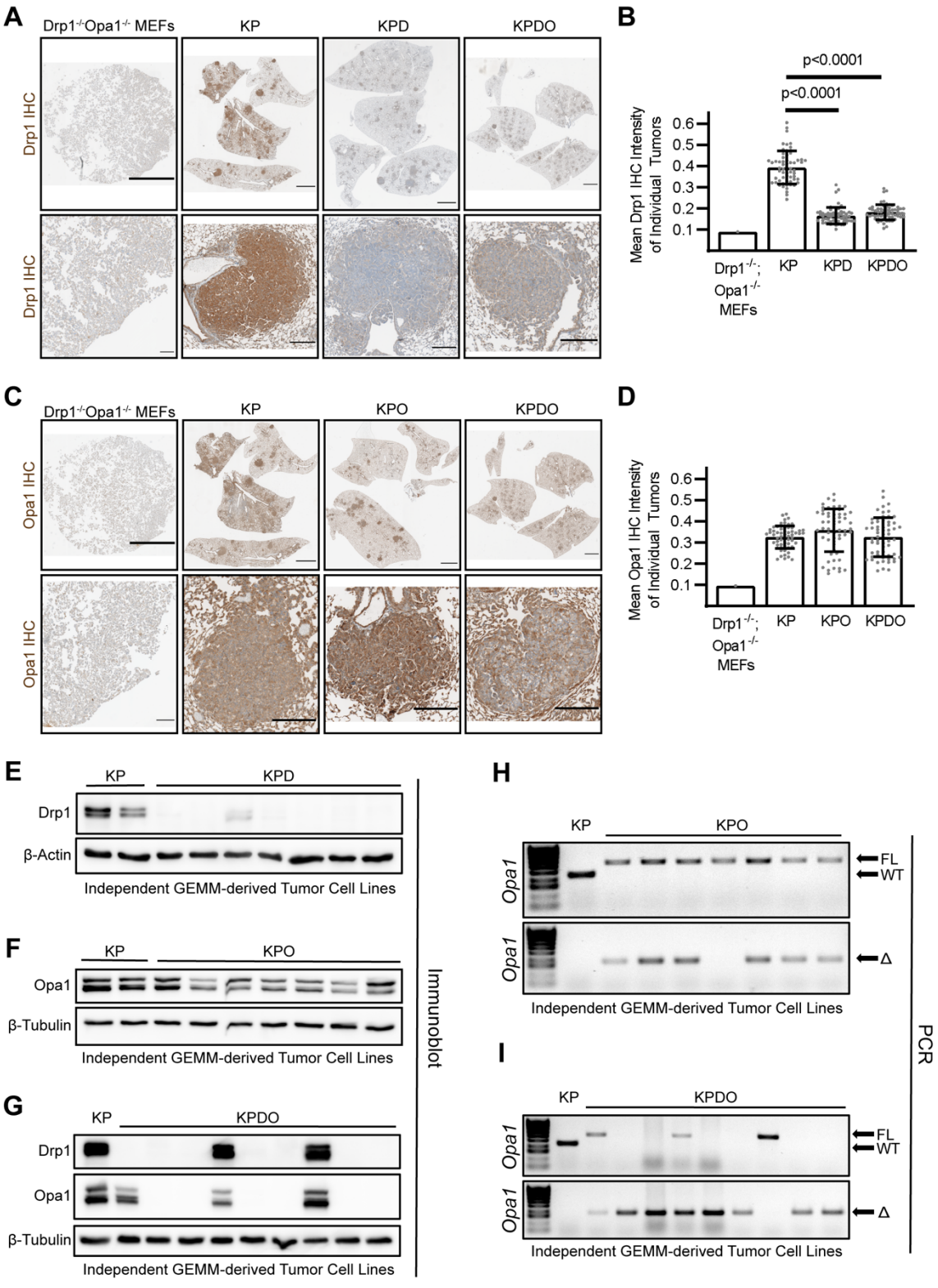
A
Drp1-/-Opa1-/- MEFs
KP
KPD
KPDO
Drp1 IHC
Drp1 IHC
B
p<0.0001
p<0.0001
Mean Drp1 IHC Intensity of Individual Tumors
0.6
0.5
0.4
0.3
0.2
0.1
Drp1-/-; Opa1-/- MEFs
KP
KPD
KPDO
C
Drp1-/-Opa1-/- MEFs
KP
KPO
KPDO
Opa1 IHC
Opa1 IHC
D
Mean Opa1 IHC Intensity of Individual Tumors
0.6
0.5
0.4
0.3
0.2
0.1
Drp1-/-; Opa1-/- MEFs
KP
KPO
KPDO
E
KP
KPD
Drp1
β-Actin
Independent GEMM-derived Tumor Cell Lines
F
KP
KPO
Opa1
β-Tubulin
Independent GEMM-derived Tumor Cell Lines
G
KP
KPDO
Drp1
Opa1
β-Tubulin
Independent GEMM-derived Tumor Cell Lines
Immunoblot
H
KP
KPO
Opa1
Opa1
FL
WT
Δ
Independent GEMM-derived Tumor Cell Lines
I
KP
KPDO
Opa1
Opa1
FL
WT
Δ
Independent GEMM-derived Tumor Cell Lines
PCR

Figure 2-4. Opa1, but not Drp1, is required for KP LUAD development

A. Representative Drp1 IHC on whole lung and tumors in indicated genotypes. KPDO MEFs are negative staining control. Scale = 2000 μm (lung), 200 μm (tumors).

B. Quantification of mean Drp1 DAB intensity of individual tumors in indicated genotypes. n=60 tumors per genotype. Kruskal-Wallis test + Dunn's multiple comparisons test.

C. Same as 3A, but Opa1 IHC.

D. Quantification of mean Opa1 DAB intensity of individual tumors in indicated genotypes. n=60 tumors per genotype.

E. Immunoblot of Drp1 in 2 KP and 7 KPD independently derived tumor cell lines.

F. Immunoblot of Opa1 in 2 KP and 7 KPO independently derived tumor cell lines.

G. Immunoblot of Drp1 and Opa1 in 1 KP and 9 KPDO independently derived tumor cell lines.

H. PCR of $Opa1^{FL}$ and $Opa1^{WT}$ alleles (top) and $Opa1^{\Delta}$ (recombined, bottom) in 1 KP and 7 independently derived KPO tumor cell lines.

I. Same as 3H, but in 1 KP and 9 independently derived KPDO tumor cell lines.

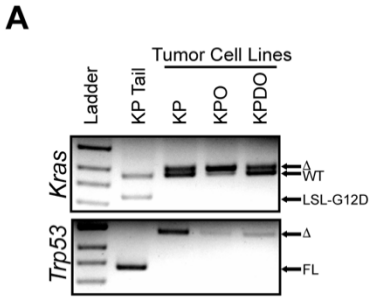

Figure 2-5. GEMM-derived LUAD cells demonstrate complete recombination of floxed *Kras* and *Trp53* alleles

A. *Kras* and *Trp53* PCR genotypes of KP mouse tail and one representative each of KP, KPO, and KPDO GEMM-derived LUAD cell lines. KP mouse tail demonstrates one wildtype (WT) and one LSL-G12D *Kras* allele and homozygous floxed (FL) *Trp53* alleles. All tumor cell lines demonstrate recombination (Δ) of the *Kras* LSL-G12D allele and both floxed *Trp53* alleles.

2.3.3 Opa1 is required to maintain mitochondrial NAD^+ regeneration

Opa1 regulates apoptosis, OXPHOS, and mitochondrial fusion. To understand what drives reduced tumor burden in KPO mice, we explored the consequences of Opa1 deletion *in vitro* using a KPO tumor cell line that retained both *Opa1*^{FL} alleles and thus is initially functionally KP. Infection of this cell line *in vitro* with AdCre, but not empty vector adenovirus (AdEV), deletes Opa1 (Figure 2-6A), whereas AdCre infection of a KP cell line has no effect on Opa1 expression (Figure 2-7A). Opa1 protein in KPO cells is almost completely undetectable three days after AdCre infection, which allows determination of the acute effects of Opa1 deletion. Expression of Drp1, VDAC and SDHA are not changed by Opa1 deletion indicating mitochondrial fission remains active and mitochondrial abundance is unaffected (Figure 2-6A).

As deletion of Opa1 has previously been reported to broadly sensitize cells to apoptosis [116, 180], we first assessed whether Opa1 deletion decreases cell viability by treating cells with established apoptosis inducers cisplatin or etoposide. Surprisingly, Opa1 deletion slightly increases relative viability of cisplatin- or etoposide-treated cells and does not alter the impact of these agents on cell accumulation (Figures 2.7B and 2.7C). Additionally, Opa1 deletion does not increase cisplatin- or etoposide-induced PARP cleavage (Figure 2-7D).

We next assessed whether Opa1 deletion inhibits tumor cell growth by inhibition of mitochondrial fusion. First, we examined mitochondrial morphology in AdEV- or AdCre-treated KPO cells and confirmed that Opa1 deletion causes mitochondrial hyperfragmentation (Figure 2-6B) as others have described [111, 116]. To determine if inhibition of fusion is sufficient to account for the effects of Opa1 deletion, we prevented fusion independently of Opa1 through CRISPR-mediated deletion of both Mfn1 and Mfn2.

Clonal Mfn1/2-targeted CRISPR cells demonstrate complete Mfn2 deletion and robust Mfn1 depletion compared to clonal control cells (Figure 2-7E). As expected, Mfn1/2 deletion causes fragmented mitochondrial morphology. However, it does not affect colony formation (Figures 2.7F and 2.7G). Together, these data suggest that Opa1 deletion does not inhibit tumor growth by inducing apoptosis or through inhibition of mitochondrial fusion.

Opa1 deletion impairs OXPHOS capacity in mouse fibroblasts [67, 111, 178, 179]. To test whether LUAD cells are similarly sensitive, we performed Seahorse mitochondrial stress tests and found that acute Opa1 deletion severely impairs basal and reserve oxygen consumption (OCR) in KPO cells (Figures 2.6C and 2.6D). This effect is not observed in KP cells and thus not due to AdCre infection itself (Figures 2.8A and 2.8B). We observe identical results in A549 cells following CRISPR-mediated Opa1 deletion (Figures 2.6E and 2.8C).

ETC dysfunction following Opa1 deletion decreases ATP synthesis in mouse fibroblasts [67, 68, 178]; however, recent evidence suggests that cancer cells primarily fulfill ATP requirements through glycolysis and instead require the ETC to couple electron flux to the oxidation of the pyrimidine precursor dihydroorotate (DHO) to orotate and NADH to NAD^+, a cofactor essential for oxidative biosynthesis [29, 31, 193, 203, 204]. We hypothesized that Opa1 deletion mediated ETC dysfunction impairs KP LUAD growth by inhibiting the ETC electron flux required for oxidation of DHO and NADH, and that mitochondrial ATP synthesis is dispensable. To determine which ETC functions are required in this model, we treated fusion-fission intact Opa1-expressing KPO cells with DMSO, oligomycin, rotenone, or CCCP (collectively ETCi) and measured cell accumulation. CCCP inactivates mitochondrial ATP synthesis through proton gradient dissipation, as confirmed by TMRE staining (Figure 2-8D), but leaves ETC electron flow intact (Figure 2-8E). Conversely,

rotenone and oligomycin diminish both mitochondrial ATP synthesis and ETC electron flux. Oligomycin and rotenone almost completely inhibit cellular accumulation compared to DMSO, while CCCP has no effect, indicating that ETC-mediated oxidation of electron carriers, but not mitochondrial ATP synthesis, is required for KP LUAD growth (Figure 2-6F). Notably, under seeding conditions almost identical to those used in ETCi experiments, Opa1 deletion phenocopies oligomycin/rotenone treatment, consistent with the effects of its deletion being due to inhibition of ETC function (Figure 2-6G).

To assess whether Opa1 deletion affects NAD^+ metabolism, we measured NAD^+/NADH and found that Opa1 deletion severely reduces this ratio, indicating dysfunction of NADH oxidation (Figure 2-6H). Impairment of ETC electron flux causes auxotrophy for pyruvate, which supports cytoplasmic NAD^+ regeneration through lactate dehydrogenase (LDH), and for uridine, which restores pyrimidine synthesis when DHO is unable to be oxidized [29, 31, 205]. To test whether Opa1 deletion inhibits KP LUAD colony formation by inhibition of pyrimidine synthesis, NAD^+ regeneration, or both, we treated cells with uridine alone and in combination with pyruvate and the alternative NAD^+-regenerating LDH substrate, alphaketobutyrate (AKB). Colony formation of Opa1-expressing cells is unaffected by treatment with uridine, pyruvate, or AKB (Figures 2.6I and 2.8F), indicating these cells meet metabolic demands for NAD^+ and uridine. Notably, pyruvate and AKB increase Opa1-null colony formation, whereas uridine has no effect either alone or with pyruvate or AKB (Figure 2-6I). These data suggest that Opa1 deletion impairs colony formation by inhibiting NAD^+ regeneration, but not pyrimidine synthesis. To determine whether Opa1 deletion sensitizes cells to inhibition of cytoplasmic NAD^+ regeneration, we measured viability of tumor cells treated with DMSO, the lactate dehydrogenase inhibitor GNE-140 [206], or the PDK inhibitor AZD7545 that activates PDH and drives pyruvate into mitochondria and away from lactate synthesis. We found Opa1-null cells demonstrate

decreased viability compared to Opa1-expressing cells when treated with GNE-140 or AZD7545 (Figure 2-8G) suggesting that Opa1 deletion induces increased reliance on cytoplasmic NAD^+ regeneration. Recent reports demonstrate that the critical and distal effect of inhibiting ETC-mediated NAD^+ regeneration is the inhibition of aspartate synthesis required for protein, RNA, and DNA synthesis [29, 31, 32, 204, 207]. Consistent with this, aspartate supplementation significantly increases colony formation of Opa1-null LUAD (Figure 2-6J). Together, these data indicate that Opa1 deletion inhibits KP LUAD by restricting ETC-mediated NAD^+ regeneration required for oxidative biosynthesis of metabolites including aspartate.

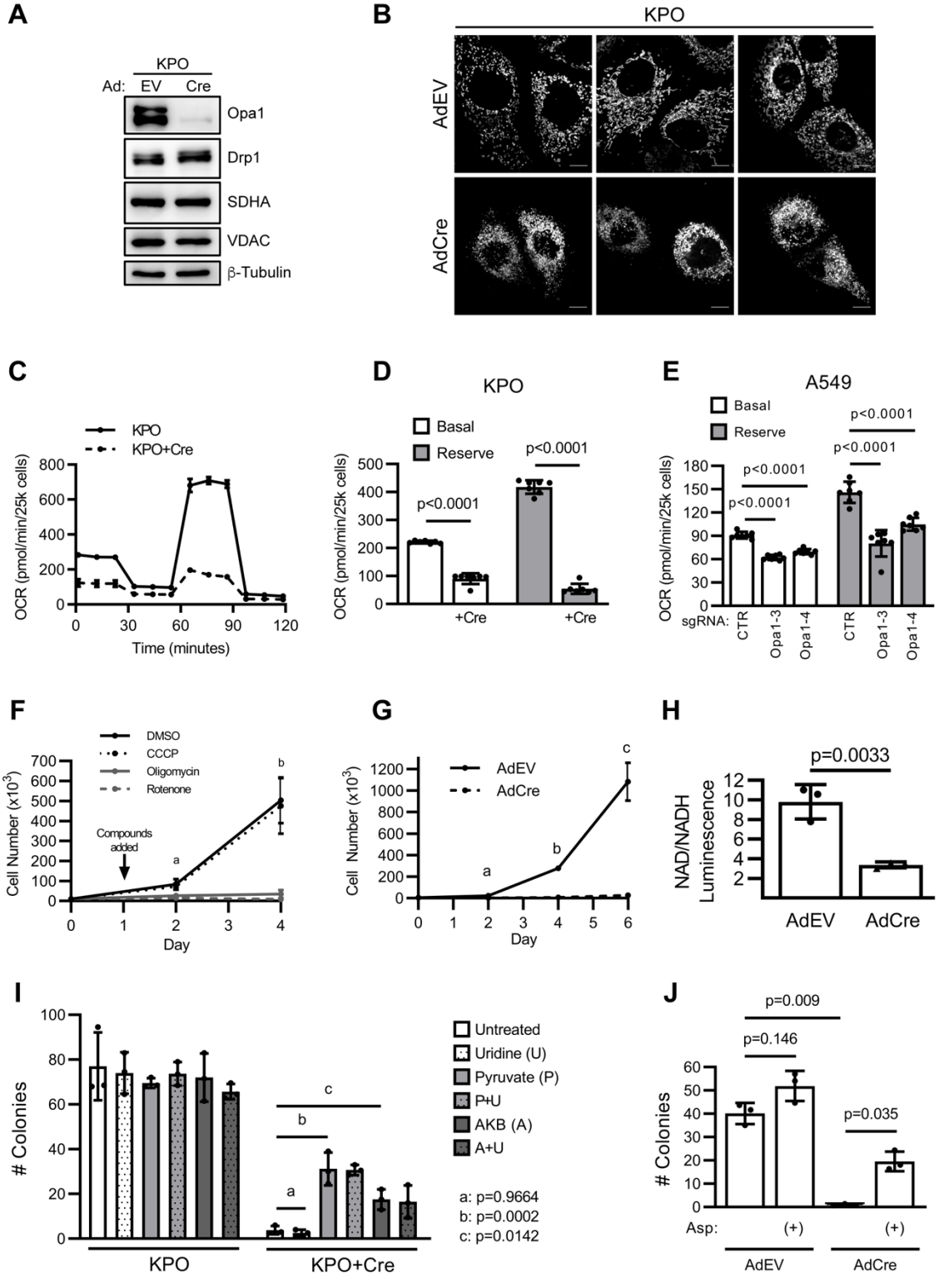
A
KPO
Ad: EV Cre
Opa1
Drp1
SDHA
VDAC
β-Tubulin
B
KPO
AdEV
AdCre
C
KPO
KPO+Cre
OCR (pmol/min/25k cells)
Time (minutes)
D
KPO
Basal
Reserve
p<0.0001
p<0.0001
OCR (pmol/min/25k cells)
+Cre
+Cre
E
A549
Basal
Reserve
p<0.0001
p<0.0001
p<0.0001
p<0.0001
OCR (pmol/min/25k cells)
sgRNA: CTR Opa1-3 Opa1-4 CTR Opa1-3 Opa1-4
F
DMSO
CCCP
Oligomycin
Rotenone
Compounds added
Cell Number (x10^3)
Day
G
AdEV
AdCre
Cell Number (x10^3)
Day
H
p=0.0033
NAD/NADH Luminescence
AdEV
AdCre
I
Colonies
Untreated
Uridine (U)
Pyruvate (P)
P+U
AKB (A)
A+U
a: p=0.9664
b: p=0.0002
c: p=0.0142
KPO
KPO+Cre
J
p=0.009
p=0.146
p=0.035
# Colonies
Asp: (+) (+)
AdEV
AdCre

Figure 2-6. Opa1 is required to maintain mitochondrial NAD^+ regeneration

A. Immunoblot of Opa1, Drp1, SDHA, and VDAC in AdEV- and AdCre-infected GEMM-derived KPO tumor cells.

B. Mitotracker Green-stained AdEV- or AdCre-infected KPO LUAD. Scale = 10 μm.

C. OCR of uninfected or AdCre-infected KPO. n=7 wells per cell condition. Mean±SD.

D. Basal and reserve OCR of uninfected or AdCre-infected KPO cells. n=7 wells per cell condition. Mean±SD. Student's T-test.

E. OCR of Opa1 A549 CRISPR cells. n=7 wells per cell condition. Mean±SD. One-way ANOVA + Dunnett's multiple comparisons test.

F. Cell accumulation of Opa1-expressing KPO cells treated with DMSO, oligomycin (10 nM), CCCP (250 nM), or rotenone (250 nM). n=3 independent experiments. Mean±SD. a:DMSO vs oligomycin/rotenone ($p<0.005$), DMSO vs CCCP ($p=0.781$), One-way ANOVA + Dunnett's multiple comparisons test. b:DMSO vs oligomycin/rotenone ($p<0.05$), DMSO vs CCCP ($p=0.989$), Welch ANOVA + Dunnett's T3 multiple comparisons test.

G. Cell accumulation of AdEV- or AdCre-infected KPO cells. a: $p=0.0041$, b: $p=0.0018$, c: $p=0.0091$. Welch's T-test.

H. NAD^+/NADH in AdEV- or AdCre-infected KPO cells. n=3 independent experiments. Mean±SD. Student's T-test.

I. Colony formation in uninfected or AdCre-infected KPO cells without treatment or treated with uridine (0.1 mg/mL), pyruvate (1 mM), alphaketobutyrate (AKB, 1 mM), or in combination. n=3 independent experiments. Mean±SD. One-way ANOVA + Dunnett's multiple comparisons test.

J. Colony formation in AdEV- or AdCre-infected KPO cells with or without aspartate (20 mM). Welch's ANOVA + Dunnett's T3 multiple comparisons test.

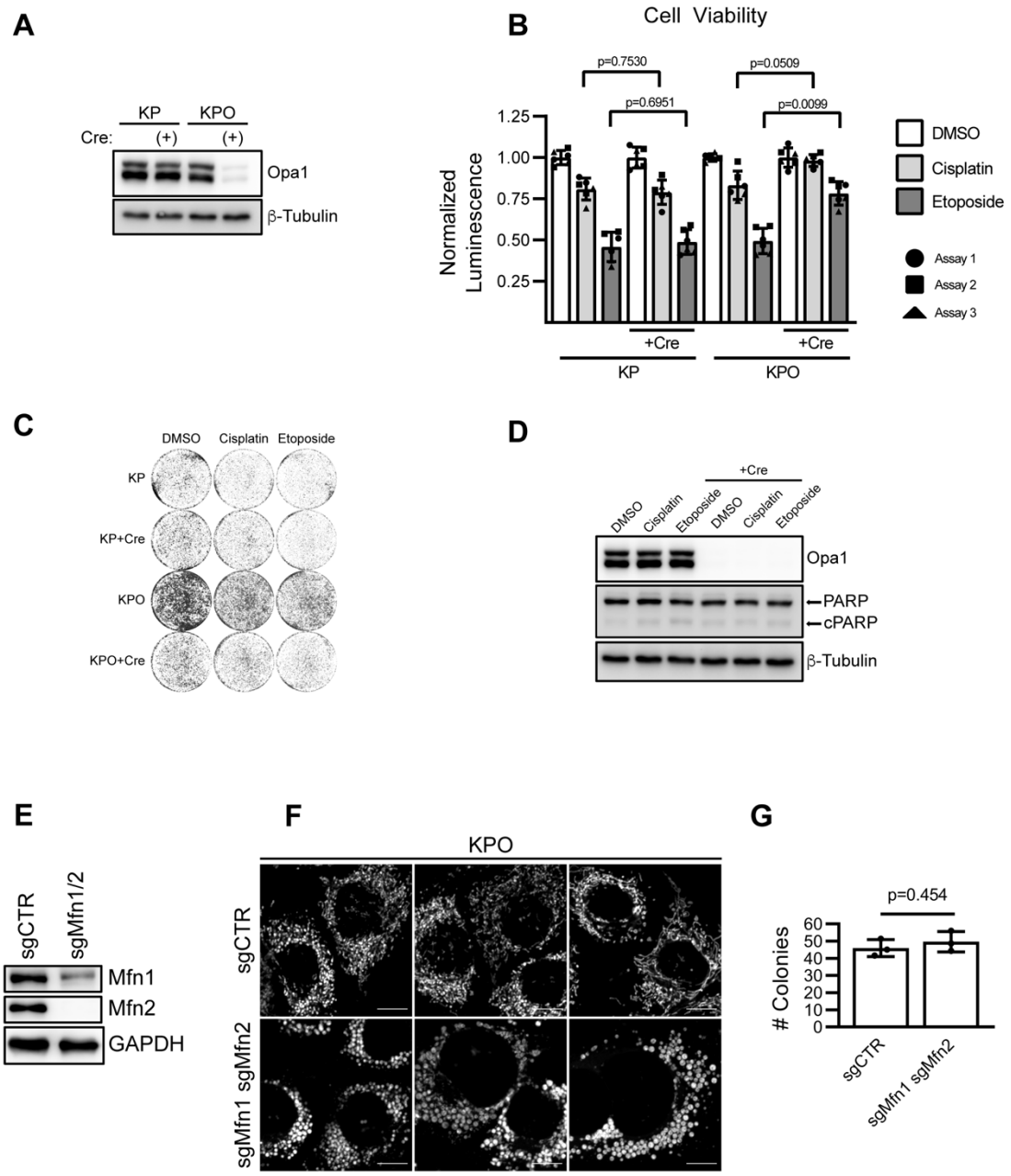
A
KP
KPO
Cre:
(+)
(+)
Opa1
β-Tubulin
B
Cell Viability
p=0.7530
p=0.6951
p=0.0509
p=0.0099
Normalized Luminescence
1.25
1.00
0.75
0.50
0.25
DMSO
Cisplatin
Etoposide
Assay 1
Assay 2
Assay 3
+Cre
+Cre
KP
KPO
C
DMSO
Cisplatin
Etoposide
KP
KP+Cre
KPO
KPO+Cre
D
+Cre
DMSO
Cisplatin
Etoposide
DMSO
Cisplatin
Etoposide
Opa1
PARP
cPARP
β-Tubulin
E
sgCTR
sgMfn1/2
Mfn1
Mfn2
GAPDH
F
KPO
sgCTR
sgMfn1 sgMfn2
G
p=0.454
# Colonies
60
50
40
30
20
10
0
sgCTR
sgMfn1 sgMfn2

Figure 2-7. Opa1 deletion does not inhibit LUAD growth by increasing apoptosis sensitivity or by inhibiting mitochondrial fusion

A. Immunoblot of Opa1 expression in uninfected or AdCre-infected GEMM-derived KP and KPO tumor cells.

B. CellTiter-Glo measurement of cell viability of uninfected or AdCre-infected KP and KPO tumor cells treated with DMSO, cisplatin (2 uM), or etoposide (2 uM) for 48 hours. All technical replicates from independent experiments are shown. Individual wells of drug-treated (non-DMSO) cells were normalized to the mean of the DMSO-treated wells within an individual experiment. Statistical analysis was performed on the mean of normalized values from individual experiments within treatment groups such that the sample size of each treatment group was equal to the number of independent experiments. n=3 independent experiments. Mean±SD. Student's T-test.

C. Crystal violet staining of uninfected or AdCre-infected KP and KPO tumor cells treated with DMSO, cisplatin (2 uM), or etoposide (2 uM) for 48 hours. Cells were seeded at 10,000 cells/12-well in 1 mL 10% FBS DMEM.

D. Immunoblot of Opa1 and PARP expression in uninfected or AdCre-infected KPO tumor cells treated with DMSO, cisplatin (2 uM), or etoposide (2 uM) for 48 hours.

E. Immunoblot of Mfn1 and Mfn2 expression in clonal control (sgCTR) or clonal Mfn1 and Mfn2 CRISPR (sgMfn1/Mfn2) KPO cells with no Cre.

F. Imaging of Mitotracker Green-stained control and Mfn1/2 CRISPR KPO cells. Scale bar = 10 μm.

G. Colony formation of control and Mfn1/2 CRISPR KPO cells. Mean±SD. Student's T-test.

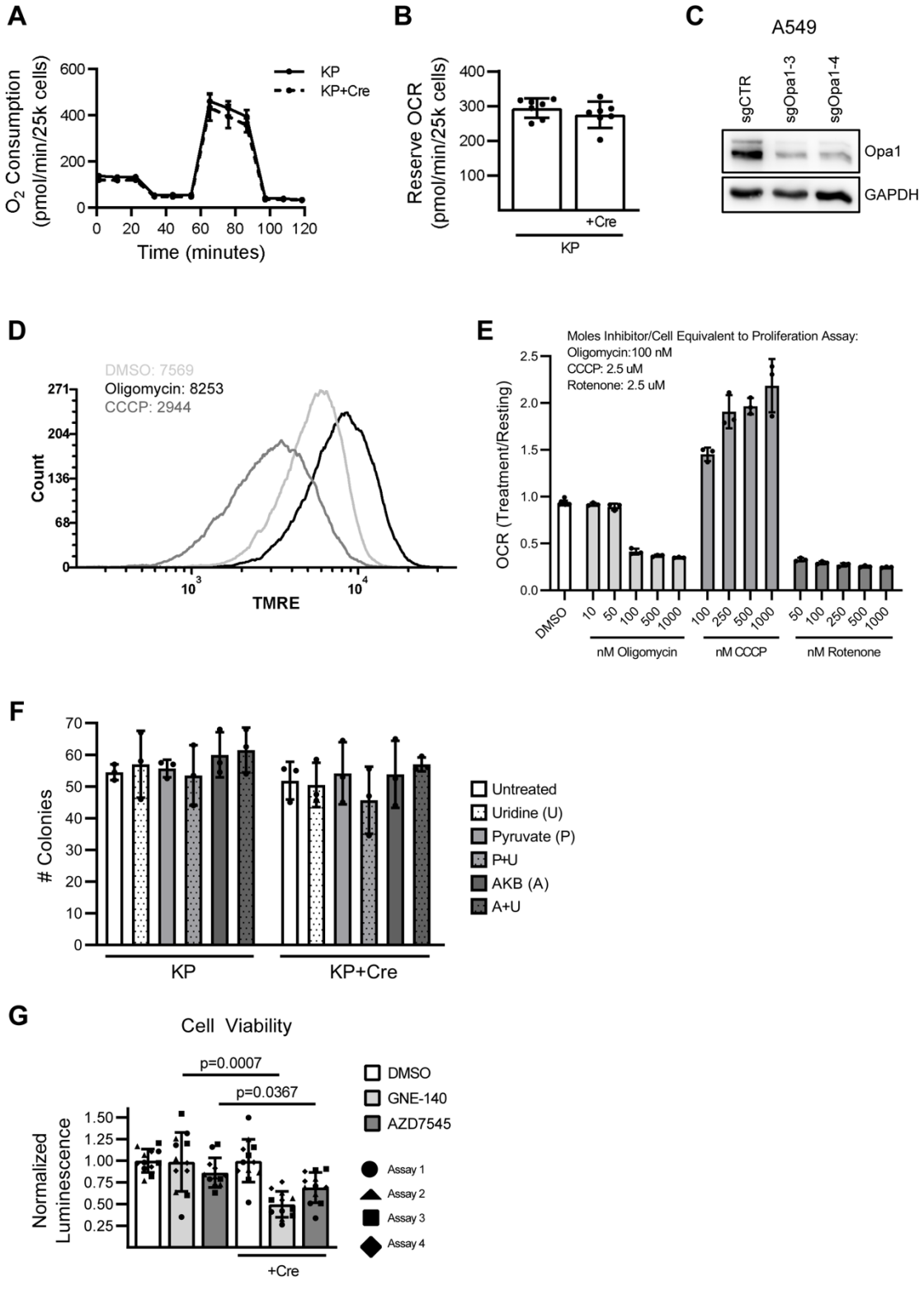
A
O_2 Consumption (pmol/min/25k cells)
600
400
200
0
0 20 40 60 80 100 120
Time (minutes)
KP
KP+Cre
B
Reserve OCR (pmol/min/25k cells)
400
300
200
100
+Cre
KP
C
A549
sgCTR
sgOpa1-3
sgOpa1-4
Opa1
GAPDH
D
DMSO: 7569
Oligomycin: 8253
CCCP: 2944
Count
271
204
136
68
0
10^3
10^4
TMRE
E
Moles Inhibitor/Cell Equivalent to Proliferation Assay:
Oligomycin:100 nM
CCCP: 2.5 uM
Rotenone: 2.5 uM
OCR (Treatment/Resting)
2.5
2.0
1.5
1.0
0.5
0.0
DMSO
10 50 100 500 1000
nM Oligomycin
100 250 500 1000
nM CCCP
50 100 250 500 1000
nM Rotenone
F
Colonies
70
60
50
40
30
20
10
0
KP
KP+Cre
Untreated
Uridine (U)
Pyruvate (P)
P+U
AKB (A)
A+U
G
Cell Viability
p=0.0007
p=0.0367
Normalized Luminescence
1.50
1.25
1.00
0.75
0.50
0.25
+Cre
DMSO
GNE-140
AZD7545
Assay 1
Assay 2
Assay 3
Assay 4

Figure 2-8. Opa1 deletion inhibits LUAD respiration and sensitizes tumor cells to pharmacologic inhibition of cytoplasmic NAD^+ regeneration.

A. OCR of untreated or AdCre-infected KP cells. n=7 wells per cell condition. Mean±SD.

B. Reserve OCR of untreated or AdCre-infected KP cells. n=7 wells per cell condition. Mean±SD.

C. Immunoblot of Opa1 expression in control (sgCTR) or two independent Opa1 CRISPR A549 cells.

D. TMRE flow cytometry of uninfected KPO tumor cells treated with equal number of moles oligomycin/CCCP per cell as the cellular accumulation experiment in Figure 4F. Cells were gated solely on live cell population (FSCxSSC). Values indicate TMRE median fluorescence intensity per group. n>20,000 cells per group.

E. Treated/resting OCR of uninfected KPO tumor cells with indicated concentrations of compounds. n=3 wells per condition. Mean±SD.

F. Colony formation in uninfected or AdCre-infected KP cells without treatment or treated with uridine (0.1 mg/mL), pyruvate (1 mM), alphaketobutyrate (AKB, 1 mM), or in combination as indicated. n=3 independent experiments.

G. CellTiter-Glo measurement of cell viability in uninfected or AdCre-infected KPO cells treated with DMSO, the lactate dehydrogenase inhibitor GNE-140 (5 uM), or the PDK1 inhibitor AZD7545 (5 uM) for 48 hours. All technical replicates from independent experiments are shown. Individual wells of drug-treated (non-DMSO) cells were normalized to the mean of the DMSO-treated wells within an individual experiment. Statistical analysis was performed on the mean of normalized values from individual experiments within treatment groups such that the sample size of each treatment group was equal to the number of independent experiments. n=4 independent experiments. Mean±SD. Student's T-test.

2.3.4 Drp1 activity drives Opa1 deletion-mediated ETC dysfunction

The effect of Opa1 deletion on KP LUAD colony formation is Drp1-dependent (Figures 2.1H and 2.1I). Although Drp1 deletion does not rescue *in vivo* tumor growth following Opa1 deletion, we isolated multiple KPDO tumor cell lines with complete *in vivo* deletion of both Opa1 and Drp1, but not a single KPO cell line that completely deleted Opa1 *in vivo*. This suggests an advantage of inactivating fission in the context of Opa1 deletion. To test whether co-deletion of Drp1 and Opa1 in KP LUAD affects ETC function and NAD^+ regeneration, we utilized a KPDO cell line that retained homozygous $Dnm1l^{FL}$ and $Opa1^{FL}$ alleles and thus is initially functionally KP. AdCre infection of this cell line deletes Drp1 and Opa1 within three days of infection (Figure 2-9A). AdEV- and AdCre-treated cells both demonstrate mixed mitochondrial morphology and while some AdCre cells demonstrate perinuclear mitochondrial aggregation (Figure 2-9B), they do not demonstrate the hyper-fragmented morphology observed in AdCre-infected KPO cells (Figure 2-6B). Notably, basal and reserve OCR are unaffected by simultaneous deletion of Drp1 and Opa1 (Figures 2.9C and 2.9D). Further, NAD^+/NADH ratio is unaffected by co-deletion of Drp1 and Opa1 (Figure 2-9E) confirming that the effects of Opa1 deletion on ETC function and NAD^+ regeneration require Drp1.

Next, we assessed whether ETC function of KPDO LUAD cells with simultaneous Drp1 and Opa1 deletion is sensitive to reintroduction of wildtype mouse $mDrp1^{WT}$ or the GTPase-inactive and fission-defective mutant $mDrp1^{K38A}$. We introduced doxycycline-inducible empty vector (EV), $mDrp1^{WT}$, or $mDrp1^{K38A}$ into KPDO+AdCre cells (Figure 2-9F) and imaged mitochondria (Figure 2-10A). EV-expressing KPDO+AdCre cells demonstrate mixed mitochondrial morphology with perinuclear aggregates, as observed in KPDO+AdCre cells, whereas $mDrp1^{WT}$-expressing cells demonstrate mitochondrial hyperfragmentation similar to KPO+AdCre cells. $mDrp1^{K38A}$-expressing KPDO+AdCre

cells demonstrate mixed morphology and perinuclear aggregates similar to EV-expressing cells, suggesting that fission is inactive in these cells. Expression of $mDrp1^{WT}$ decreases basal and reserve OCR in KPDO+AdCre cells, whereas expression of $mDrp1^{K38A}$ does not (Figures 2.9G and 2.9H). As an additional approach, we constitutively expressed luciferase, $mDrp1^{WT}$, or $mDrp1^{K38A}$ in a separate KPDO cell line that retained Opa1 but deleted Drp1 *in vivo* and found that expression of $mDrp1^{WT}$, but not EV or $mDrp1^{K38A}$, inhibits colony formation (Figure 2-10B). As a third approach, we generated control (sgCTR) and Drp1-targeted KPO CRISPR cells to establish KP, KPO, KPD, and KPDO conditions upon AdCre infection (Figure 2-9I). A clonal control cell line demonstrates mixed mitochondrial morphology whereas two independent sgDrp1 clones demonstrate complete mitochondrial tubulation, confirming loss of mitochondrial fission (Figure 2-10C). As expected, Opa1 deletion in sgCTR cells significantly decreases basal and reserve OCR, and Drp1 deletion rescues this phenotype (Figure 2-9J and S5D), although more modestly than in KPDO cells with simultaneous Cre-mediated Opa1 and Drp1 deletion. Additionally, acute Drp1 deletion alone mildly decreases OCR. Collectively, these data suggest that mitochondrial fission mediates the effects of Opa1 deletion on ETC function, NAD^+ regeneration, and colony formation.

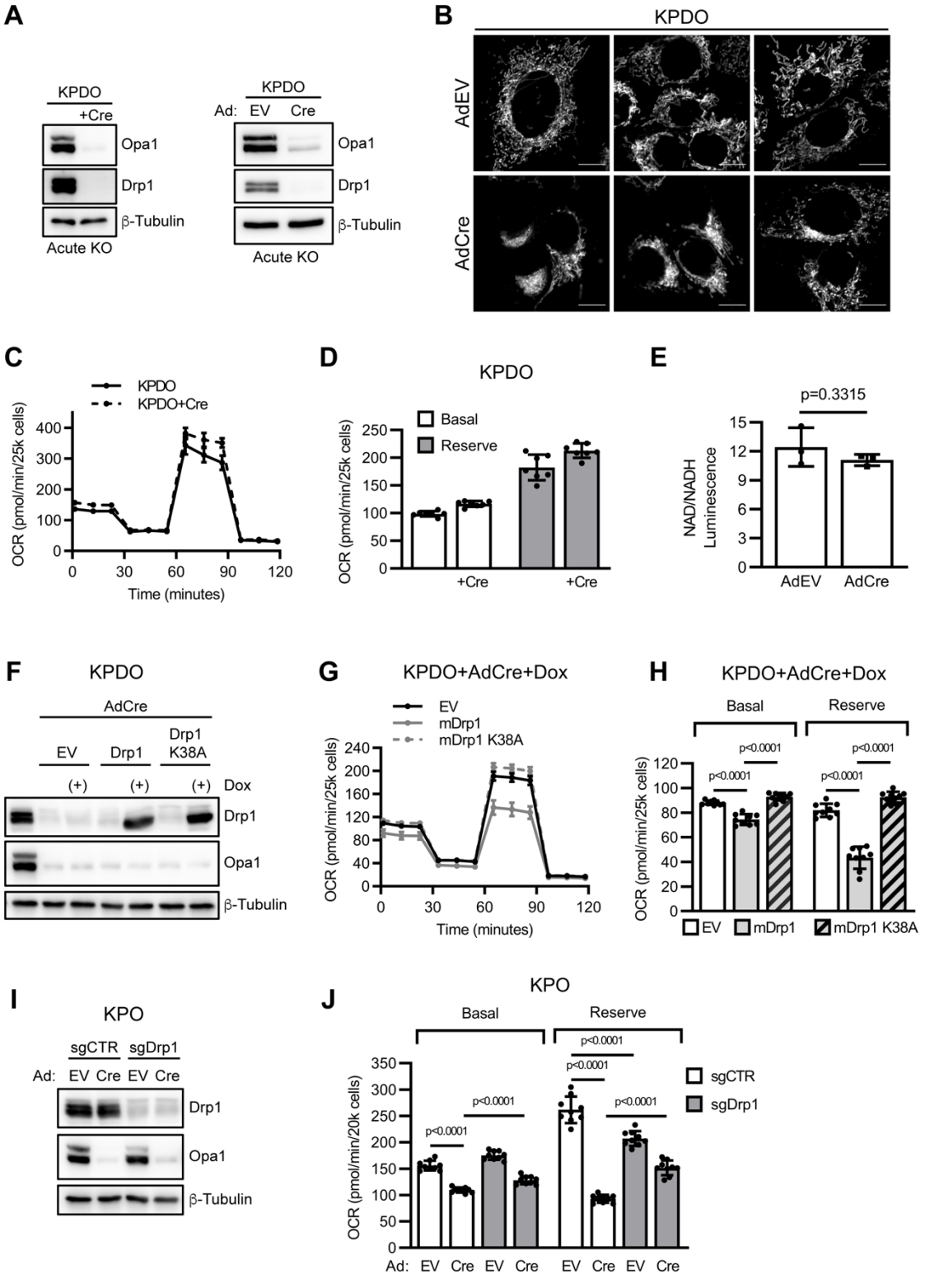
A
KPDO
+Cre
Opa1
Drp1
β-Tubulin
Acute KO
KPDO
Ad: EV Cre
Opa1
Drp1
β-Tubulin
Acute KO
B
KPDO
AdEV
AdCre
C
KPDO
KPDO+Cre
OCR (pmol/min/25k cells)
Time (minutes)
D
KPDO
Basal
Reserve
OCR (pmol/min/25k cells)
+Cre
+Cre
E
p=0.3315
NAD/NADH Luminescence
AdEV
AdCre
F
KPDO
AdCre
EV
Drp1
Drp1 K38A
(+) (+) (+) Dox
Drp1
Opa1
β-Tubulin
G
KPDO+AdCre+Dox
EV
mDrp1
mDrp1 K38A
OCR (pmol/min/25k cells)
Time (minutes)
H
KPDO+AdCre+Dox
Basal
Reserve
p<0.0001
OCR (pmol/min/25k cells)
EV
mDrp1
mDrp1 K38A
I
KPO
sgCTR sgDrp1
Ad: EV Cre EV Cre
Drp1
Opa1
β-Tubulin
J
KPO
Basal
Reserve
p<0.0001
OCR (pmol/min/20k cells)
sgCTR
sgDrp1
Ad: EV Cre EV Cre EV Cre EV Cre

Figure 2-9. Drp1 activity drives Opa1 deletion-mediated ETC dysfunction

A. Immunoblot of Drp1 and Opa1 in untreated and AdCre-infected KPDO cells (left), and AdEV- or AdCre-infected KPDO (right).

B. Mitotracker Green-stained AdEV- or AdCre-infected KPDO cells. Scale = 10 μm.

C. OCR of untreated or AdCre-infected KPDO cells. n=7 wells per cell condition. Mean±SD.

D. Basal and reserve OCR of untreated or AdCre-infected KPDO cells. n=7 wells per condition. Mean±SD.

E. NAD^+/NADH in AdEV- or AdCre-infected KPDO cells. n=3 independent experiments. Mean±SD. Student's T-test.

F. Immunoblot of Drp1 and Opa1 in uninfected or AdCre-infected KPDO cells with doxycycline-inducible empty vector (EV), wildtype mouse Drp1 (mDrp1), or GTPase-inactive fission-defective $mDrp1^{K38A}$.

G. OCR of AdCre-infected and doxycycline-induced KPDO cells. n=9 wells per cell condition. Mean±SD.

H. Basal and reserve OCR of AdCre-infected and doxycycline-induced KPDO cells. n=9 wells per condition. Mean±SD. One-way ANOVA + Sidak's multiple comparisons test.

I. Immunoblot of Drp1 and Opa1 in mixed-population AdEV- or AdCre-infected control (sgCTR) and sgDrp1 KPO CRISPR cells.

J. Basal and reserve OCR of mixed-population AdEV- or AdCre-infected KPO sgCTR or sgDrp1 CRISPR cells. n=9 wells per condition. Mean±SD. One-way ANOVA + Sidak's multiple comparisons test.

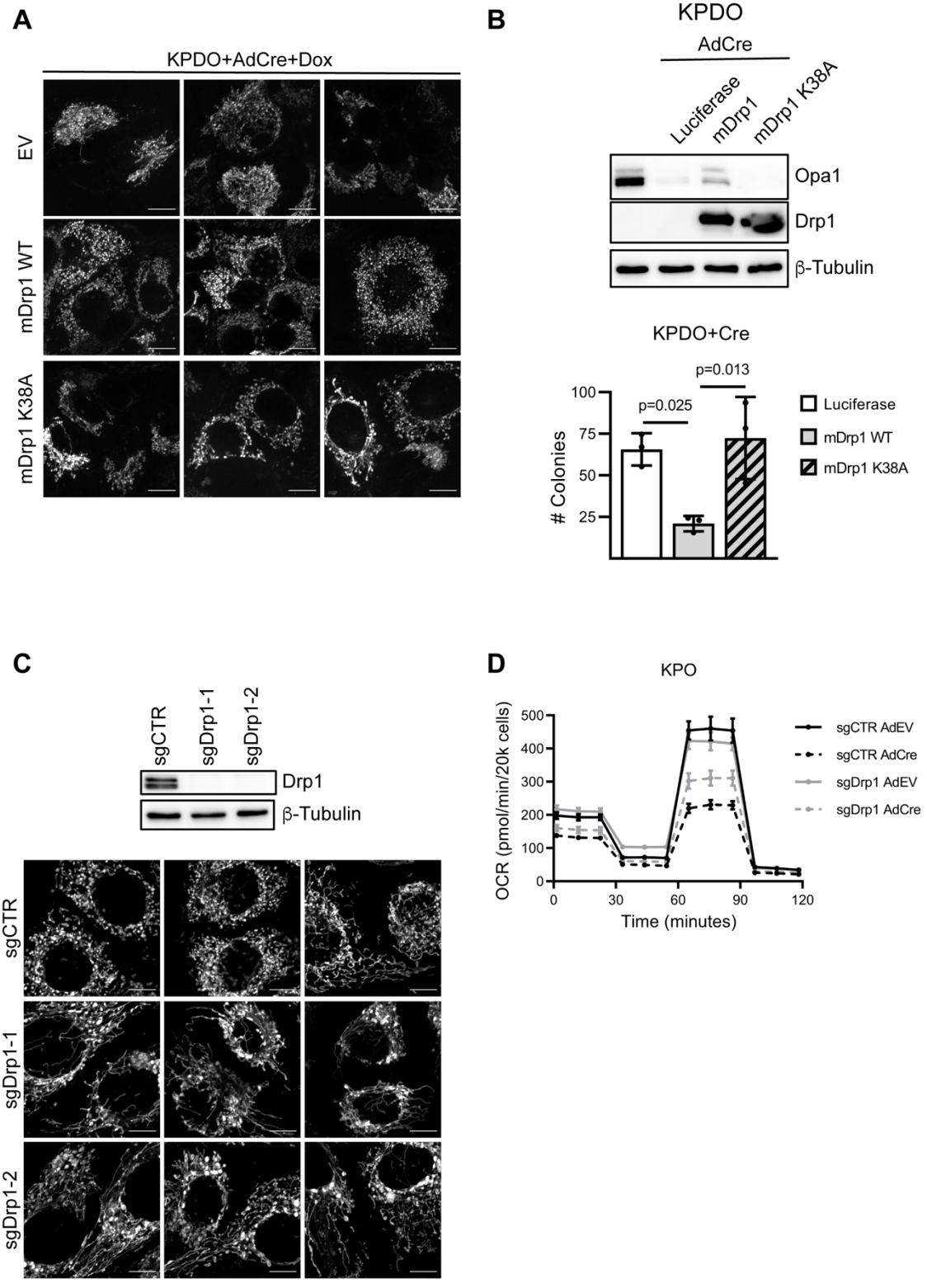
A
KPDO+AdCre+Dox
EV
mDrp1 WT
mDrp1 K38A
B
KPDO
AdCre
Luciferase
mDrp1
mDrp1 K38A
Opa1
Drp1
β-Tubulin
KPDO+Cre
p=0.025
p=0.013
# Colonies
100
75
50
25
Luciferase
mDrp1 WT
mDrp1 K38A
C
sgCTR
sgDrp1-1
sgDrp1-2
Drp1
β-Tubulin
sgCTR
sgDrp1-1
sgDrp1-2
D
KPO
OCR (pmol/min/20k cells)
500
400
300
200
100
0
0
30
60
90
120
Time (minutes)
sgCTR AdEV
sgCTR AdCre
sgDrp1 AdEV
sgDrp1 AdCre

Figure 2-10. Assessment of LUAD mitochondrial morphology and colony formation under Opa1 and/or Drp1 deletion

A. Imaging of Mitotracker Green-stained AdCre-infected KPDO LUAD with doxycycline-induced empty vector (EV), wildtype mouse Drp1 (mDrp1 WT), or GTPase-inactive and fission-defective mDrp1 K38A. Scale bar = 10 μm.

B. Immunoblot of Drp1 and Opa1 expression and colony formation in a KPDO LUAD tumor cell line that deleted Drp1 and retained Opa1 in vivo and was transduced to constitutively express luciferase or mDrp1 WT or K38A.

C. Immunoblot of Drp1 expression and Mitotracker Green imaging in one sgCTR and two sgDrp1 KPO CRISPR clonal cell lines. Scale bar = 10 μm.

D. Seahorse OCR curves of AdEV- or AdCre-infected mixed-population CRISPR KPO cells.

2.3.5 Drp1 mediates ETC disassembly and dysmorphic cristae from Opa1 deletion

The ETC is embedded in the inner mitochondrial membrane (IMM) and its function is dependent on cristae morphology [67]. Although Opa1 is a key regulator of cristae remodeling [110, 111, 116, 180], its exact function in this context is unclear. The role of Drp1 in cristae remodeling is also unclear, but fission promotes apoptotic cristae disorganization [93]. We hypothesized that Drp1 disrupts cristae during steady-state mitochondrial dynamics, not only during apoptosis, and that Opa1 reorganizes cristae following fission events.

To assess how Opa1 deletion affects ETC function and cristae homeostasis in the presence and absence of Drp1, we used KPO and KPDO tumor cells that delete retained floxed alleles following *in vitro* AdCre infection (Figure 2-11A). Since we observed a decrease in NAD^+/NADH in Opa1-deleted cells expressing Drp1, we assessed assembly of ETC complexes and the activity of ETC complex I, which oxidizes NADH to NAD^+. Notably, AdCre-infected KPO cells, but not KPDO cells, exhibit decreased abundance of multiple assembled ETC complexes visualized by clear-native PAGE (cnPAGE) analysis of mitochondrial extracts (Figure 2-11B). Further, Opa1 deletion, but not simultaneous Opa1 and Drp1 deletion decreases complex I activity (Figures 2.11C and 2.11D). Equal loading of mitochondrial isolates was confirmed by immunoblot analysis of SDHA and VDAC (Figure 2-11E). These data suggest that Drp1-expressing cells require Opa1 to maintain ETC assembly and complex I function and that cells lacking Drp1 preserve functional ETC complexes in the absence of Opa1.

Opa1 disruption depletes mitochondrial DNA (mtDNA) and disrupts cristae morphology [111, 114, 116]. We reasoned that either depletion of mtDNA-encoded ETC subunits or disrupted cristae could affect ETC assembly and function following acute Opa1 deletion.

We therefore analyzed cristae structure and mtDNA abundance in AdEV- or AdCre-infected KPO and KPDO cells. Transmission electron microscopy (TEM) revealed that lamellar cristae, in which the cristae membrane contacts the inner boundary membrane (IBM), are abundant in the mitochondria of Opa1-expressing cells. Opa1 deletion decreases the proportion of mitochondria with lamellar cristae and increases the proportion of mitochondria with tubular or no discernable cristae, but this effect is not observed following co-deletion of Opa1 and Drp1 (Figures 2.11F-H and 2.12A). We next assessed whether Opa1 deletion affects abundance of mtDNA relative to nuclear DNA by measuring levels of mtDNA genes *ND1* and *16S* and the nuclear gene *HK2* by quantitative PCR. Acute Opa1 deletion reduces abundance of mtDNA to two-thirds that of Opa1-expressing cells, but not if Drp1 is also deleted (Figures 2.11I and 2.11J); however, the impact of acute Opa1 deletion on global mtDNA-encoded ETC protein abundance is uncertain, especially on acute gene deletion timescales. These data suggest that at steady state, mitochondrial fission drives dysmorphic cristae, mtDNA loss, and decreased ETC function if unopposed by Opa1.

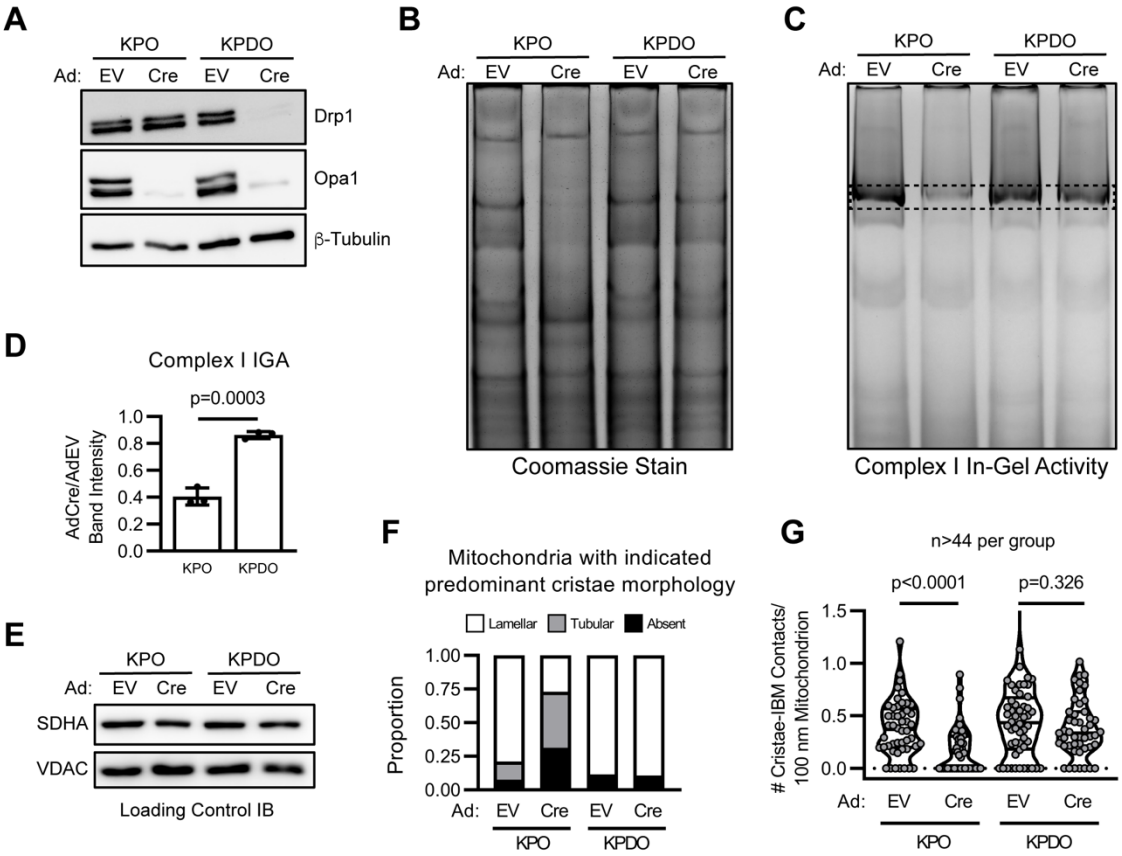
A
KPO
KPDO
Ad: EV Cre EV Cre
Drp1
Opa1
β-Tubulin
B
KPO
KPDO
Ad: EV Cre EV Cre
Coomassie Stain
C
KPO
KPDO
Ad: EV Cre EV Cre
Complex I In-Gel Activity
D
Complex I IGA
p=0.0003
AdCre/AdEV Band Intensity
1.0
0.8
0.6
0.4
0.2
0.0
KPO
KPDO
E
KPO
KPDO
Ad: EV Cre EV Cre
SDHA
VDAC
Loading Control IB
F
Mitochondria with indicated predominant cristae morphology
Lamellar
Tubular
Absent
Proportion
1.00
0.75
0.50
0.25
0.00
Ad: EV Cre EV Cre
KPO
KPDO
G
n>44 per group
p<0.0001
p=0.326
# Cristae-IBM Contacts/ 100 nm Mitochondrion
1.5
1.0
0.5
0.0
Ad: EV Cre EV Cre
KPO
KPDO
H
KPO
KPDO
AdEV
AdCre
AdEV
AdCre
I
KPO
p=0.0394
p=0.0045
ND1
16S
mtDNA/HK2
700
600
500
400
300
200
100
0
Ad: EV Cre EV Cre
J
KPDO
p=0.655
p=0.528
ND1
16S
mtDNA/HK2
1400
1200
1000
800
600
400
200
0
Ad: EV Cre EV Cre

Figure 2-11. Drp1 mediates ETC disassembly and dysmorphic cristae following Opa1 knockout

A. Immunoblot of Drp1 and Opa1 in AdEV- and AdCre-infected KPO and KPDO cells.

B. Coomassie-stained clear native PAGE of mitochondrial isolates from AdEV- or AdCre-infected KPO and KPDO cells. n= 3 independent experiments.

C. Clear native PAGE + complex I in-gel activity (IGA) assay of mitochondrial isolates from AdEV- or AdCre-infected KPO and KPDO cells. n= 3 independent experiments.

D. Quantification of complex I IGA assay intensity. n=3 independent experiments. Mean±SD. Student's T-test.

E. Immunoblot of SDHA and VDAC in native PAGE samples.

F. Transmission electron microscopy (TEM) quantitation of dominant cristae morphology (lamellar, tubular, or absent) in individual mitochondria from AdEV- or AdCre-treated KPO and KPDO cells.

G. TEM quantitation of number cristae contacting the inner boundary membrane (IBM) per 100 nm per mitochondrion in AdEV- or AdCre-treated KPO and KPDO cells. n>44 mitochondria per condition. Violin plot shows quartiles and median. Mann-Whitney test.

H. Representative TEM images in AdEmpty- or AdCre-infected KPO and KPDO cells. Magnification = 30k. Scale = 200 nm. See also Figure S1.

I. Quantitative PCR abundance of mitochondrial genes *ND1* and *16S* versus nuclear gene *HK2* in AdEV- or AdCre-treated KPO cells. n=3 independent experiments. Mean±SD. Student's T-test.

J. Same as 6I, but in KPDO cells.

A

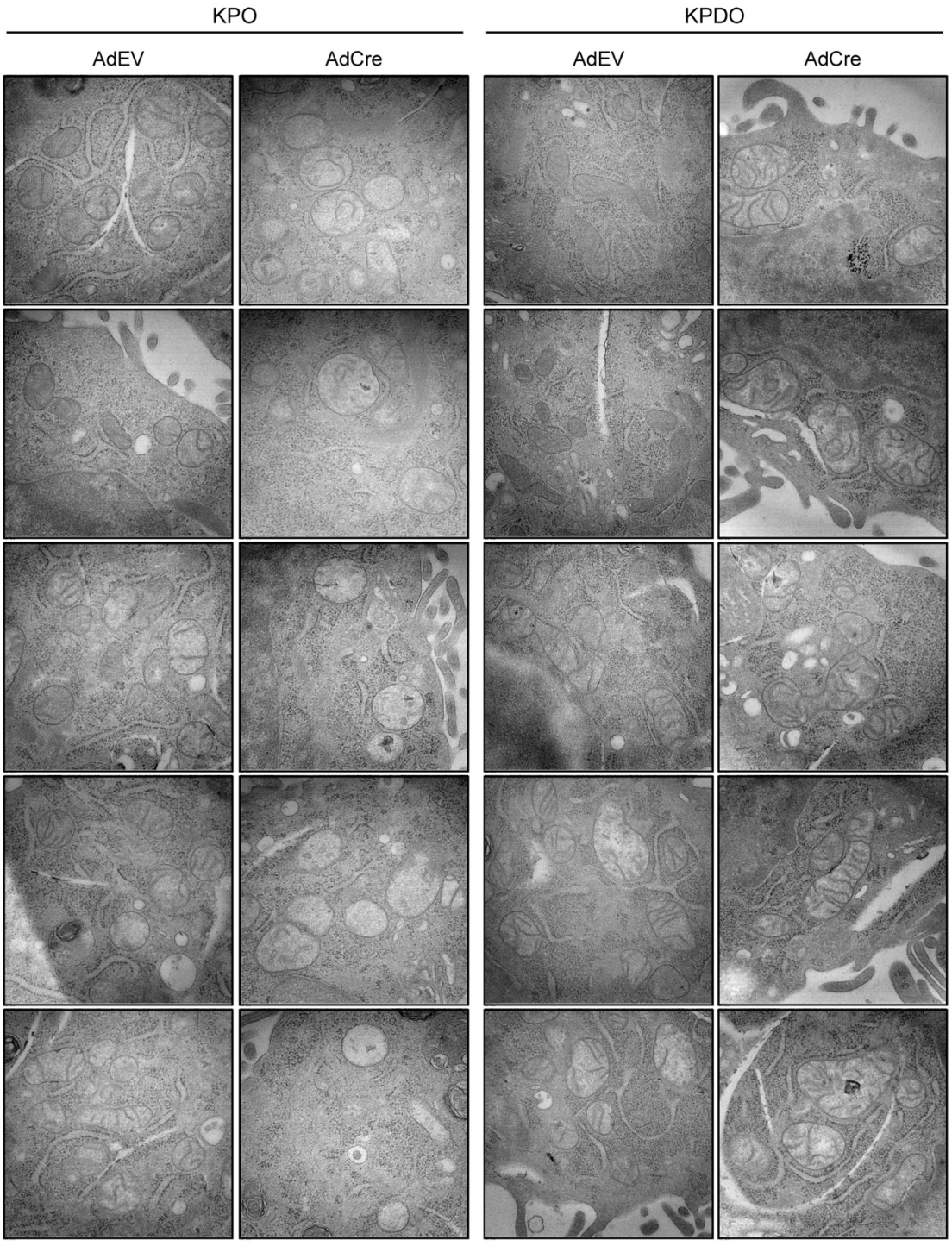

Figure 2-12. Opa1 deletion impairs mitochondrial cristae morphology in a Drp1-dependent manner

A. Additional representative TEM images of mitochondria and cristae morphology in AdEV- or AdCre-infected KPO and KPDO tumor cells. Magnification = 30k. Scale bar = 200 nm.

2.3.6 Chronic inhibition of mitochondrial dynamics inhibits LUAD ETC function

Our results demonstrate that the effects of acute Opa1 deletion are mediated by unopposed mitochondrial fission; however, that simultaneous Drp1 deletion rescues colony formation, ETC assembly and function, and cristae morphology *in vitro,* but not tumor development *in vivo,* suggests that additional unidentified factors influence the sensitivity of *in vivo* tumor development to mitochondrial dynamics disruption. Two testable possibilities for this discrepancy are the tumor cell environment and the timing of gene deletion.

Recent work demonstrated that environment affects tumor metabolism, including that of KRas-mutant lung adenocarcinoma [40, 208], prompting development of media that resembles human plasma [19, 209]. These media do not perfectly recapitulate the microenvironment of mouse KP LUAD because the tumor microenvironment differs from mouse plasma [38] and mouse plasma differs from human plasma [209]; however, they likely model the *in vivo* environment better than high-glucose DMEM. To assess if more-physiologic media affects the rescue of Opa1 deletion by simultaneous Drp1 deletion, we performed colony formation and NAD^+/NADH assays using KPDO cells (Figure 2-9A) in human plasma-like medium (HPLM). We found that simultaneous Drp1 and Opa1 deletion in HPLM results in a mild decrease in NAD^+/NADH (Figure 2-13A) but does not affect colony formation (Figure 2-13B). We also found that re-expression of $mDrp1^{WT}$ decreases NAD^+/NADH compared to EV- or $mDrp1^{K38A}$-expressing cells (Figure 2-13C), indicating that fission activity promotes a decrease in ETC function in Opa1-depleted cells even in more-physiologic media conditions. These data suggest that differences in extracellular metabolite availability likely do not explain the discrepancy between the effects of Drp1 and Opa1 co-deletion on *in vitro* colony formation versus *in vivo* tumor development.

Another distinction between colony formation and the GEMM is the time elapsed between gene deletion and experimental endpoint. We purposefully assessed *in vitro* phenotypes within 1 week of gene deletion to capture acute interactions between Drp1 and Opa1. We assessed GEMM tumor burden at 10 weeks post-initiation to allow enough time for adenocarcinoma-grade lesion development and to maximize assay sensitivity to genetic disruptions that affect tumor development. GEMM tumor burden may therefore reflect both acute and chronic effects of gene deletion due to the ten-fold increase in dynamics disruption time compared to *in vitro* systems. To assess whether chronic disruption of mitochondrial dynamics affects ETC function, we assayed OCR in three independent KP and three independent KPDO cell lines that completely deleted Opa1 and Drp1 *in vivo* (Figure 2-13D). KPDO cells with *in vivo* Drp1 and Opa1 deletion demonstrate significantly decreased OCR, indicating that ETC function is inhibited under conditions of chronic Drp1 and Opa1 deletion (Figures 2.13E and 2.13F). This suggests either that Drp1 deletion leads to loss of ETC function over time, independent of Opa1, or that the ability of Drp1 deletion to restore the effects of Opa1 deletion on ETC function diminish over time. We next generated control and Drp1-targeted KPO CRISPR clones over the course of six weeks and assayed OCR after acute AdEV or AdCre infection. We found that chronic Drp1 deletion inhibits OCR in the presence of Opa1 (Figures 2.13G and 2.13H), consistent with a role for Drp1-dependent fission in the long-term maintenance of mitochondrial function. Notably, acute Opa1 deletion in chronic Drp1 CRISPR cells has no significant effect on OCR suggesting that even chronic inactivation of fission mitigates the effects of Opa1 deletion on ETC function. Collectively, these data indicate that chronic Drp1 deletion leads to decreased mitochondrial function but is still protective against the effects of acute Opa1 loss. We note the possibility that chronic loss of both Drp1 and Opa1 is more detrimental to ETC function than chronic loss of Drp1 alone, suggesting that disruptions to cristae that require Opa1-mediated repair can arise over time in the absence of Drp1-

dependent fission events. In support of this, continuous fission-independent cristae remodeling has been recently reported using live-cell super resolution imaging [210, 211].

Our findings support a model in which steady-state mitochondrial fusion and fission dynamics constantly restructure both outer and inner mitochondrial membrane morphology (Figure 2-13I). Mitochondrial fission locally disrupts cristae morphology and ETC assembly and function, including the NAD^+ regeneration required for oxidative synthesis (OxSyn) in highly proliferative tumor cells. Opa1 is required for mitochondrial fusion and to repair cristae and ETC at sites of fission. Thus, the consequences of acute Opa1 deletion in Drp1-expressing cells are profoundly fragmented mitochondrial outer membrane morphology with dysmorphic cristae and reduced ETC function. Importantly, this model predicts that the short-term effects of Opa1 deletion can be prevented by simultaneous inactivation of fission, but that long-term inactivation of fusion-fission cycling causes mitochondrial dysfunction.

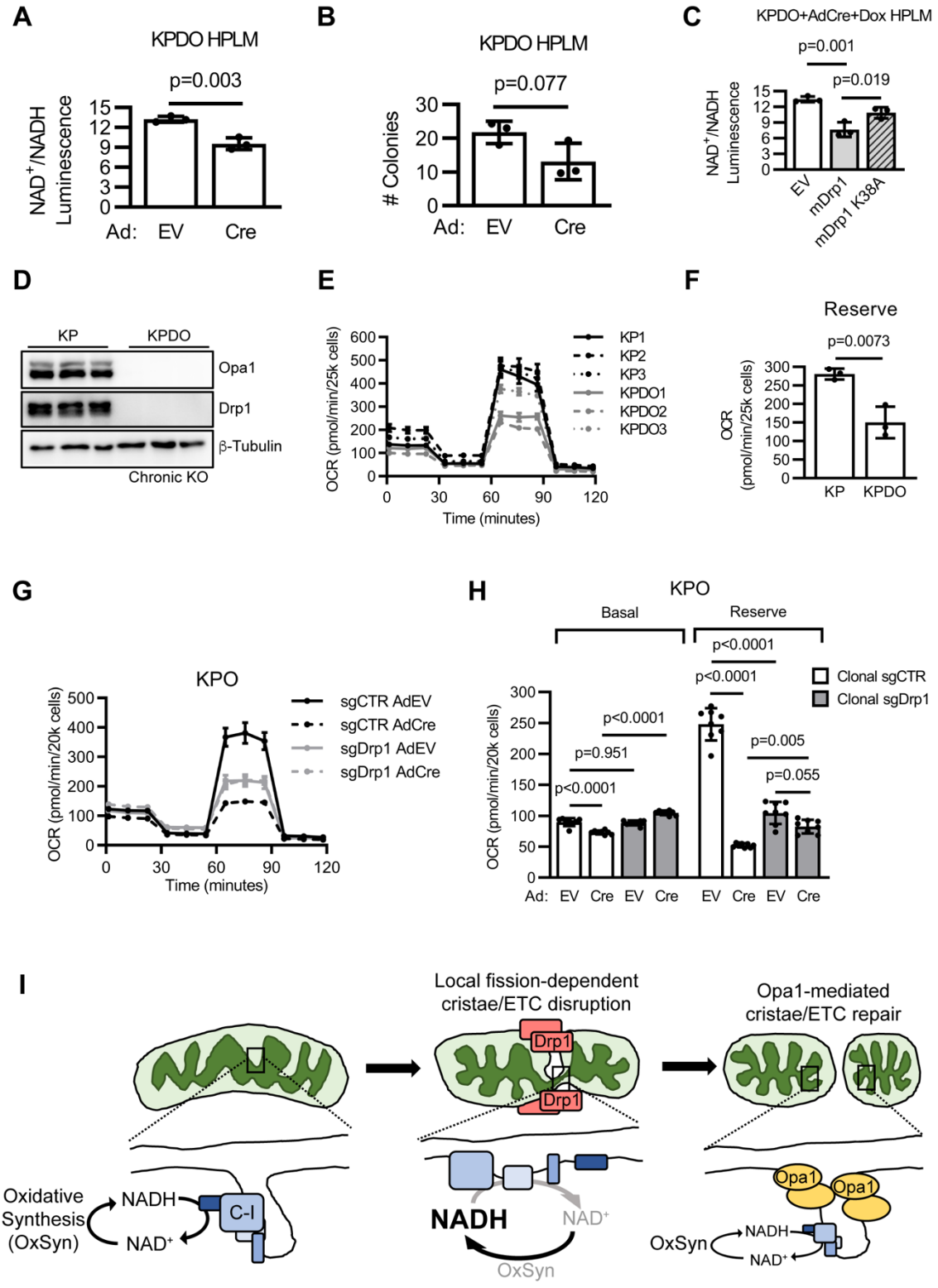
A
KPDO HPLM
p=0.003
NAD+/NADH Luminescence
Ad: EV Cre
B
KPDO HPLM
p=0.077
# Colonies
Ad: EV Cre
C
KPDO+AdCre+Dox HPLM
p=0.001
p=0.019
NAD+/NADH Luminescence
EV
mDrp1
mDrp1 K38A
D
KP
KPDO
Opa1
Drp1
β-Tubulin
Chronic KO
E
KP1
KP2
KP3
KPDO1
KPDO2
KPDO3
OCR (pmol/min/25k cells)
Time (minutes)
F
Reserve
p=0.0073
OCR (pmol/min/25k cells)
KP
KPDO
G
KPO
sgCTR AdEV
sgCTR AdCre
sgDrp1 AdEV
sgDrp1 AdCre
OCR (pmol/min/20k cells)
Time (minutes)
H
KPO
Basal
Reserve
p<0.0001
p<0.0001
Clonal sgCTR
Clonal sgDrp1
p<0.0001
p=0.951
p<0.0001
p=0.005
p=0.055
OCR (pmol/min/20k cells)
Ad: EV Cre EV Cre EV Cre EV Cre
I
Local fission-dependent cristae/ETC disruption
Opa1-mediated cristae/ETC repair
Drp1
Drp1
Oxidative Synthesis (OxSyn)
NADH
NAD+
C-I
NADH
NAD+
OxSyn
Opa1
Opa1
OxSyn
NADH
NAD+

Figure 2-13. Chronic mitochondrial dynamics gene deletion inhibits LUAD ETC function

A. NAD^+/NADH in AdEV- or AdCre-infected KPDO cells cultured in HPLM. n=3 independent experiments. Mean±SD. Student's T-test.

B. Colony formation in AdEV- or AdCre-infected KPDO cells cultured in HPLM. n=3 independent experiments. Mean±SD. Student's T-test.

C. NAD^+/NADH in AdCre-infected KPDO cells expressing empty vector (EV), $mDrp1^{WT}$, or $mDrp1^{K38A}$ cultured in HPLM. n=3 independent experiments. Mean±SD. One-way ANOVA + Sidak's multiple comparisons test.

D. Immunoblot of Drp1 and Opa1 in KP and KPDO cells. KPDO cells deleted Drp1 and Opa1 *in vivo.* n=3 independently derived cell lines per genotype.

E. OCR of KP and KPDO cells. n=3 independent cell lines per genotype. Mean±SD.

F. Each point = mean reserve OCR of one KP or KPDO cell line. n=7 wells for each of 3 independent cell lines per genotype. Mean±SD. Student's T-test.

G. OCR of clonal control (sgCTR) or clonal Drp1 (sgDrp1) KPO CRISPR cells infected with AdEV or AdCre. n=8 wells per condition. Mean±SD.

H. Basal and reserve OCR of clonal control and Drp1 KPO CRISPR acutely infected with AdEV or AdCre. n=8 wells per condition. Mean±SD. One-way ANOVA + Sidak's multiple comparisons test.

I. Model of Drp1 and Opa1 restructuring the inner mitochondrial membrane and their effects on ETC function and NAD^+ regeneration.

2.4 Discussion

This work demonstrates that Opa1 is required *in vitro* and *in vivo* for KRas-mutant LUAD growth and development by promoting the ETC-mediated NAD^+ regeneration necessary for oxidative biosynthesis. We find the cell growth and metabolic phenotypes that arise from Opa1 knockout are reversible *in vitro* by simultaneous deletion of Drp1 or inactivation of its GTPase catalytic domain. This indicates that mitochondrial fission that is unopposed by Opa1 is catastrophic to mitochondrial function and ultimately cell growth and survival. In stark contrast, Drp1 deletion demonstrates no effect on KP LUAD tumor cell growth *in vitro* or on tumor development *in vivo*. This is surprising given the requirement for Drp1 in a PDAC model with identical KP genetics [182], and in *BRAF*-mutant melanoma, another MAPK-driven tumor [84]. This suggests that the consequences of disrupting mitochondrial dynamics are tissue specific.

Opa1-dependent ETC functions are likely tissue-specific. For instance, skeletal muscle requires Opa1 for ETC-mediated ATP synthesis [212], whereas tumors require ETC-mediated NAD^+ regeneration and synthesize ATP through glycolysis. Recent work has found that mitochondrial ATP synthesis comes at the expense of rapid NAD^+ regeneration, as generation of the proton gradient required by mitochondrial ATP synthase slows ETC electron flux and thus NADH oxidation [193]. It would be interesting to assess whether tumor cells regulate Drp1 and Opa1 to maximize ETC flux and NADH oxidation at the expense of ATP synthesis, potentially through fission-mediated increase in proton leakage to counteract the slowing of ETC electron flux.

Pharmacological Opa1 inhibition may be therapeutically valuable for highly proliferative tumors with substantial ETC-mediated NAD^+ regeneration requirements and hyperactive mitochondrial fission, such as those with activating mutations in *KRAS* or other MAPK

activators. Given KP LUAD can develop with heterozygous deletion of Opa1 and decreased Opa1 protein expression, we suspect that Opa1 activity must be inhibited by more than 50%. It is possible that ETC function in fission-stimulated tumors would be more adversely affected by acute Opa1 inhibition than normal tissues. Supporting this, mouse hepatocytes tolerate complete Opa1 depletion *in vivo* and Opa1 silencing reverses liver steatosis characterized by megamitochondria [213].

Drp1 deletion rescues the effects of acute Opa1 deletion on colony formation and ETC function, but not *in vivo* tumor development; however, Drp1 deletion also permits isolation of Opa1-null tumor cell lines, suggesting that Opa1 deletion prevents tumor initiation and that simultaneous Drp1 deletion rescues initiation, but not progression. Notably, chronic Drp1 deletion leads to decreased ETC function, but does not inhibit tumor progression in KPD mice. We speculate that tumors with Opa1 and Drp1 deletion undergo initiation, but that ETC dysfunction from combined chronic Drp1 deletion and accumulation of fission-independent cristae disruptions unrepaired by Opa1 inhibit tumor progression. In addition, we cannot rule out other functions of Opa1 that are important *in vivo* but not *in vitro* and that are not impacted by Drp1-dependent fission activity.

Opa1, the mitochondrial contact site and cristae organizing system (MICOS) complex, and ATP synthase dimers regulate cristae morphology [64–66, 116, 214–217] through mechanisms that remain unclear. Our work suggests that cristae are disrupted by fission and must be repaired to maintain ETC function. The sequence of action of Opa1, MICOS, and ATP synthase dimers in orchestration of cristae structure remain unclear, though recent work suggests Opa1 is epistatic to the core MICOS protein, MIC60 [121]. MIC60 densely populates cristae junctions, whereas Opa1 localizes to cristae membranes and the IBM [120]. This suggests that Opa1 forms new cristae by directly folding the IMM,

while MICOS maintains cristae structure by securing cristae junctions to the outer mitochondrial membrane and inhibiting Opa1 from fusing opposing leaflets of the IMM at cristae junctions. This model is consistent with a requirement for Opa1 only when fission disrupts cristae and predicts that MICOS is required to anchor cristae even in the absence of Drp1. Future work will delineate how fission and MICOS interact to affect cristae structure.

We find that acute Opa1 deletion impacts both cristae morphology and mtDNA content in a Drp1-dependent manner. We cannot rule out the possibility that Drp1 disrupts cristae indirectly through direct loss of mtDNA, which encodes two subunits of ATP synthase. Decreased expression of ATP synthase subunits would decrease assembly and dimer formation, which could disrupt cristae. In this alternative model, Opa1 activity would preserve cristae structure by preventing the fission-induced loss of mtDNA.

Collectively, this work establishes the dependency of LUAD cells on mitochondrial ETC-mediated NAD^+ regeneration and elucidates how Opa1 opposes Drp1-mediated mitochondrial fission to promote ETC assembly and function through IMM restructuring. This work supports a need for future research that will inform the approach and efficacy of inhibiting mitochondrial dynamics in specific tumor types and the development of more potent and specific inhibitors of dynamics effectors.

3 Chapter 3. Perspectives and Future Directions

The work presented in this dissertation presents two main findings:

1) The requirements for mitochondrial dynamics are specific to tissue-of-origin and stage of tumorigenesis. Our lab previously found KRas-mutant PDAC is extraordinarily sensitive to inactivation of mitochondrial fission by deletion of Drp1, whereas LUAD with *KRAS* and *TP53* driver mutations identical to those used in PDAC is relatively insensitive to disruption of fission. Additionally, the work in this dissertation suggests that Opa1 deletion prevents tumor initiation, and that simultaneous Drp1 deletion rescues tumor initiation, but not progression.

2) The mitochondrial inner membrane is constantly remodeled on acute timescales by the reciprocal actions of Drp1 and Opa1, and mitochondrial fission that is unbalanced by Opa1 inhibits mitochondrial ETC function and tumor development.

3.1 Mitochondrial dynamics themes

These findings highlight a number of themes that guide our understanding of how mitochondrial dynamics promote mitochondrial function and tumorigenesis:

What are the basic functions of dynamics components?

The basic functions of mitochondrial dynamics components have been thoroughly elucidated over the past 20 years in primarily non-cancer systems including yeast and mouse fibroblasts. Most notably, Drp1 executes mitochondrial fission and binds OMM receptors to do so; Opa1 is required for IMM fusion and preservation of cristae. The systems used for these studies offered relative ease of genetic disruption and ideal

imaging; however, further layers of mitochondrial dynamics are critical to consider if we seek to understand how these processes affect tumor biology, as outlined below.

On what timescales do dynamics components act?

It is clear that mitochondrial dynamics exert acute and chronic effects on mitochondria. Drp1 causes mitochondrial fragmentation on acute timescales and participates in organelle quality control over prolonged periods of time. Our studies demonstrate that acute CRISPR-mediated Drp1 deletion in KP LUAD exerts little effect on ETC function, whereas chronic Drp1 deletion substantially decreases ETC function. Conversely, we find that acute Opa1 deletion severely inhibits ETC function. Our model suggests that Opa1 is required to oppose Drp1-mediated cristae remodeling and predicts that in order to observe rescue of ETC function by Drp1 deletion in Opa1 knockout cells, Drp1 must be inactivated at the same time as, or slightly before, Opa1, and that functional readouts must be performed shortly thereafter. This recognizes that fission occurs rapidly and that in the absence of Opa1, the effects of unopposed fission on cristae and ETC function will manifest quickly. If these experimental conditions are not met, other facets of mitochondrial dynamics that influence mitochondrial function such as Drp1-independent fission or cristae remodeling and lack of organelle quality control could confound results. In order to address this, experimental approach should consider and implement timing of gene deletion.

We leveraged GEMM-derived tumor cell lines that retained floxed mitochondrial dynamics alleles and provide precise and timely gene disruption. Drawbacks of this approach were that we could not inactivate floxed genes independently (i.e. Drp1 first, then Opa1) and complete protein depletion required 2-3 days. If understanding the biology of interest requires differential timing of gene deletion, it would be useful to generate mice or mouse-

derived cells with one gene of interest flanked by loxP sites and the other flanked by FRT sites. Inducible expression or adenoviral delivery of Cre and/or flippase recombinases would therefore permit more control over timing of gene deletion. If protein depletion must be achieved faster than gene deletion itself can mediate, degron systems could be employed, although introduction of degron machinery into specific mitochondrial compartments may be challenging.

How do dynamics processes interact?

Most work to-date has identified seemingly independent functions of Drp1 and Opa1 by disrupting single genes. Our work identifies how Opa1 and Drp1 interact on acute timescales and we find the nature of this interaction has profound implications for mitochondrial function and tumor biology. These findings make understanding mitochondrial dynamics from a systems level essential. Rationale for this in our own experiments stems from the different effects of Drp1 disruption in KRas-mutant PDAC versus LUAD. Whereas directly targeting Drp1 may be efficacious in PDAC, its effect in LUAD is unremarkable; however, a broader understanding that 1) LUAD may have substantial respiration requirements, 2) that fission is hyperactivated by KRas, and 3) that Opa1 inhibition acutely inhibits tumor ETC function in a fission-dependent manner, makes it possible that instead of targeting Drp1 in LUAD, Opa1 inhibition may be more efficacious.

How does the oncogenic cellular milieu affect mitochondrial dynamics?

Our lab discovered that oncogenic Ras signaling hyperactivates mitochondrial fission through direct Erk2 phosphorylation of Drp1. These findings alone demonstrate that the mitochondrial dynamics landscape in normal cells is different from that in tumor cells, especially those with mutations in MAPK components. Much research has elucidated how mitochondria-dependent tumor metabolism differs from normal tissue. Understanding the

differences in mitochondrial dynamics in cells with oncogenic signaling and how they influence metabolism will be critical to evaluating whether inhibition of dynamics machinery is efficacious against certain tumor types and whether it is tolerable in normal tissues.

How does tissue-of-origin affect tumor mitochondrial dynamics requirements?

KRas-mutant PDAC and BRAF-mutant melanoma are sensitive to Drp1 disruption, but KRas-mutant LUAD is insensitive to Drp1 disruption *in vitro* and *in vivo*. This discrepancy demonstrates that there is still much to be discovered regarding how tissue-of-origin influences tumor metabolism in cells with identical driver mutations and how tumor metabolism is influenced by mitochondrial dynamics and extracellular environment. Further understanding in this area is critical to informing a potential approach to tumor therapy targeting mitochondrial dynamics.

These themes of dynamics machinery function, timescales of action, interaction, cell signaling, and tissue-of-origin will guide future research into mitochondrial dynamics. The following section outlines avenues of future investigation that often weave together multiple themes. When we have already begun approaching certain questions below, we demonstrate preliminary and unpublished findings.

3.2 Future directions

3.2.1 Differentiating effects of Drp1 deletion in KRas-mutant PDAC vs. LUAD

One of the surprising findings of this work is that acute deletion of Drp1 in KRas-mutant LUAD has no effect on colony formation *in vitro* or tumor burden *in vivo*. Conversely, our lab previously found that acute inhibition of Drp1 inhibits KRas-driven cellular transformation, metabolism, and *in vivo* PDAC tumorigenesis. This distinction is

reminiscent of other metabolic differences between KP LUAD and KP PDAC such as the differential engagement of branched chain amino acid metabolism [39], and indicates that tumors with identical initiating genetics demonstrate profound differences in metabolism based on tissue-of-origin. We also find that chronic inhibition of mitochondrial fission induces mitochondrial dysfunction in both PDAC and LUAD, suggesting that inhibition of fusion-fission cycling as opposed to acute morphological changes, drives this effect without respect to tumor tissue-of-origin. Therefore, acute Drp1 inhibition (within 1-2 weeks of protein depletion) should be used to best evaluate the mechanisms driving differential sensitivity to Drp1 inhibition in PDAC versus LUAD. Technically, we can acutely inhibit Drp1 by CRISPR-mediated deletion or shRNA knockdown, but the most precise and effective technique is *in vitro* adenovirus Cre infection of tumor cells that possess floxed alleles for Drp1.

The ideal experimental approach to assess the effects of acute Drp1 deletion in mouse PDAC and LUAD would be to generate homozygous floxed *Dnm1l* (Drp1)-retaining PDAC and LUAD tumor cells in the KP model from the same mouse to control for genetic background. This is theoretically achievable using KPDC (KPD + pancreas-specific *Pdx-1 CreERT2)* mice and initiating PDAC through tamoxifen injection and LUAD through intratracheal AdCre at appropriate timepoints such that tumor harvest occurs at the same time. One potential difficulty of this approach is the differential selection for tumor cells that retain Drp1 in LUAD versus PDAC *in vivo.* We find Drp1 is dispensable to LUAD *in vivo* and that tumor cell lines derived from KPD mice successfully deleted Drp1, suggesting that for this tumor model, we would have to screen many independent LUAD cell lines to identify those with chance retention of Drp1. Because the LUAD model generates hundreds of individual tumors per mouse, it is feasible to establish many tumor cell lines from the same animal and screen them independently for Drp1 retention.

Conversely, retention of Drp1 exerts a significant survival advantage to PDAC *in vivo*, so the fraction of Drp1-retaining PDAC tumor cell lines in this model is expected to be higher than that of LUAD.

Once PDAC and LUAD cell lines with retained floxed *Dnm1l* alleles are established, the effects of Drp1 deletion in these two tumor systems should be assessed shortly after AdEVor AdCre infection. Basic cell-level phenotypes to assess should include 1) cell accumulation under standard culture conditions (typically in high-glucose DMEM or similar medium) as well as under physiologic media (HPLM or Plasmax media) conditions and nutrient-restricted conditions (i.e. low-glucose, galactose, low FBS), and 2) sensitivity to apoptosis by analysis of cleaved PARP and cell viability by CellTiter-Glo. Additionally, the effects of Drp1 deletion on tumor metabolism should be assessed by Seahorse bioanalyzer and metabolomics. Together these initial endeavors would reveal, in broad strokes, how Drp1 deletion affects cell growth, health, and metabolism.

The KP PDAC and KP LUAD tumor microenvironments are known to be distinct [38], and thus the difference in available extracellular metabolites may dictate *in vivo* sensitivity to Drp1 deletion. To discern whether LUAD and PDAC demonstrate differential sensitivity to Drp1 deletion *in vivo* due to environmental factors, it would be worthwhile to perform orthotopic and subcutaneous injection tumor models and compare tumor growth within cell lines between compartments and between cell lines within compartments (Figure 3-1). If KP PDAC and KP LUAD grow well under Drp1 deletion in the lung but not pancreas, this would suggest that some extracellular factors in the pancreas restrict KP tumor growth under Drp1 deletion irrespective of tumor-intrinsic characteristics imparted by tissue-of-origin. If Drp1-null KP LUAD grows well in the pancreas and lung, but Drp1-null KP PDAC does not grow in either, this would suggest that factors intrinsic to lung tumors permit

tumor growth under Drp1 deletion regardless of environment, whereas PDAC is restricted regardless of environment. The subcutaneous space provides an environment to which both cell types are naïve and would allow determination of whether effects of transplantation in the lungs or pancreas are specific to those compartments. Identification of any environmental factors that influence tumor sensitivity to Drp1 deletion is critical to further understanding how mitochondrial fission shapes tumor metabolism and growth, and would allow for better tumor modeling *in vitro* as media could be developed to better resemble the particular extracellular environment of interest.

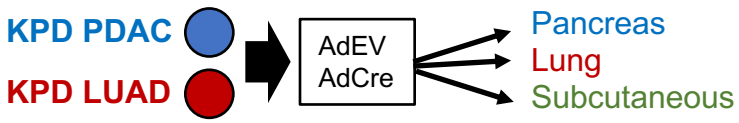

Figure 3-1. Experimental overview for evaluating the effects of extracellular environment on sensitivity of KP PDAC and LUAD to Drp1 deletion

3.2.2 Effects of Opa1 and Drp1 co-deletion on tumor progression *in vivo*

Another exciting finding from our work is that Drp1 deletion rescues ETC assembly and function and tumor cell growth *in vitro*, but not tumor development *in vivo*; however, we isolated many tumor cell lines with complete *in vivo* Drp1 and Opa1 deletion and no cell lines with only Opa1 deletion. This indicates that Drp1 deletion confers some advantage to Opa1-deleted cells that allows for persistence *in vivo* for the entirety of the GEMM and then growth *in vitro* during tumor cell line establishment. These findings also suggest that Opa1 deletion inhibits tumor initiation and that Drp1 deletion rescues initiation, but not progression, *in vivo*.

To address the discrepancy between the rescue of Opa1 deletion by Drp1 deletion *in vitro* versus *in vivo*, we assessed the effects of environment and duration of dual gene deletion

on tumor cell ETC function. We found that Opa1/Drp1 deletion was not substantially detrimental to ETC function in cells cultured in more-physiologic media, indicating that environmental metabolites likely do not drive the discrepancy. We also found that chronic Drp1 deletion inhibits ETC function, but is still sufficient to rescue the effects of Opa1 deletion.

To better describe the *in vivo* effects of Drp1 deletion on Opa1 deletion-mediated decrease in tumor burden, it would be useful to measure number of tumor foci and tumor grade distribution, as opposed to the rudimentary metric of total tumor burden, in KP, KPO, and KPDO mice. To reduce experimental variation and maximize efficiency of recombination, lentivirus Cre should be used and metrics should be normalized to total lung area of field analyzed. Additionally, all lesions should be screened for complete dynamics gene deletion by IHC or RNA in-situ hybridization before being quantitated. Lung adenocarcinoma progresses from initiating cell to atypical adenomatous hyperplasia (AAH) to adenoma and then finally to adenocarcinoma. If Opa1 deletion alone inhibits initiation we would expect zero Opa1-null foci. If Drp1 deletion rescues tumor initiation from Opa1 deletion, but not complete progression, we would expect equal number of tumor foci of lower grade than KP tumors. The ten-week GEMM incubation time used in this study is likely appropriate for initial follow-up studies as KP mice demonstrate a substantial distribution of tumor grades, indicating that it would be sensitive to genetic disruptions that inhibit progression and collapse the distribution towards earlier-grade lesions.

In order to identify why Drp1 deletion does not rescue tumor progression *in vivo* following Opa1 deletion, it would be worthwhile to perform orthotopic injection studies in luciferase-expressing KPDO tumor cells with retained floxed *Dnm1l* and *Opa1* alleles. These cells

offer temporal control of gene deletion that should be leveraged for the specific question asked. AdCre-mediated gene deletion before implantation would permit assessment of how Drp1/Opa1-null tumor cells grow *in vivo;* however, introduction of a doxycycline-inducible Cre transgene would allow gene deletion *in vivo* if we suspect that the environmental context of gene deletion influences tumor outcomes. After implantation, tumor growth should be monitored through serial luciferase bioluminescent imaging. We expect that if the orthotopic transplantation approach recapitulates the GEMM, Drp1/Opa1-deleted cells will not grow tumors. If this is the case, mechanistic workup to identify why tumor growth is inhibited should include assessment of apoptotic markers and global tumor metabolism within a few days post-injection.

These studies would provide more clarity on the effects of Opa1/Drp1 co-deletion in LUAD tumorigenesis and would indicate whether specific tumor development stages exhibit distinct requirements for mitochondrial dynamics.

3.2.3 Mechanisms of ETC disassembly by Opa1 deletion

Our findings from Chapter 2 demonstrate that acute Opa1 deletion inhibits ETC assembly and complex I function; however, the mechanism driving this phenomenon remains unclear. We proposed that acute Opa1 deletion decreases ETC assembly either by decreasing the abundance of mitochondrial DNA-encoded protein subunits of ETC complexes I, III, IV, and V, or that Opa1 deletion disrupts proper cristae morphology that promotes ETC assembly.

To determine whether acute Opa1 deletion affects protein expression of ETC subunits in a Drp1-dependent manner, we assessed levels of ETC components by Western blot under conditions of Opa1 deletion or Opa1 and Drp1 co-deletion. We included mitochondrial-

(mtDNA) and nuclear- (nDNA) encoded subunits to identify whether potential changes to abundance of ETC proteins was specific to those that are encoded by mitochondria, or whether nuclear subunits are also affected which may indicate ETC complex destabilization and degradation. We find that although acute Opa1 deletion does not cause a universal decrease in mitochondrial DNA-encoded ETC subunit abundance, it significantly decreases levels of the mtDNA-encoded complex IV subunit MTCO2 in a Drp1-dependent manner (Figures 3-2A and 3-2B). Surprisingly, although we observe a substantial decrease in *in vitro* complex I activity following acute Opa1 deletion, there is no decrease in expression of either the mtDNA- or the nDNA-encoded complex I subunits we assessed. This indicates that although acute Opa1 deletion reduces abundance of mtDNA by about one-third, this does not lead to a universal decrease in mtDNA-encoded ETC subunits that would explain the substantial decrease in ETC assembly or decrease in complex I activity we observe from Opa1 deletion in KP LUAD.

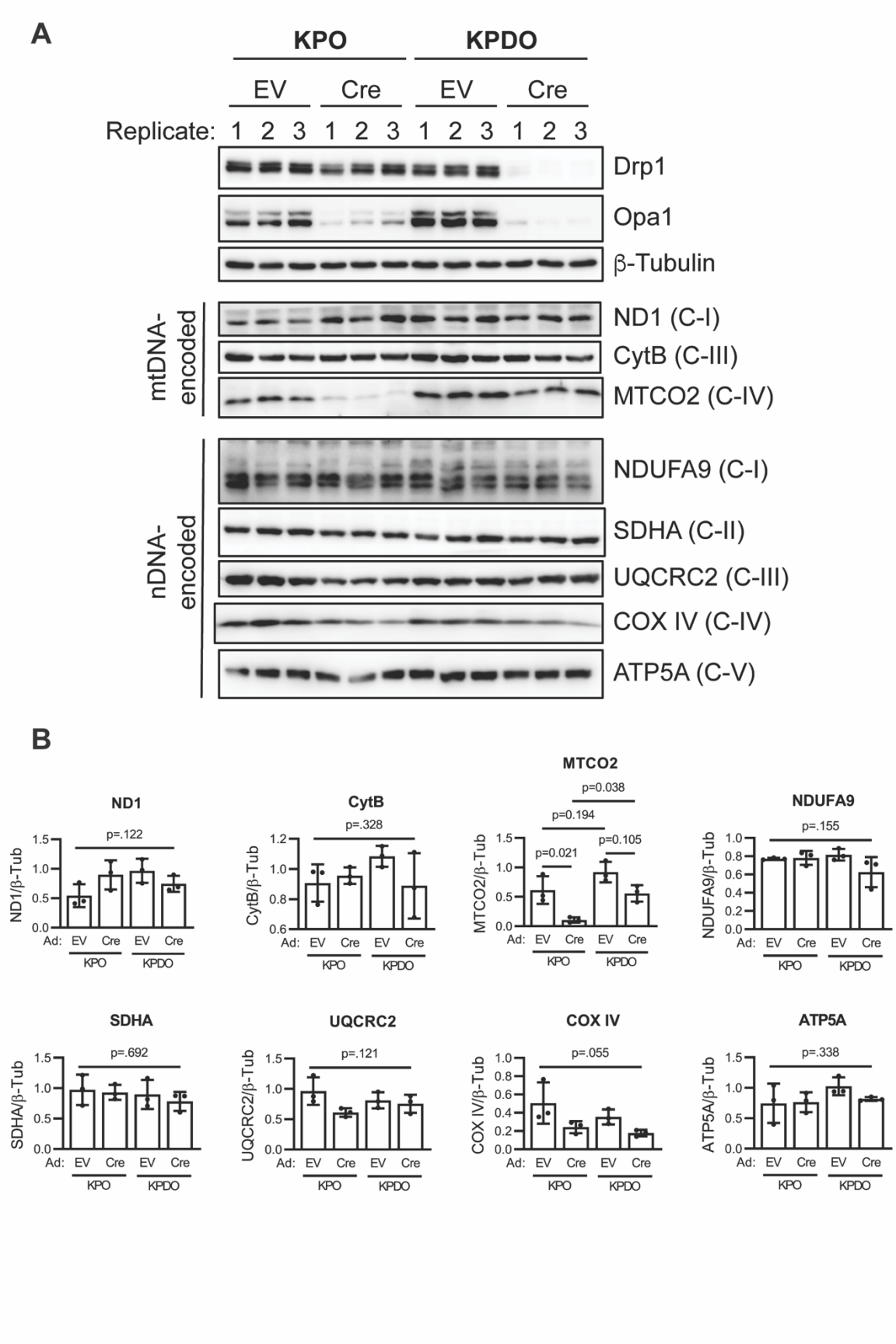
A
KPO
KPDO
EV
Cre
EV
Cre
Replicate: 1 2 3 1 2 3 1 2 3 1 2 3
Drp1
Opa1
β-Tubulin
mtDNA-encoded
ND1 (C-I)
CytB (C-III)
MTCO2 (C-IV)
nDNA-encoded
NDUFA9 (C-I)
SDHA (C-II)
UQCRC2 (C-III)
COX IV (C-IV)
ATP5A (C-V)
B
ND1
p=.122
ND1/β-Tub
CytB
p=.328
CytB/β-Tub
MTCO2
p=0.038
p=0.194
p=0.021
p=0.105
MTCO2/β-Tub
NDUFA9
p=.155
NDUFA9/β-Tub
SDHA
p=.692
SDHA/β-Tub
UQCRC2
p=.121
UQCRC2/β-Tub
COX IV
p=.055
COX IV/β-Tub
ATP5A
p=.338
ATP5A/β-Tub
Ad: EV Cre EV Cre
KPO KPDO

Figure 3-2. Acute Opa1 deletion does not universally decrease abundance of mtDNA-encoded ETC proteins

A. Immunoblot of Drp1, Opa1, and numerous mtDNA- and nDNA-encoded ETC subunits in KPO and KPDO tumor cells acutely treated with AdEV or AdCre. n=3 replicates of lysates harvested on separate days (all replicates shown). C-I = complex I, C-II = complex II, C-III = complex III, C-IV = complex IV, C-V = complex V.

B. Immunoblot densitometry of ETC subunits normalized to β-Tubulin in indicated tumor cells. One-way ANOVA (all) + Sidak's multiple comparisons test (MTCO2).

We reasoned that because Opa1 deletion does not cause a universal decrease in mtDNA-encoded ETC component expression upon acute Opa1 deletion, the inhibition of complex I activity and decrease in MTCO2 expression may instead be caused by an Opa1 deletion-mediated decrease in ETC complex or supercomplex *assembly* required for ETC function and stability. Deletion of cytochrome C [218] or subunits of complex III [219] or IV [220, 221] destabilize complex I and maturation of complexes I and IV occur at supercomplexes [222], so it is possible that Opa1 deletion inhibits complex I assembly directly or indirectly by disrupting assembly of other ETC components.

To determine whether the function or assembly of specific ETC complexes is disrupted by acute Opa1 deletion, we performed native PAGE followed by either *in vitro* complex IV activity assay or in-gel denaturation and immunoblotting, respectively. We find that acute Opa1 deletion inhibits complex IV activity and assembly of structures containing subunits of complexes I, III, and IV (Figure 3-3). Notably, we also find that assembly of complex II and complex V are unaffected, suggesting that Opa1 deletion does not universally inhibit ETC assembly. Further, complex I activity signal appears at high molecular weights indicating that most of the complex I activity in KP LUAD occurs within supercomplexes, as others have noted [223]. Together, these results indicate that acute Opa1 deletion may inhibit ETC function by destabilizing or inhibiting assembly of complex I, III, IV, or a combination of these.

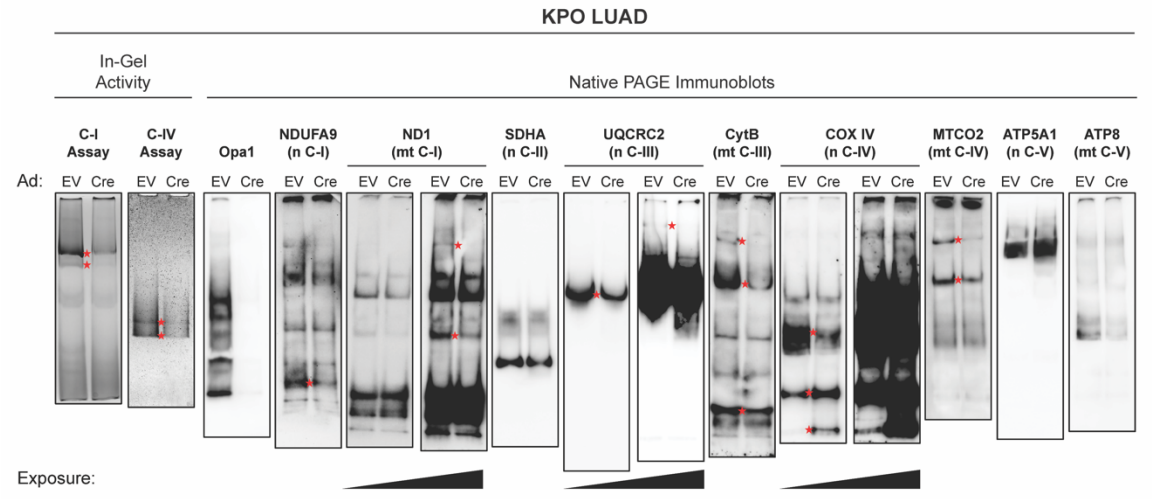

Figure 3-3. Acute Opa1 deletion inhibits complex IV activity and ETC assembly

Complex I and IV in-gel activity assays (left) and native PAGE immunoblots of mtDNA- or nDNA-encoded ETC subunits in KPO LUAD with acute AdEV or AdCre infection. Red stars indicate substantial differences in band intensity between EV and Cre samples.

Two distinct models for ETC assembly have been proposed. The elasticity model posits that ETC complexes I, III, and IV are initially formed independently by assembly of their individual subunits and sub-complex modules and then fully assembled complexes assemble into supercomplexes, the most well-described of which is the complex I,III_2,IV respirasome [62]. In contrast, the cooperative assembly model posits that incomplete complex I, III, and IV structures first assemble with each other into larger structures that promote the complete assembly and function of each individual complex. The mechanics of ETC assembly were recently and thoroughly reviewed [224].

Although the exact mechanism by which Opa1 deletion affects ETC assembly remains to be discovered, the most striking effect of Opa1 deletion that native PAGE immunoblot reveals is differential assembly of nuclear-encoded COX IV-containing structures. Opa1 deletion causes substantially decreased abundance of higher molecular weight COX IV-containing structures and an increased abundance of smaller structures. COX IV is assembled into a pre-complex IV module with mtDNA-encoded MTCO1. It is therefore possible that Opa1 deletion inhibits NAD^+ regeneration by inhibiting complex IV assembly required for stability and function of other ETC complexes or supercomplexes. Targeted monitoring of ETC assembly using individual proteins as proxies for ETC complexes is difficult because ETC structures are formed by many subunits that organize hierarchically. To instead monitor assembly of ETC complexes in a less-biased manner, complexome profiling (CP) was recently developed [225]. This approach measures abundance of all proteins of interest by molecular weight, and therefore at different stages of assembly, following native PAGE. Additionally, samples from separate mitochondrial preparations can be analyzed at the same time by combining CP with stable isotope labeling of amino acids in culture (SILAC), allowing for comparison of relative peptide densities between

samples [226]. SILAC CP would therefore be an appropriate approach to assess whether and how Opa1 deletion affects ETC assembly in KP LUAD.

Our work demonstrates that the effects of Opa1 deletion are caused by unopposed Drp1-mediated mitochondrial fission. We hypothesize that Opa1 is acutely required to oppose fission-induced disruptions to cristae morphology that inhibit ETC function, so it would be interesting to perform complexome profiling to assess how acute Opa1 deletion affects ETC assembly in cells expressing or lacking Drp1. We predict that tumor cells with simultaneous Drp1 and Opa1 deletion will assemble ETC appropriately. This notion disagrees with assertions that direct interactions between Opa1 and ETC components [227, 228] or Opa1 and ETC assembly factors [229] are important, as others have suggested. We instead propose that Opa1 is critical to preservation of cristae architecture required for ETC assembly and that Opa1 is unnecessary for ETC assembly if fission-induced disruption to cristae structure is disabled.

3.2.4 Effects of dynamics disruption on cristae reorganization

Our findings suggest that Drp1-mediated mitochondrial fission that is unopposed by Opa1 causes cristae disruption leading to ETC disassembly and dysfunction. We observe by TEM that Opa1 deletion results in severely dysmorphic cristae in Drp1-expressing cells, but not cells that simultaneously delete Drp1 and Opa1; however, TEM provides only a snapshot of cristae morphology due to the requirement of cell fixation for this approach. To instead monitor the dynamics of cristae remodeling under Drp1 and/or Opa1 deletion, super resolution live-cell microscopy must be performed. Traditional confocal microscopy has been historically incapable of resolving individual cristae, which have an average width of 20 nm, due to diffraction limitations imposed by the lenses and wavelengths of light used. The development of super resolution microscopy tools such as Airyscan and

stimulated emission-depletion (STED) have permitted recent live-cell imaging of cristae [210, 211, 230–232]. Super resolution microscopy will allow us to better understand how mitochondrial fusion-fission dynamics affect cristae restructuring in real time. Super resolution microscopy of cristae is often performed after staining cells with fluorescent mitochondrial-localized dyes that are enriched at the inner mitochondrial membrane, such as Mitotracker Green. Mitotracker Green is relatively photostable compared to other dyes used for the same purpose (i.e. Nonyl Acridine Orange [NAO]) and allows for timelapse microscopy. It will therefore be the reagent of use for the following proposed future work.

One possible explanation for decreased ETC function in chronic Drp1/Opa1 knockout cells is that Drp1-independent cristae reorganization in the absence of Opa1 leads to ETC dysfunction over longer timescales. This notion makes two testable predictions: 1) cristae are reorganized in Drp1-null cells, and 2) cells with chronic, but not acute, Drp1/Opa1 deletion will demonstrate dysmorphic cristae. Cristae in Drp1-null cells look relatively normal by TEM [93], but this does not indicate whether they are restructured or static. Additionally, although cristae are constantly remodeled on the order of seconds [210], it is unknown if Drp1 is required for this process. To easily test the first prediction, steady-state cristae remodeling should be assessed in Drp1-expressing and Drp1-null cells. To test the second prediction, TEM should be performed on cells with acute or chronic Drp1/Opa1 deletion and their dynamics-expressing controls. The expectation for this is that cells with acute Drp1/Opa1 deletion will demonstrate normal cristae morphology as we observed in this study, but that chronic deletion impairs cristae structure.

Our work posits that Drp1-mediated fission causes local cristae dysmorphism that must be repaired by Opa1 to restore ETC function. To properly assess the effects of Drp1 on cristae morphology at sites of fission in cells expressing or lacking Opa1, live-cell imaging

that captures cristae structure before, during, and after fission events should be performed. The ideal setup for this experiment would be to image cristae in individual mitochondria within Drp1-expressing cells at steady-state and immediately after Opa1 deletion. We find that Opa1 deletion in Drp1-expressing cells causes severe mitochondrial fragmentation and cristae disruption at the earliest timepoint that immunoblot confirms Opa1 deletion after AdCre infection (3 days post-infection); therefore, it would be almost impossible to capture the desired events and ensure complete Opa1 deletion before the mitochondrial network has completely fragmented and had cristae structure disrupted. As an alternative experimental approach, we introduced doxycycline-inducible mDrp1 fused to RFP into a KPDO tumor cell line that deleted Drp1 *in vivo* but retained Opa1 (Figure 3-4A). In this system, we could delete Opa1 and preserve mitochondrial structure until we induce Drp1 expression. Although Opa1-expressing cells demonstrated tubular mitochondria suggesting low fission activity (Figure 3-4B), many Opa1-deleted cells harbored fragmented mitochondria (Figure 3-4D). This indicated that the slight expression leakage of the Drp1-RFP transgene was sufficient to cause fission and that we had missed the window of observing cristae morphology as mitochondria transition from tubular to fragmented. Additionally, we expressed the mDrp1-RFP to try and capture Drp1 foci, but found the RFP signal was low and requires further optimization, and thus that imaging channel is not included in the data below.

Although our system requires further optimization, we were able to make a few key observations. First, we found we can technically observe individual cristae in subcellular regions of single cells using Airyscan super resolution microscopy and plot Mitotracker Green signal intensities across lines (yellow in the images below) running parallel to the main axes of individual mitochondria (Figures 3-4B-3-4E). These plots demonstrate peaks corresponding to cristae of about 20 nm width and valleys of about 20 nm width.

Additionally, we can observe cristae restructuring in individual, even highly-fragmented, mitochondria on the timescale of seconds (Figure 3-4F). This initial experimental approach lacks certainty regarding the protein expression status of Drp1 and Opa1 in any individual cell imaged; however, these data are initial proof that this imaging can be performed. As mentioned above, the ideal setup for these experiments would be to instantaneously deplete Opa1 from the cell and image mitochondria as fission progresses. This could be achieved using a degron system, but Opa1 is localized to the mitochondrial inner membrane within cristae and the intermembrane space, so degron components would have to be targeted accordingly. Alternatively, mitochondria could be imaged very shortly after treatment with an Opa1 inhibitor. All known functions of Opa1 require its GTPase activity [111], and thus inhibitors that interfere with the Opa1 GTPase domain could effectively prevent Opa1 activity almost instantaneously. We used the Opa1 inhibitor MYLS22 to inhibit Opa1 and found it prevents colony formation of KP LUAD. We therefore predict that if MYLS22 inhibits Opa1 GTPase function, it could be used to prevent Opa1 action and image cristae structure at sites of fission.

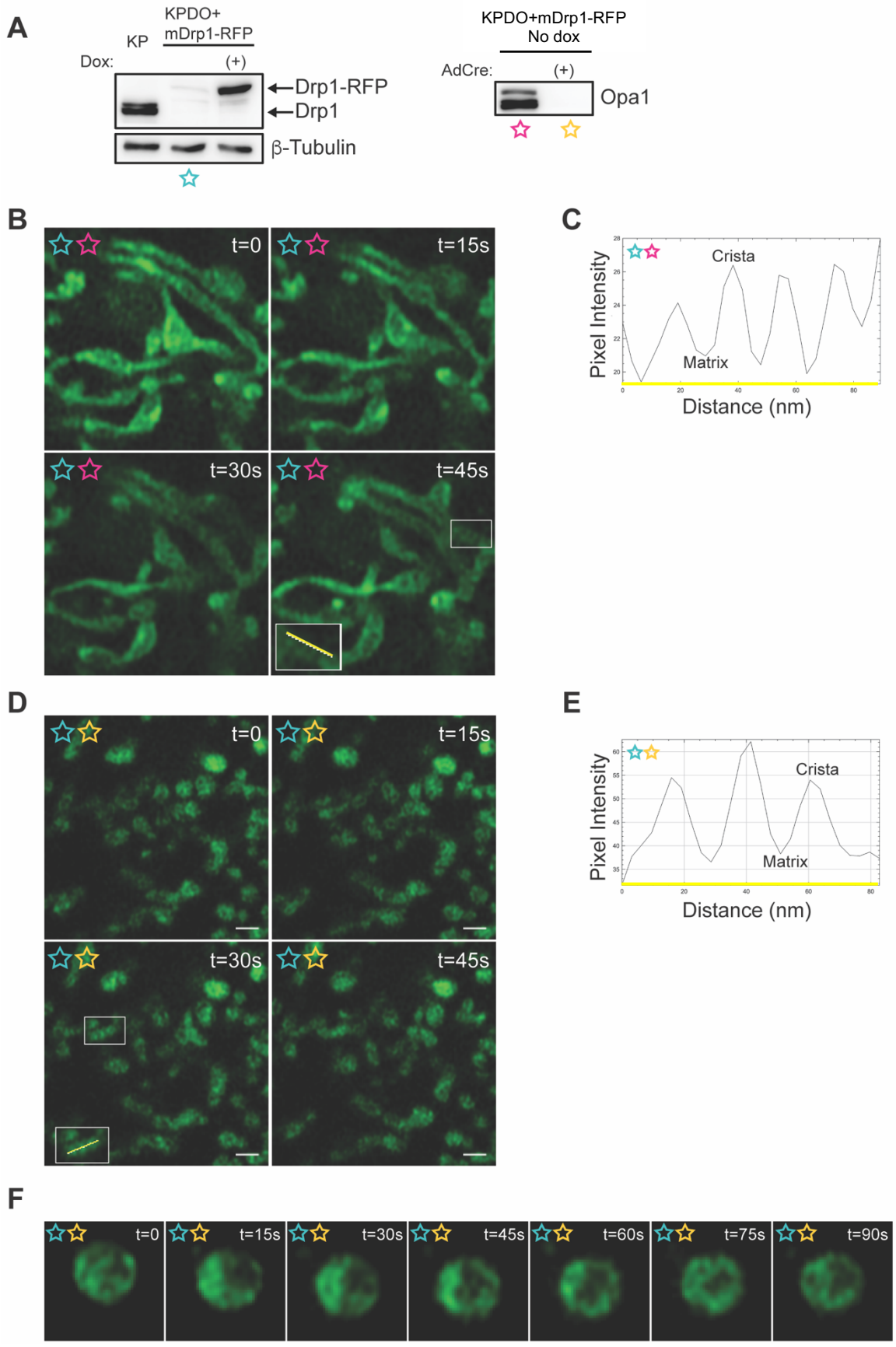
A
KP
KPDO+
mDrp1-RFP
Dox:
(+)
Drp1-RFP
Drp1
β-Tubulin
KPDO+mDrp1-RFP
No dox
AdCre:
(+)
Opa1
B
t=0
t=15s
t=30s
t=45s
C
Crista
Matrix
Pixel Intensity
Distance (nm)
D
t=0
t=15s
t=30s
t=45s
E
Crista
Matrix
Pixel Intensity
Distance (nm)
F
t=0
t=15s
t=30s
t=45s
t=60s
t=75s
t=90s

Figure 3-4. Airyscan imaging of cristae reorganization in live KPDO LUAD cells

A. (Left) Immunoblot of Drp1 expression in KP and KPDO cells (left). KP serve as endogenous Drp1 expression control. KPDO cells deleted Drp1 *in vivo,* but retained Opa1, and were transduced with inducible mDrp1-RFP. Dox = 2 ug/mL for 24 hrs. (Right) Opa1 expression in non-doxycycline-treated KPDO mDrp1-RFP cells with or without AdCre treatment. Colored stars indicate conditions used in imaging panels. All cells imaged are non-dox-treated KPDO mDrp1-RFP cells. The only distinction between sets of imaged cells is AdCre treatment.

B. Timelapse of individual mitochondria within a single subcellular frame of a Mitotracker Green-stained non-doxycycline-treated KPDO mDrp1-RFP cell without AdCre infection. Yellow line at t=45s indicates line used for intensity profiling across a single mitochondrion (plot shown in C).

C. Pixel intensity plot of the yellow line from B. Intensity maxima occur at individual cristae, intensity minima occur in the matrix separating cristae.

D. Timelapse of individual mitochondria within a single subcellular frame of a Mitotracker Green-stained non-doxycycline-treated KPDO mDrp1-RFP cell infected with AdCre. Yellow line at t=30s indicates line used for intensity profiling across a single mitochondrion (plot shown in D). Scale = 100 nm.

E. Pixel intensity plot of the yellow line from D. Intensity maxima occur at individual cristae, intensity minima occur in the matrix separating cristae.

F. Timelapse of one single mitochondrion within an AdCre-infected and Mitotracker Green-stained non-doxycycline-treated KPDO mDrp1-RFP cell.

Live-cell cristae monitoring also has the potential to illuminate the intriguing relationship between fission, Opa1 proteolytic processing, and cristae dynamics. Opa1 exists in many protein isoforms; the two IMM-embedded “long” isoforms (isoforms a and b) result from translation of differentially spliced mRNA isoforms 7 and 1, respectively, and harbor cleavage sites at which inner mitochondrial membrane proteases Oma1 or YME1L act (Figure 3-5A). Cleavage of the two long isoforms generates three intermembrane space-soluble “short” isoforms (isoforms c, d, and e) and results in five isoforms present in many cell types (Figure 3-5B). YME1L promotes basal mitochondrial proteostasis through cleavage of IMM proteins including Opa1 protein isoform a [233] and YME1L-mediated Opa1 cleavage is stimulated by hypoxia and nutrient stress [234, 235]. Oma1 cleaves both a and b long isoforms at S1 sites into c and e isoforms under conditions of stress, including respiratory inhibition by ETC inhibitors CCCP or oligomycin [236] and under oxidative stress [110]. Interestingly, Opa1 is also cleaved by Oma1 when Drp1 is knocked down or deleted [92]. The exact functions that long and short isoforms of Opa1 perform are controversial and there is no indication that the functions of one long isoform differ from those of another long isoform, or those of one short isoform from another short isoform. Expression of only the long isoform preserves mitochondrial fusion, mtDNA maintenance, and mitochondrial energetics [109–111, 237]. The functions of short isoforms of Opa1 are less certain, as some indicate that cells expressing short isoforms alone are incapable of fusion whereas others indicate short forms are sufficient for fusion [238]. In general, it appears that to exogenously reconstitute complete Opa1 function, both Opa1 long and short forms must be expressed in cells [111, 112], highlighting the importance of regulating Opa1 proteolytic cleavage.

It was recently proposed that Drp1 knockout-induced Oma1 cleavage of Opa1 acts as a mechanism to prevent mitochondrial hyperfusion associated with decreased ETC function

[239]. Given our findings that Drp1 and Opa1 interact by regulating cristae structure and ETC function, we question whether Drp1 deletion promotes Opa1 cleavage as a mechanism to avoid cristae disruption and ETC failure, as opposed to its effects on gross mitochondrial morphology. To address this possibility, we propose to assess the effects of Drp1 deletion on cristae structure and remodeling and ETC function in cells expressing long-only Opa1 that cannot be cleaved by Opa1. To confirm whether any effects of Drp1 deletion in these cells are mediated Drp1 enzymatic function, expression of $Drp1^{K38A}$ could be introduced and phenotypes monitored for rescue.

To approach these questions, we first assessed whether Opa1 isoform abundance is affected by Drp1 deletion in KP cells. We found that KPD MEFs demonstrate increased abundance of short Opa1 protein isoform c compared to KP MEFs in three independent cell lines per genotype (Figure 3-5C). We also confirmed this effect in two KP and two KPD independent mouse LUAD cell lines (Figure 3-5D). We then used mixed-population CRISPR-mediated Oma1 deletion to evaluate whether the increased abundance of short Opa1 isoform c in two independent KPD LUAD cell lines is generated by Oma1. We found that Oma1 deletion substantially reduces the abundance of Opa1 isoform c, but does not completely eliminate it (Figure 3-5E). It is unclear why short Opa1 isoform c expression is not completely abolished by Oma1 deletion in KPD LUAD, when Oma1 deletion completely eliminates this isoform in clonal SV40 large T antigen-immortalized MEFs [110]. It is possible that a small population of Oma1-targeted CRISPR cells retained Oma1 in the mixed population, although the knockout efficiency was robust, or that the cells required more time to completely eliminate already-synthesized Oma1 following gene deletion. Alternatively, it is possible that Opa1 processing is somehow modified in lung-derived cells or by oncogenic KRas signaling and generates Opa1 isoform c independent of Oma1.

To assess whether constitutive expression of long Opa1 in Drp1-null KP LUAD affects cristae dynamics and ETC function, we propose to express uncleavable long Opa1 in KPD LUAD. We will do this by expressing long Opa1 derived from mRNA isoform 1 (Iso1) with deletion of the 10 amino acids surrounding the Oma1 cleavage site (Iso1ΔS1, Figure 3-5F). We generated this construct and expressed it in KPO LUAD to confirm that upon AdCre deletion of endogenous Opa1, the transgene is expressed as constitutively long Opa1 and does not generate the normal distribution in Opa1 isoform abundance (Figure 3-5G). We will introduce this Opa1 construct into KPDO tumor cells that retained Opa1 and Drp1 in vivo and additionally express empty vector, mDrp1^{WT}, or mDrp1^{K38A}. Acute AdCre infection of these cells will delete endogenous Drp1 and Opa1 and leave only uncleavable Opa1 along with no Drp1, wildtype Drp1, or fission-defective Drp1^{K38A}. These cells will then be used for live cell cristae imaging and ETC function analysis. Our hypothesis is that expression of long-only Opa1 in cells lacking mitochondrial fission will promote cristae dysmorphism and inhibit ETC function.

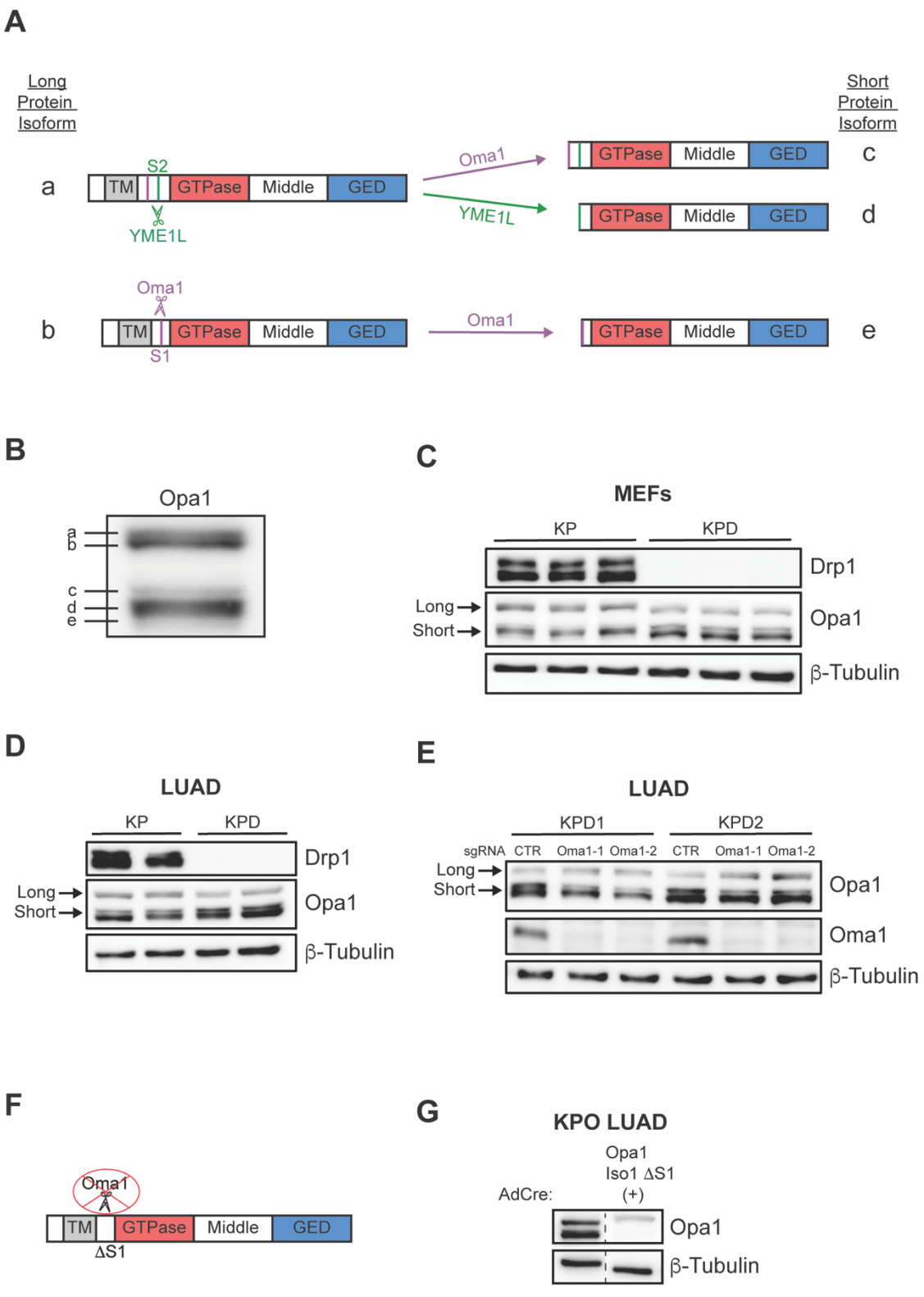
A
Long Protein Isoform
Short Protein Isoform
a
S2
TM
GTPase
Middle
GED
YME1L
Oma1
YME1L
c
d
b
Oma1
S1
Oma1
e
B
Opa1
a
b
c
d
e
C
MEFs
KP
KPD
Drp1
Long
Short
Opa1
β-Tubulin
D
LUAD
KP
KPD
Drp1
Long
Short
Opa1
β-Tubulin
E
LUAD
KPD1
KPD2
sgRNA
CTR
Oma1-1
Oma1-2
CTR
Oma1-1
Oma1-2
Long
Short
Opa1
Oma1
β-Tubulin
F
Oma1
TM
GTPase
Middle
GED
ΔS1
G
KPO LUAD
Opa1
Iso1 ΔS1
AdCre:
(+)
Opa1
β-Tubulin

Figure 3-5. Drp1 deletion induces Oma1-mediated cleavage of Opa1

A. Schematic of Opa1 protein isoforms. Long protein isoform a harbors S1 (Oma1-targeted) and S2 (YME1L-targeted) cleavage sites. Long protein isoform a yields short protein isoform c when cleaved by Oma1 and isoform d when cleaved by YME1L. Long protein isoform b harbors only the S1 Oma1 cleavage site and yields short isoform e when cleaved.

B. Example of Opa1 immunoblot demonstrating isoform distribution in KP MEFs with individual protein isoforms labeled.

C. Drp1 and Opa1 immunoblots in 3 independent KP and 3 independent KPD MEF cell lines.

D. Drp1 and Opa1 immunoblots in 2 independent KP and 2 independent KPD LUAD cell lines.

E. Opa1 and Oma1 immunoblots in 2 independent KPD LUAD cell lines with control sgRNA (sgCTR) or one of two independent Oma1-targeting sgRNAs.

F. Schematic of Opa1 protein isoform b with Oma1 cleavage site deleted (ΔS1). Protein isoform b is translated from Opa1 mRNA isoform 1 and thus this protein is referred to as Opa1 Iso1ΔS1. Deletion of Oma1 cleavage site yields an IMM-embedded long-only Opa1 isoform.

G. Opa1 Immunoblot in KPO LUAD cells that are untreated (left) or treated with AdCre and expressing Opa1 Iso1ΔS1. Images have been stitched together from same original blot, from which intervening lanes were removed.

3.2.5 Effects of KRas-driven Drp1 activity on Opa1 cleavage

The work outlined in Chapter 2 of this dissertation demonstrates a functional relationship between Drp1 and Opa1 that affects cristae structure and ETC function. Mitochondrial fission is hyperactivated by KRas signaling through Erk2-mediated phosphorylation of Drp1 on serine 616. As demonstrated in Section 3.2.4 and Figure 3-5, Drp1 *deletion* results in increased Oma1-mediated cleavage of long Opa1 to short Opa1; however, it is unknown whether Ras-mediated Drp1 *hyperactivation* affects Opa1 cleavage. Investigation of whether oncogenic KRas signaling affects Opa1 processing and function through activation of Drp1 would provide a broader understanding of how mitochondrial fusion and fission dynamics are orchestrated by cancer signaling.

To broadly assess whether KRas mutation status affects Opa1 cleavage, Opa1 isoform distribution should be assessed in KRas wildtype and mutant cells of shared background. Introduction of oncogenic KRas into cell types including MEFs and 293T would allow easy assessment of Opa1 isoforms in cells with or without oncogenic Ras. Conversely, the $Kras^{G12D}$ allele in KP mouse LUAD could be CRISPR-inactivated using a guide RNA targeting the mutant allele. Although this allele varies from wildtype by just one nucleotide, the nucleotide is immediately downstream of the CRISPR PAM site, which may offer greater specificity for the mutant allele than if the nucleotide were more downstream. Alternatively, MAPK inhibitors like the MEK inhibitor trametinib could be used to determine whether MAPK activity affects Opa1 isoform distribution. If hyperactive MAPK signaling does affect Opa1 isoform distribution, we could identify whether phosphorylation of Drp1 at the known Erk2 phosphorylation site, S616, by using mutants at this residue. Because Drp1 deletion leads to conversion of long Opa1 to short Opa1, we anticipate that activation of Drp1 by phosphorylation at S616 would have the opposite effect. We hypothesize that cells with hyperactive fission driven by Drp1 S616 phosphorylation would demonstrate an

increased long Opa1:short Opa1 ratio than those without hyperactive fission. We therefore predict that the Opa1 isoform distribution in cells expressing phosphomimetic Drp1 S616D would have higher long Opa1:short Opa1 compared to wildtype Drp1-expressing cells. Conversely, we predict that cells with phospho-dead Drp1 S616A will demonstrate decreased long Opa1:short Opa1 compared to cells expressing wildtype or S616D Drp1. To date, long Opa1 seems to be more functional than short Opa1 in reconstituting the functions of endogenous Opa1 that exists as a mixture of the two. If the mechanism outlined above exists, Drp1 activation by MAPK signaling would be coupled with increased ratio of long Opa1:short Opa1 that may have implications for Opa1 function.

3.2.6 Identify whether pharmacological Opa1 inhibition is therapeutic for LUAD

We found that KP LUAD tumor cell growth is inhibited by the first-in-class Opa1 inhibitor, MYLS22. Mechanistic evaluation in KP LUAD revealed that Opa1 inhibition causes ETC disassembly and dysfunction of NADH oxidation in a Drp1-dependent manner. Additionally, Opa1 deletion-mediated inhibition of mitochondrial NAD^+ regeneration sensitized cells to inhibition of cytoplasmic NAD^+ regeneration through lactate dehydrogenase A (LDHA). This suggests that under conditions of ETC inhibition, cells shift the burden of NAD^+ regeneration from the ETC to the cytoplasm. Recent work has found that pharmacologic LDHA inhibition increases mitochondrial metabolism, which, along with our work, indicates that a switch in the compartment responsible for NAD^+ regeneration can be bidirectional [206, 240]. Additionally, simultaneous inhibition of ETC function and LDHA has the greatest anti-tumor effect. Together, these studies make it critical to explore whether Opa1 inhibition alone or in combination with LDHA inhibition is a viable therapeutic strategy for targeting tumors with fission-activating mutations in MAPK components.

NADH must be oxidized to allow oxidative synthesis of critical metabolites to continue. Oxidation of glucose in the cytoplasm by glycolysis generates NADH that must be oxidized to allow further rounds of glycolysis, whereas mitochondrial NADH must be regenerated to allow further rounds of oxidative metabolism by the Krebs cycle. Glycolysis-derived NADH is oxidized to NAD^+ through LDHA, which transfers electrons from NADH to pyruvate to regenerate NAD^+ and form lactate that is excreted from the cell. Alternatively, glycolytic NADH can donate electrons to the malate-aspartate shuttle (MAS) or glycerol 3-phosphate shuttle (G3PS) that both transfer electrons from cytosolic NADH to the mitochondrial electron transport chain to regenerate cytosolic NAD^+ and promote mitochondrial ATP synthesis; however, the MAS and G3PS differ in the pathway of electron movement. The MAS proceeds in one direction by NADH-mediated reduction of cytosolic oxaloacetate to malate that moves into the mitochondrial matrix via the malate-alphaketoglutarate antiporter. Once in the matrix, malate is oxidized back to oxaloacetate and generates NADH that is then oxidized by ETC complex I. Conversely, the G3PS proceeds by cytosolic NADH-mediated reduction of dihydroxyacetone phosphate (DHAP) into glycerol 3-phosphate. Glycerol 3-phosphate then directly donates electrons to coenzyme Q of the ETC and thus does not generate electron carriers in the mitochondrial matrix. Recent work proposed that the Warburg effect, or oxidation of glucose to lactate under aerobic conditions, is driven by saturation of the MAS and G3PS that then necessitates cytosolic NADH oxidation by LDHA [241]. The rate of ETC-mediated regeneration of NAD^+ is limited by the flux of electrons through the ETC and eventual deposition onto oxygen. Any perturbation of ETC electron flux should therefore limit activity of ETC-requiring NADH oxidation pathways such as the MAS, G3PS, and ETC complex I.

Our work demonstrates Opa1 deletion-mediated and fission-dependent ETC disassembly and respiratory collapse in KP LUAD. We also find that Opa1-deleted cells demonstrate decreased cell viability compared to Opa1-expressing cells when treated with the LDHA inhibitor GNE-140. We interpret these data as a shift of NAD^+ regeneration burden from the mitochondrial ETC to cytoplasmic LDHA under conditions of Opa1 deletion. To assess whether Opa1 deletion affects the path of NADH-derived electrons, we should perform LDHA, G3PS, and MAS flux analyses as recently described [241]. Because the MAS translocates NADH-derived electrons across the IMM independent of the ETC, whereas the G3PS directly loads electrons into the ETC, we hypothesize that Opa1 deletion-mediated ETC dysfunction will cause mitochondrial NADH-derived electrons to flow through the MAS, but not G3PS, in reverse relative to those from cytosolic NADH-derived electrons. In order for electrons to flow in reverse through the G3PS, ETC complex I would have to oxidize NADH and then reduce ubiquinone, which would have to then reduce DHAP. Because our results demonstrate severely decreased complex I function under Opa1 deletion, this avenue is likely unavailable to excess NADH-derived electrons. Additionally, we anticipate that the flux through LDH will be substantially increased as it would be required to directly or indirectly oxidize both cytosolic- and mitochondrial-derived NADH.

LDH exists as two isoenzymes, encoded by *LDHA* and *LDHB*. LDHA catalyzes the conversion of pyruvate to lactate and regenerates NAD^+, whereas LDHB catalyzes the opposite reaction. Each isoenzyme is required for oncogenic KRas-driven LUAD tumorigenesis [242–244]. Human lung tumors uptake environmental lactate *in vivo* through the MCT1 transporter, convert it to pyruvate through LDHB, and channel lactate-derived pyruvate into mitochondria for oxidative biosynthesis [37, 245]. This pathway provides the cell with carbon that it uses to synthesize metabolites, but requires NAD^+ for

the initial conversion of lactate to pyruvate. In lung tumor cells with systems capable of efficiently regenerating NAD^+, lactate is therefore an important fuel source; however, it is uncertain whether ETC dysfunction, specifically by Opa1 deletion, makes use of environmental lactate deleterious. It would be very interesting to assess how pharmacologic Opa1 inhibition affects KP LUAD growth *in vivo* alone and in combination with either LDHA inhibition or LDHB inhibition. We hypothesize that, as *in vitro*, LDHA inhibition combined with Opa1 inhibition will inhibit tumor growth *in vivo.* Additionally, inhibition of LDHB may somewhat rescue tumor growth from Opa1 deletion if LDHB-mediated NADH synthesis is a significant sink of NAD^+ *in vivo*. Because most human lung tumors are identified at late stage, it would be appropriate to assess whether Opa1 inhibition alone or in combination with LDHA inhibition, slows or prevents growth of already-formed tumors. To assess this, tumors should be established using the KP GEMM or with orthotopic transplantation, and treatment should be initiated after tumors have already formed.

Overall, these studies will elucidate how Opa1 deletion affects which machineries manage NADH-derived electron burden and how Opa1 deletion combined with LDH inhibition affects tumor growth *in vivo*.

3.3 Concluding Remarks

Lung adenocarcinomas are devastating tumors with enormous global mortality. Understanding LUAD genetics and how frequent driver mutations, such as those in *KRAS,* affect cellular metabolism will reveal novel future therapeutic avenues to treat those with this cancer. Mitochondria are the central metabolic regulators of cells and their fusion-fission dynamics can have powerful, and as we demonstrate, reciprocal, effects on their function. Recent advances in our knowledge of mitochondrial function coupled with

technical advances such as super resolution live-cell microscopy of individual organelles makes studying how mitochondrial dynamics affect each other and tumor cells incredibly exciting and yields previously unattainable discoveries. Ultimately, leveraging the effects of oncogenic signaling on mitochondrial dynamics may prove to be efficacious, but requires understanding of how dynamics processes affect each other and of how dynamics vary between tissues.

3.4 Materials and Methods:

Native PAGE + Complex IV in-gel activity assay

Native PAGE was performed on mitochondrial isolates as described in the Methods section of chapter 2. For complex IV in-gel activity assay, gels were incubated in 50 mM sodium phosphate buffer pH 7.2 + 0.05 mM cytochrome C + 2.3 mM diaminobenzidine at room temperature for 2 hours. After incubation, reaction was stopped by switching buffer for 10% acetic acid and gels were imaged.

Native PAGE immunoblot:

Native PAGE was performed on mitochondrial isolates as described in the Methods section of chapter 2. Gels were denatured in transfer buffer supplemented with 0.25% SDS on a shaker for 1 hour at RT before transfer to PVDF membrane, block in 5% milk TBST, and antibody probing.

Super resolution live-cell imaging of cristae dynamics:

Cells were seeded in coverslip-thin glass wells and adhered overnight. The next day, cells were stained with 150 nM Mitotracker Green for 1 hour at 37C in standard medium before being rinsed in PBS and having media replaced with DMEM no phenol red + 1% FBS. Imaging was performed on Zeiss LSM 900 or 980 (Keck Center). Airyscan imaging was

performed and Airyscan was set to maximize resolution. Imaging parameters: 63X or 100X objective, laser power 0.5-2%, digital gain 850-900V, digital zoom 8-10x, scanning time/pixel 4-9 μs, time series 15-30s/image. Image processing: background subtraction in FIJI = rolling ball filter (50 pixels)

References:

1. Murphy SL, Xu J, Kochanek KD, Arias E (2021) Mortality in the United States, 2020
2. Richardson L, Dowling N, Henley J (2022) An Update on Cancer Deaths in the United States. cdc.gov/cancer/dcpc/research/update-on-cancer-deaths/index.htm. Accessed 29 Mar 2022
3. WHO (2020) The top 10 causes of death
4. NIH NCI Adenocarcinoma of the lung and bronchus SEER Explorer
5. Greulich H (2010) The genomics of lung adenocarcinoma: Opportunities for targeted therapies. Genes and Cancer 1:1200–1210. https://doi.org/10.1177/1947601911407324
6. cBioPortal Lung Adenocarcinoma
7. Friedman PN, Chen X, Bargonetti J, Prives C (1993) The p53 protein is an unusually shaped tetramer that binds directly to DNA. Proc Natl Acad Sci U S A 90:3319–3323. https://doi.org/10.1073/pnas.90.8.3319
8. El-Deiry WS, Kern SE, Pietenpop JA, et al (1992) Definition of a consensus binding site for p53. Nature 1:45–49
9. Midthun D (2021) Overview of the initial treatment and prognosis of lung cancer. In: UpToDate
10. Gonzalez-Rajal A, Hastings JF, Watkins DN, et al (2020) Breathing New Life into the Mechanisms of Platinum Resistance in Lung Adenocarcinoma. Front Cell Dev Biol 8:1–6. https://doi.org/10.3389/fcell.2020.00305
11. Soria J-C, Ohe Y, Vansteenkiste J, et al (2018) Osimertinib in Untreated EGFR - Mutated Advanced Non–Small-Cell Lung Cancer . N Engl J Med 378:113–125. https://doi.org/10.1056/nejmoa1713137
12. Kohl NE, Mosser SD, DeSolms SJ, et al (1993) Selective inhibition of ras-dependent transformation by a farnesyltransferase inhibitor. Science (80-) 260:1934–1937. https://doi.org/10.1126/science.8316833
13. Ostrem JM, Peters U, Sos ML, et al (2013) K-Ras(G12C) inhibitors allosterically control GTP affinity and effector interactions. Nature 503:548–551. https://doi.org/10.1038/nature12796
14. West H (2021) Management of advanced non-small cell lung cancer lacking a driver mutation: Immunotherapy. In: UpToDate
15. Roller DG, Hoang SA, Rawls KD, et al (2021) Validation of a multicellular tumor microenvironment system for modeling patient tumor biology and drug response. Sci Rep 11:1–15. https://doi.org/10.1038/s41598-021-84612-z
16. THEODORE T. PUCK, PH.D., PHILIP I. MARCUS ASJC (1956) CLONAL GROWTH PLATzS 10 TO 12 (Received for publication , October 17 , 1955) The conventional methods available for routine growth of animal ceils in vitro demand the presence of a large cell population in order that sustained multiplication be initiate. J Exp Med 103:273–284
17. Benton G, Kleinman HK, George J, Arnaoutova I (2011) Multiple uses of basement membrane-like matrix (BME/Matrigel) in vitro and in vivo with cancer cells. Int J Cancer 128:1751–1757. https://doi.org/10.1002/ijc.25781
18. Han K, Pierce SE, Li A, et al (2020) CRISPR screens in cancer spheroids identify 3D growth-specific vulnerabilities. Nature 580:136–141. https://doi.org/10.1038/s41586-020-2099-x
19. Lagziel S, Gottlieb E, Shlomi T (2020) Mind your media. Nat Metab 2:1369–1372. https://doi.org/10.1038/s42255-020-00299-y
20. Yoshida K, Gowers KHC, Lee-Six H, et al (2020) Tobacco smoking and somatic mutations in human bronchial epithelium. Nature 578:266–272.

https://doi.org/10.1038/s41586-020-1961-1
21. DuPage M, Dooley AL, Jacks T (2009) Conditional mouse lung cancer models using adenoviral or lentiviral delivery of Cre recombinase. Nat Protoc 4:1064–1072. https://doi.org/10.1038/nprot.2009.95
22. Chung WJ, Daemen A, Cheng JH, et al (2017) Kras mutant genetically engineered mouse models of human cancers are genomically heterogeneous. Proc Natl Acad Sci U S A 114:E10947–E10955. https://doi.org/10.1073/pnas.1708391114
23. Racker E, Resnick RJ, Feldman R (1985) Glycolysis and methylaminoisobutyrate uptake in rat-1 cells transfected with ras or myc oncogenes. Proc Natl Acad Sci U S A 82:3535–3538. https://doi.org/10.1073/pnas.82.11.3535
24. Chiaradonna F, Sacco E, Manzoni R, et al (2006) Ras-dependent carbon metabolism and transformation in mouse fibroblasts. Oncogene 25:5391–5404. https://doi.org/10.1038/sj.onc.1209528
25. Gaglio D, Metallo CM, Gameiro PA, et al (2011) Oncogenic K-Ras decouples glucose and glutamine metabolism to support cancer cell growth. Mol Syst Biol 7:1–15. https://doi.org/10.1038/msb.2011.56
26. Schell JC, Olson KA, Jiang L, et al (2014) A role for the mitochondrial pyruvate carrier as a repressor of the warburg effect and colon cancer cell growth. Mol Cell 56:400–413. https://doi.org/10.1016/j.molcel.2014.09.026
27. Christofk HR, Vander Heiden MG, Harris MH, et al (2008) The M2 splice isoform of pyruvate kinase is important for cancer metabolism and tumour growth. Nature 452:230–233. https://doi.org/10.1038/nature06734
28. Weinberg F, Hamanaka R, Wheaton WW, et al (2010) Mitochondrial metabolism and ROS generation are essential for Kras-mediated tumorigenicity. Proc Natl Acad Sci U S A 107:8788–8793. https://doi.org/10.1073/pnas.1003428107
29. Birsoy K, Wang T, Chen WW, et al (2015) An Essential Role of the Mitochondrial Electron Transport Chain in Cell Proliferation Is to Enable Aspartate Synthesis. Cell 162:540–551. https://doi.org/10.1016/j.cell.2015.07.016
30. Alkan HF, Walter KE, Luengo A, et al (2018) Cytosolic Aspartate Availability Determines Cell Survival When Glutamine Is Limiting. Cell Metab 28:706-720.e6. https://doi.org/10.1016/j.cmet.2018.07.021
31. Sullivan LB, Gui DY, Hosios AM, et al (2015) Supporting Aspartate Biosynthesis Is an Essential Function of Respiration in Proliferating Cells. Cell 162:552–563. https://doi.org/10.1016/j.cell.2015.07.017
32. Garcia-Bermudez J, Baudrier L, La K, et al (2018) Aspartate is a limiting metabolite for cancer cell proliferation under hypoxia and in tumours. Nat Cell Biol 20:775–781. https://doi.org/10.1038/s41556-018-0118-z
33. Gouw AM, Eberlin LS, Margulis K, et al (2017) Oncogene KRAS activates fatty acid synthase, resulting in specific ERK and lipid signatures associated with lung adenocarcinoma. Proc Natl Acad Sci U S A 114:4300–4305. https://doi.org/10.1073/pnas.1617709114
34. Ricoult S, Yecies J, Ben-Sahra I, Manning B (2016) Oncogenic PI3K and K-Ras stimulate de novo lipid synthesis through mTORC1 and SREBP. Oncogene. https://doi.org/10.1038/onc.2015.179.Oncogenic
35. Hatzivassiliou G, Zhao F, Bauer DE, et al (2005) ATP citrate lyase inhibition can suppress tumor cell growth. Cancer Cell 8:311–321. https://doi.org/10.1016/j.ccr.2005.09.008
36. Chen PH, Cai L, Huffman K, et al (2019) Metabolic Diversity in Human Non-Small Cell Lung Cancer Cells. Mol Cell 76:838-851.e5. https://doi.org/10.1016/j.molcel.2019.08.028

37. Hensley CT, Faubert B, Yuan Q, et al (2016) Metabolic Heterogeneity in Human Lung Tumors. Cell 164:681–694. https://doi.org/10.1016/j.cell.2015.12.034
38. Sullivan MR, Danai L V., Lewis CA, et al (2019) Quantification of microenvironmental metabolites in murine cancers reveals determinants of tumor nutrient availability. Elife 8:1–27. https://doi.org/10.7554/eLife.44235
39. Mayers JR, Torrence ME, Danai L V., et al (2016) Tissue of origin dictates branched-chain amino acid metabolism in mutant Kras-driven cancers. Science (80-) 353:1161–1165. https://doi.org/10.1126/science.aaf5171
40. Davidson SM, Papagiannakopoulos T, Olenchock BA, et al (2016) Environment impacts the metabolic dependencies of ras-driven non-small cell lung cancer. Cell Metab 23:517–528. https://doi.org/10.1016/j.cmet.2016.01.007
41. Nakano K, Vousden KH (2001) PUMA, a novel proapoptotic gene, is induced by p53. Mol Cell 7:683–694. https://doi.org/10.1016/S1097-2765(01)00214-3
42. Oda E, Ohki R, Murasawa H, et al (2000) Noxa, a BH3-only member of the Bcl-2 family and candidate mediator of p53-induced apoptosis. Science (80-) 288:1053–1058. https://doi.org/10.1126/science.288.5468.1053
43. Wolff S, Erster S, Palacios G, Moll UM (2008) p53's mitochondrial translocation and MOMP action is independent of Puma and Bax and severely disrupts mitochondrial membrane integrity. Cell Res 18:733–744. https://doi.org/10.1038/cr.2008.62
44. Mihara M, Erster S, Zaika A, et al (2003) P53 Has a Direct Apoptogenic Role At the Mitochondria. Mol Cell 11:577–590. https://doi.org/10.1016/S1097-2765(03)00050-9
45. Werth JL, Thayer SA (1994) Mitochondria buffer physiological calcium loads in cultured rat dorsal root ganglion neurons. J Neurosci 14:348–356. https://doi.org/10.1523/jneurosci.14-01-00348.1994
46. Jouaville LS, Pinton P, Bastianutto C, et al (1999) Regulation of mitochondrial ATP synthesis by calcium: Evidence for a long-term metabolic priming. Proc Natl Acad Sci U S A 96:13807–13812. https://doi.org/10.1073/pnas.96.24.13807
47. Tarasov AI, Griffiths EJ, Rutter GA (2012) Regulation of ATP production by mitochondrial Ca2+. Cell Calcium 52:28–35. https://doi.org/10.1016/j.ceca.2012.03.003
48. Orrenius S, Zhivotovsky B, Nicotera P (2003) Regulation of cell death: The calcium-apoptosis link. Nat Rev Mol Cell Biol 4:552–565. https://doi.org/10.1038/nrm1150
49. De Stefani D, Raffaello A, Teardo E, et al (2011) A forty-kilodalton protein of the inner membrane is the mitochondrial calcium uniporter. Nature 476:336–340. https://doi.org/10.1038/nature10230
50. Baughman JM, Perocchi F, Girgis HS, et al (2011) Integrative genomics identifies MCU as an essential component of the mitochondrial calcium uniporter. Nature 476:341–345. https://doi.org/10.1038/nature10234
51. Friel DD, Tsien RW (1994) An FCCP-sensitive Ca2+ store in bullfrog sympathetic neurons and its participation in stimulus-evoked changes in [Ca2+](i). J Neurosci 14:4007–4024. https://doi.org/10.1523/jneurosci.14-07-04007.1994
52. Rizzuto R, Pinton P, Carrington W, et al (1998) Close contacts with the endoplasmic reticulum as determinants of mitochondrial Ca2+ responses. Science (80-) 280:1763–1766. https://doi.org/10.1126/science.280.5370.1763
53. Danese A, Patergnani S, Bonora M, et al (2017) Calcium regulates cell death in cancer: Roles of the mitochondria and mitochondria-associated membranes (MAMs). Biochim Biophys Acta - Bioenerg 1858:615–627. https://doi.org/10.1016/j.bbabio.2017.01.003

54. De Brito OM, Scorrano L (2008) Mitofusin 2 tethers endoplasmic reticulum to mitochondria. Nature 456:605–610. https://doi.org/10.1038/nature07534
55. Kaufman B, Durisic N, Mativetsky J, et al (2007) The Mitochondrial Transcription Factor TFAM Coordinates the Assembly of Multiple DNA Molecules into Nucleoid-like Structures. Mol Biol Cell 18:3250–3263. https://doi.org/10.1091/mbc.E07
56. Kukat C, Davies KM, Wurm CA, et al (2015) Cross-strand binding of TFAM to a single mtDNA molecule forms the mitochondrial nucleoid. Proc Natl Acad Sci U S A 112:11288–11293. https://doi.org/10.1073/pnas.1512131112
57. Garrido N, Gripaaric L, Jokitalo E, et al (2003) Composition and Dynamics of Human Mitochondrial Nucleoids. Mol Biol Cell 13:4100–4109. https://doi.org/10.1091/mbc.E02
58. Ojala D, Montoya J, Attardi G (1981) tRNA punctuation model of RNA processing in human mitochondria. Nature 470–474
59. Ali AT, Boehme L, Carbajosa G, et al (2019) Nuclear genetic regulation of the human mitochondrial transcriptome. Elife 8:1–23. https://doi.org/10.7554/eLife.41927
60. Grasso C, Eccles DA, Boukalova S, et al (2020) Mitochondrial DNA Affects the Expression of Nuclear Genes Involved in Immune and Stress Responses in a Breast Cancer Model. Front Physiol 11:1–12. https://doi.org/10.3389/fphys.2020.543962
61. Fetterman JL, Ballinger SW (2019) Mitochondrial genetics regulate nuclear gene expression through metabolites. Proc Natl Acad Sci U S A 116:15763–15765. https://doi.org/10.1073/pnas.1909996116
62. Acín-Pérez R, Fernández-Silva P, Peleato ML, et al (2008) Respiratory Active Mitochondrial Supercomplexes. Mol Cell 32:529–539. https://doi.org/10.1016/j.molcel.2008.10.021
63. Fedor JG, Hirst J (2018) Mitochondrial Supercomplexes Do Not Enhance Catalysis by Quinone Channeling. Cell Metab 28:525-531.e4. https://doi.org/10.1016/j.cmet.2018.05.024
64. Blum TB, Hahn A, Meier T, et al (2019) Dimers of mitochondrial ATP synthase induce membrane curvature and self-assemble into rows. Proc Natl Acad Sci U S A 116:4250–4255. https://doi.org/10.1073/pnas.1816556116
65. Paumard P (2002) The ATP synthase is involved in generating mitochondrial cristae morphology. EMBO J 21:221–230. https://doi.org/10.1093/emboj/21.3.221
66. Strauss M, Hofhaus G, Schröder RR, Kühlbrandt W (2008) Dimer ribbons of ATP synthase shape the inner mitochondrial membrane. EMBO J 27:1154–1160. https://doi.org/10.1038/emboj.2008.35
67. Cogliati S, Frezza C, Soriano ME, et al (2013) Mitochondrial cristae shape determines respiratory chain supercomplexes assembly and respiratory efficiency. Cell 155:160–171. https://doi.org/10.1016/j.cell.2013.08.032
68. Gomes LC, Benedetto G Di, Scorrano L (2011) During autophagy mitochondria elongate, are spared from degradation and sustain cell viability. Nat Cell Biol 13:589–598. https://doi.org/10.1038/ncb2220
69. Oettinghaus B, D'Alonzo D, Barbieri E, et al (2016) DRP1-dependent apoptotic mitochondrial fission occurs independently of BAX, BAK and APAF1 to amplify cell death by BID and oxidative stress. Biochim Biophys Acta - Bioenerg 1857:1267–1276. https://doi.org/10.1016/j.bbabio.2016.03.016
70. Rolland SG, Motori E, Memar N, et al (2013) Impaired complex IV activity in response to loss of LRPPRC function can be compensated by mitochondrial hyperfusion. Proc Natl Acad Sci U S A 110:. https://doi.org/10.1073/pnas.1303872110

71. Cho HM, Ryu JR, Jo Y, et al (2019) Drp1-Zip1 Interaction Regulates Mitochondrial Quality Surveillance System. Mol Cell 73:364-376.e8. https://doi.org/10.1016/j.molcel.2018.11.009
72. Lieber T, Jeedigunta SP, Palozzi JM, et al (2019) Mitochondrial fragmentation drives selective removal of deleterious mtDNA in the germline. Nature 570:380–384. https://doi.org/10.1038/s41586-019-1213-4
73. Friedman JR, Lackner LL, West M, et al (2011) ER tubules mark sites of mitochondrial division. Science (80-) 334:358–362. https://doi.org/10.1126/science.1207385
74. Ingerman E, Perkins EM, Marino M, et al (2005) Dnm1 forms spirals that are structurally tailored to fit mitochondria. J Cell Biol 170:1021–1027. https://doi.org/10.1083/jcb.200506078
75. Gandre-Babbe S, van der Bliek AM (2008) The Novel Tail-anchored Membrane Protein Mff Controls Mitochondrial and Peroxisomal Fission in Mammalian Cells. Mol Biol Cell 19:2402–2412. https://doi.org/10.1091/mbc.E07
76. Otera H, Wang C, Cleland MM, et al (2010) Mff is an essential factor for mitochondrial recruitment of Drp1 during mitochondrial fission in mammalian cells. J Cell Biol 191:1141–1158. https://doi.org/10.1083/jcb.201007152
77. Yoon Y, Krueger EW, Oswald BJ, McNiven MA (2003) The Mitochondrial Protein hFis1 Regulates Mitochondrial Fission in Mammalian Cells through an Interaction with the Dynamin-Like Protein DLP1. Mol Cell Biol 23:5409–5420. https://doi.org/10.1128/mcb.23.15.5409-5420.2003
78. James DI, Parone PA, Mattenberger Y, Martinou JC (2003) hFis1, a novel component of the mammalian mitochondrial fission machinery. J Biol Chem 278:36373–36379. https://doi.org/10.1074/jbc.M303758200
79. Palmer CS, Osellame LD, Laine D, et al (2011) MiD49 and MiD51, new components of the mitochondrial fission machinery. EMBO Rep 12:565–573. https://doi.org/10.1038/embor.2011.54
80. Kamerkar SC, Kraus F, Sharpe AJ, et al (2018) Dynamin-related protein 1 has membrane constricting and severing abilities sufficient for mitochondrial and peroxisomal fission. Nat Commun 9:. https://doi.org/10.1038/s41467-018-07543-w
81. Fonseca TB, Sánchez-Guerrero Á, Milosevic I, Raimundo N (2019) Mitochondrial fission requires DRP1 but not dynamins. Nature 570:E34–E42. https://doi.org/10.1038/s41586-019-1296-y
82. Lee JE, Westrate LM, Wu H, et al (2016) Multiple dynamin family members collaborate to drive mitochondrial division. Nature 540:139–143. https://doi.org/10.1038/nature20555
83. Kashatus JA, Nascimento A, Myers LJ, et al (2015) Erk2 phosphorylation of Drp1 promotes mitochondrial fission and MAPK-driven tumor growth. Mol Cell 57:537–551. https://doi.org/10.1016/j.molcel.2015.01.002
84. Serasinghe MN, Wieder SY, Renault TT, et al (2015) Mitochondrial division is requisite to RAS-induced transformation and targeted by oncogenic MAPK pathway inhibitors. Mol Cell 57:521–536. https://doi.org/10.1016/j.molcel.2015.01.003
85. Taguchi N, Ishihara N, Jofuku A, et al (2007) Mitotic phosphorylation of dynamin-related GTPase Drp1 participates in mitochondrial fission. J Biol Chem 282:11521–11529. https://doi.org/10.1074/jbc.M607279200
86. Chang CR, Blackstone C (2007) Cyclic AMP-dependent protein kinase phosphorylation of Drp1 regulates its GTPase activity and mitochondrial morphology. J Biol Chem 282:21583–21587. https://doi.org/10.1074/jbc.C700083200

87. Harder Z, Zunino R, McBride H (2004) Sumo1 Conjugates Mitochondrial Substrates and Participates in Mitochondrial Fission. Curr Biol 14:340–345. https://doi.org/10.1016/j.cub.2004.02.004
88. Figueroa-Romero C, Iñiguez-Lluhí JA, Stadler J, et al (2009) SUMOylation of the mitochondrial fission protein Drp1 occurs at multiple nonconsensus sites within the B domain and is linked to its activity cycle. FASEB J 23:3917–3927. https://doi.org/10.1096/fj.09-136630
89. Frank S, Gaume B, Bergmann-Leitner ES, et al (2001) The Role of Dynamin-Related Protein 1, a Mediator of Mitochondrial Fission, in Apoptosis. Dev Cell 1:515–525. https://doi.org/10.1016/S1534-5807(01)00055-7
90. Wasiak S, Zunino R, McBride HM (2007) Bax/Bak promote sumoylation of DRP1 and its stable association with mitochondria during apoptotic cell death. J Cell Biol 177:439–450. https://doi.org/10.1083/jcb.200610042
91. Parone PA, James DI, Da Cruz S, et al (2006) Inhibiting the Mitochondrial Fission Machinery Does Not Prevent Bax/Bak-Dependent Apoptosis. Mol Cell Biol 26:7397–7408. https://doi.org/10.1128/mcb.02282-05
92. Estaquier J, Arnoult D (2007) Inhibiting Drp1-mediated mitochondrial fission selectively prevents the release of cytochrome c during apoptosis. Cell Death Differ 14:1086–1094. https://doi.org/10.1038/sj.cdd.4402107
93. Otera H, Miyata N, Kuge O, Mihara K (2016) Drp1-dependent mitochondrial fission via MiD49/51 is essential for apoptotic cristae remodeling. J Cell Biol 212:531–544. https://doi.org/10.1083/jcb.201508099
94. Karbowski M, Arnoult D, Chen H, et al (2004) Quantitation of mitochondrial dynamics by photolabeling of individual organelles shows that mitochondrial fusion is blocked during the Bax activation phase of apoptosis. J Cell Biol 164:493–499. https://doi.org/10.1083/jcb.200309082
95. Ban-Ishihara R, Ishihara T, Sasaki N, et al (2013) Dynamics of nucleoid structure regulated by mitochondrial fission contributes to cristae reformation and release of cytochrome c. Proc Natl Acad Sci U S A 110:11863–11868. https://doi.org/10.1073/pnas.1301951110
96. Kageyama Y, Hoshijima M, Seo K, et al (2014) Parkin-independent mitophagy requires D rp1 and maintains the integrity of mammalian heart and brain . EMBO J 33:2798–2813. https://doi.org/10.15252/embj.201488658
97. Ikeda Y, Shirakabe A, Maejima Y, et al (2015) Endogenous Drp1 mediates mitochondrial autophagy and protects the heart against energy stress. Circ Res 116:264–278. https://doi.org/10.1161/CIRCRESAHA.116.303356
98. Shirakabe A, Zhai P, Ikeda Y, et al (2016) Drp1-dependent mitochondrial autophagy plays a protective role against pressure overload-induced mitochondrial dysfunction and heart failure. Circulation 133:1249–1263. https://doi.org/10.1161/CIRCULATIONAHA.115.020502
99. Pernaute B, Pérez-Montero S, Sánchez Nieto JM, et al (2022) DRP1 levels determine the apoptotic threshold during embryonic differentiation through a mitophagy-dependent mechanism. Dev Cell 57:1316-1330.e7. https://doi.org/10.1016/j.devcel.2022.04.020
100. Santel A, Fuller MT (2001) Control of mitochondrial morphology by a human mitofusin. J Cell Sci 114:867–874
101. Chen H, Detmer SA, Ewald AJ, et al (2003) Mitofusins Mfn1 and Mfn2 coordinately regulate mitochondrial fusion and are essential for embryonic development. J Cell Biol 160:189–200. https://doi.org/10.1083/jcb.200211046
102. Huo Y, Sun W, Shi T, et al (2022) The MFN1 and MFN2 mitofusins promote clustering between mitochondria and peroxisomes. Commun Biol 5:1–11.

https://doi.org/10.1038/s42003-022-03377-x
103. Naon D, Zaninello M, Giacomello M, et al (2016) Critical reappraisal confirms that Mitofusin 2 is an endoplasmic reticulum-mitochondria tether. Proc Natl Acad Sci U S A 113:11249–11254. https://doi.org/10.1073/pnas.1606786113
104. Olichon A, Emorine LJ, Descoins E, et al (2002) The human dynamin-related protein OPA1 is anchored to the mitochondrial inner membrane facing the inter-membrane space. FEBS Lett 523:171–176. https://doi.org/10.1016/S0014-5793(02)02985-X
105. Delettre C, Griffoin JM, Kaplan J, et al (2001) Mutation spectrum and splicing variants in the OPA1 gene. Hum Genet 109:584–591. https://doi.org/10.1007/s00439-001-0633-y
106. McQuibban GA, Saurya S, Freeman M (2003) Mitochondrial membrane remodelling regulated by a conserved rhomboid protease. Nature 423:537–541. https://doi.org/10.1038/nature01633
107. Cipolat S, Rudka T, Hartmann D, et al (2006) Mitochondrial Rhomboid PARL Regulates Cytochrome c Release during Apoptosis via OPA1-Dependent Cristae Remodeling. Cell 126:163–175. https://doi.org/10.1016/j.cell.2006.06.021
108. Ehses S, Raschke I, Mancuso G, et al (2009) Regulation of OPA1 processing and mitochondrial fusion by m-AAA protease isoenzymes and OMA1. J Cell Biol 187:1023–1036. https://doi.org/10.1083/jcb.200906084
109. Ishihara N, Fujita Y, Oka T, Mihara K (2006) Regulation of mitochondrial morphology through proteolytic cleavage of OPA1. EMBO J 25:2966–2977. https://doi.org/10.1038/sj.emboj.7601184
110. Anand R, Wai T, Baker MJ, et al (2014) The i-AAA protease YME1L and OMA1 cleave OPA1 to balance mitochondrial fusion and fission. J Cell Biol 204:919–929. https://doi.org/10.1083/jcb.201308006
111. Del Dotto V, Mishra P, Vidoni S, et al (2017) OPA1 Isoforms in the Hierarchical Organization of Mitochondrial Functions. Cell Rep 19:2557–2571. https://doi.org/10.1016/j.celrep.2017.05.073
112. Ge Y, Shi X, Boopathy S, et al (2020) Two forms of opa1 cooperate to complete fusion of the mitochondrial inner-membrane. Elife 9:1–22. https://doi.org/10.7554/eLife.50973
113. Guan K, Farh L, Marshall TK, Deschenes RJ (1993) Normal mitochondrial structure and genome maintenance in yeast requires the dynamin-like product of the MGM1 gene. Curr Genet 24:141–148. https://doi.org/10.1007/BF00324678
114. Elachouri G, Vidoni S, Zanna C, et al (2011) OPA1 links human mitochondrial genome maintenance to mtDNA replication and distribution. Genome Res 21:12–20. https://doi.org/10.1101/gr.108696.110
115. Sidarala V, Zhu J, Levi-D'Ancona E, et al (2022) Mitofusin 1 and 2 regulation of mitochondrial DNA content is a critical determinant of glucose homeostasis. Nat Commun 13:1–16. https://doi.org/10.1038/s41467-022-29945-7
116. Olichon A, Baricault L, Gas N, et al (2003) Loss of OPA1 perturbates the mitochondrial inner membrane structure and integrity, leading to cytochrome c release and apoptosis. J Biol Chem 278:7743–7746. https://doi.org/10.1074/jbc.C200677200
117. Wunderlich FT, Waisman A, Merkwirth C, et al (2008) Prohibitins control cell proliferation and apoptosis by regulating OPA1-dependent cristae morphogenesis in mitochondria. Genes Dev 22:476–488. https://doi.org/10.1101/gad.460708.derstood
118. Stephan T, Brüser C, Deckers M, et al (2020) MICOS assembly controls mitochondrial inner membrane remodeling and crista junction redistribution to

mediate cristae formation. EMBO J 39:1–24. https://doi.org/10.15252/embj.2019104105
119. Hu C, Shu L, Huang X, et al (2020) OPA1 and MICOS Regulate mitochondrial crista dynamics and formation. Cell Death Dis 11:. https://doi.org/10.1038/s41419-020-03152-y
120. Barrera M, Koob S, Dikov D, et al (2016) OPA1 functionally interacts with MIC60 but is dispensable for crista junction formation. FEBS Lett 590:3309–3322. https://doi.org/10.1002/1873-3468.12384
121. Glytsou C, Calvo E, Cogliati S, et al (2016) Optic Atrophy 1 Is Epistatic to the Core MICOS Component MIC60 in Mitochondrial Cristae Shape Control. Cell Rep 17:3024–3034. https://doi.org/10.1016/j.celrep.2016.11.049
122. Prieto J, León M, Ponsoda X, et al (2016) Early ERK1/2 activation promotes DRP1-dependent mitochondrial fission necessary for cell reprogramming. Nat Commun 7:. https://doi.org/10.1038/ncomms11124
123. Pyakurel A, Savoia C, Hess D, Scorrano L (2015) Extracellular Regulated Kinase Phosphorylates Mitofusin 1 to Control Mitochondrial Morphology and Apoptosis. Mol Cell 58:244–254. https://doi.org/10.1016/j.molcel.2015.02.021
124. Tondera D, Santel A, Schwarzer R, et al (2004) Knockdown of MTP18, a novel phosphatidylinositol 3-kinase-dependent protein, affects mitochondrial morphology and induces apoptosis. J Biol Chem 279:31544–31555. https://doi.org/10.1074/jbc.M404704200
125. Kim DI, Lee KH, Gabr AA, et al (2016) Aβ-Induced Drp1 phosphorylation through Akt activation promotes excessive mitochondrial fission leading to neuronal apoptosis. Biochim Biophys Acta - Mol Cell Res. https://doi.org/10.1016/j.bbamcr.2016.09.003
126. Agarwal E, Altman BJ, Ho Seo J, et al (2019) Myc Regulation of a Mitochondrial Trafficking Network Mediates Tumor Cell Invasion and Metastasis. Mol Cell Biol 39:. https://doi.org/10.1128/mcb.00109-19
127. Prieto J, Seo AY, León M, et al (2018) MYC Induces a Hybrid Energetics Program Early in Cell Reprogramming. Stem Cell Reports 11:1479–1492. https://doi.org/10.1016/j.stemcr.2018.10.018
128. von Eyss B, Jaenicke LA, Kortlever RM, et al (2015) A MYC-Driven Change in Mitochondrial Dynamics Limits YAP/TAZ Function in Mammary Epithelial Cells and Breast Cancer. Cancer Cell 28:743–757. https://doi.org/10.1016/j.ccell.2015.10.013
129. Toyama EQ, Herzig S, Courchet J, et al (2016) Metabolism: AMP-activated protein kinase mediates mitochondrial fission in response to energy stress. Science (80-) 351:275–281. https://doi.org/10.1126/science.aab4138
130. Xie Q, Wu Q, Horbinski CM, et al (2015) Mitochondrial control by DRP1 in brain tumor initiating cells. Nat Neurosci 18:501–510. https://doi.org/10.1038/nn.3960
131. Batlle E, Clevers H (2017) Cancer stem cells revisited. Nat. Med. 23:1124–1134
132. Beck B, Blanpain C (2013) Unravelling cancer stem cell potential. Nat. Rev. Cancer 13:727–738
133. Chen J, Li Y, Yu TS, et al (2012) A restricted cell population propagates glioblastoma growth after chemotherapy. Nature 488:522–526. https://doi.org/10.1038/nature11287
134. Hu J, Yuan X, Xu Q, et al (2012) Cancer stem cells in glioblastoma. Stem Cells Cancer Stem Cells, Vol 1 Stem Cells Cancer Stem Cells, Ther Appl Dis Inj Vol 1 113–120. https://doi.org/10.1007/978-94-007-1709-1_14
135. Dick JE, Bonnet D (1997) Human Acute Myeloid Leukaemia is organised as a heirarchy that originates from a primitive haematopoetic cell. Nat Med 3:730–737

136. Tian Y, Huang Z, Wang Z, et al (2014) Identification of novel molecular markers for prognosis estimation of acute myeloid leukemia: Over-expression of PDCD7, FIS1 and Ang2 may indicate poor prognosis in pretreatment patients with acute myeloid leukemia. PLoS One 9:5–10. https://doi.org/10.1371/journal.pone.0084150
137. Fillmore CM, Kuperwasser C (2008) Human breast cancer cell lines contain stem-like cells that self-renew, give rise to phenotypically diverse progeny and survive chemotherapy. Breast Cancer Res 10:1–13. https://doi.org/10.1186/bcr1982
138. Al-Hajj M, Wicha M, Benito-Hernandez A, et al (2003) Prospective Identification of Tumorigenic Breast Cancer Cells. Proc Natl Acad Sci 100:
139. Masciale V, Grisendi G, Banchelli F, et al (2019) Isolation and Identification of Cancer Stem-Like Cells in Adenocarcinoma and Squamous Cell Carcinoma of the Lung: A Pilot Study. Front Oncol 9:1–12. https://doi.org/10.3389/fonc.2019.01394
140. Herreros-Pomares A, de-Maya-Girones JD, Calabuig-Fariñas S, et al (2019) Lung tumorspheres reveal cancer stem cell-like properties and a score with prognostic impact in resected non-small-cell lung cancer. Cell Death Dis 10:1–14. https://doi.org/10.1038/s41419-019-1898-1
141. De Sousa E Melo F, Kurtova A V., Harnoss JM, et al (2017) A distinct role for Lgr5 + stem cells in primary and metastatic colon cancer. Nature 543:676–680. https://doi.org/10.1038/nature21713
142. O'Brien CA, Pollett A, Gallinger S, Dick JE (2007) A human colon cancer cell capable of initiating tumour growth in immunodeficient mice. Nature 445:106–110. https://doi.org/10.1038/nature05372
143. Bertolini G, Roz L, Perego P, et al (2009) Highly tumorigenic lung cancer CD133+ cells display stem-like features and are spared by cisplatin treatment. Proc Natl Acad Sci U S A 106:16281–16286. https://doi.org/10.1073/pnas.0905653106
144. Singh SK, Hawkins C, Clarke ID, et al (2004) Identification of human brain tumour initiating cells. Nature 432:396–401. https://doi.org/10.1038/nature03128
145. Prager BC, Xie Q, Bao S, Rich JN (2019) Cancer Stem Cells: The Architects of the Tumor Ecosystem. Cell Stem Cell 24:41–53
146. Shimokawa M, Ohta Y, Nishikori S, et al (2017) Visualization and targeting of LGR5 + human colon cancer stem cells. Nature 545:187–192. https://doi.org/10.1038/nature22081
147. Prigione A, Fauler B, Lurz R, et al (2010) The senescence-related mitochondrial/oxidative stress pathway is repressed in human induced pluripotent stem cells. Stem Cells 28:721–733. https://doi.org/10.1002/stem.404
148. Zhang J, Khvorostov I, Hong JS, et al (2011) UCP2 regulates energy metabolism and differentiation potential of human pluripotent stem cells. EMBO J 30:4860–4873. https://doi.org/10.1038/emboj.2011.401
149. DeBerardinis RJ, Chandel NS (2020) We need to talk about the Warburg effect. Nat Metab 2:127–129. https://doi.org/10.1038/s42255-020-0172-2
150. Sperber H, Mathieu J, Wang Y, et al (2015) The metabolome regulates the epigenetic landscape during naive-to-primed human embryonic stem cell transition. Nat Cell Biol 17:1523–1535. https://doi.org/10.1038/ncb3264
151. Kaelin WG, McKnight SL (2013) Influence of metabolism on epigenetics and disease. Cell 153:56–69. https://doi.org/10.1016/j.cell.2013.03.004
152. Lee J V., Carrer A, Shah S, et al (2014) Akt-dependent metabolic reprogramming regulates tumor cell Histone acetylation. Cell Metab 20:306–319. https://doi.org/10.1016/j.cmet.2014.06.004
153. Wellen KE, Hatzivassiliou G, Sachdeva UM, et al (2009) ATP-citrate lyase links cellular metabolism to histone acetylation. Science (80-) 324:1076–1080.

https://doi.org/10.1126/science.1164097
154. Carey BW, Finley LWS, Cross JR, et al (2015) Intracellular α-ketoglutarate maintains the pluripotency of embryonic stem cells. Nature 518:413–416. https://doi.org/10.1038/nature13981
155. Selak MA, Armour SM, MacKenzie ED, et al (2005) Succinate links TCA cycle dysfunction to oncogenesis by inhibiting HIF-α prolyl hydroxylase. Cancer Cell 7:77–85. https://doi.org/10.1016/j.ccr.2004.11.022
156. Wang C, Shao L, Pan C, et al (2019) Elevated level of mitochondrial reactive oxygen species via fatty acid β-oxidation in cancer stem cells promotes cancer metastasis by inducing epithelial-mesenchymal transition. Stem Cell Res Ther 10:. https://doi.org/10.1186/s13287-019-1265-2
157. Hamanaka RB, Glasauer A, Hoover P, et al (2013) Mitochondrial Reactive Oxygen Species Promote Epidermal Differentiation and Hair Follicle Development. 6:1–10
158. MacKenzie ED, Selak MA, Tennant DA, et al (2007) Cell-Permeating α-Ketoglutarate Derivatives Alleviate Pseudohypoxia in Succinate Dehydrogenase-Deficient Cells. Mol Cell Biol 27:3282–3289. https://doi.org/10.1128/mcb.01927-06
159. Rodríguez-Colman MJ, Schewe M, Meerlo M, et al (2017) Interplay between metabolic identities in the intestinal crypt supports stem cell function. Nature 543:424–427. https://doi.org/10.1038/nature21673
160. Ma R, Ma L, Weng W, et al (2020) DUSP6 SUMOylation protects cells from oxidative damage via direct regulation of Drp1 dephosphorylation. Sci Adv 6:. https://doi.org/10.1126/sciadv.aaz0361
161. Xue D, Zhou X, Qiu J (2020) Emerging role of NRF2 in ROS-mediated tumor chemoresistance. Biomed Pharmacother 131:110676. https://doi.org/10.1016/j.biopha.2020.110676
162. Guha M, Srinivasan S, Ruthel G, et al (2014) Mitochondrial retrograde signaling induces epithelial-mesenchymal transition and generates breast cancer stem cells. Oncogene 33:5238–5250. https://doi.org/10.1038/onc.2013.467
163. Srinivasan S, Koenigstein A, Joseph J, et al (2010) Role of mitochondrial reactive oxygen species in osteoclast differentiation. Ann N Y Acad Sci 1192:245–252. https://doi.org/10.1111/j.1749-6632.2009.05377.x
164. Khacho M, Clark A, Svoboda DS, et al (2016) Mitochondrial Dynamics Impacts Stem Cell Identity and Fate Decisions by Regulating a Nuclear Transcriptional Program. Cell Stem Cell 19:232–247. https://doi.org/10.1016/j.stem.2016.04.015
165. Folmes CDL, Nelson TJ, Martinez-Fernandez A, et al (2011) Somatic oxidative bioenergetics transitions into pluripotency-dependent glycolysis to facilitate nuclear reprogramming. Cell Metab 14:264–271. https://doi.org/10.1016/j.cmet.2011.06.011
166. Civenni G, Bosotti R, Timpanaro A, et al (2019) Epigenetic Control of Mitochondrial Fission Enables Self-Renewal of Stem-like Tumor Cells in Human Prostate Cancer. Cell Metab 30:303-318.e6. https://doi.org/10.1016/j.cmet.2019.05.004
167. Lagadinou ED, Sach A, Callahan K, et al (2013) BCL-2 inhibition targets oxidative phosphorylation and selectively eradicates quiescent human leukemia stem cells. Cell Stem Cell 12:329–341. https://doi.org/10.1016/j.stem.2012.12.013
168. Pei S, Minhajuddin M, Adane B, et al (2018) AMPK/FIS1-Mediated Mitophagy Is Required for Self-Renewal of Human AML Stem Cells. Cell Stem Cell 23:86-100.e6. https://doi.org/10.1016/j.stem.2018.05.021
169. Ye X, Tam WL, Shibue T, et al (2015) Distinct EMT programs control normal mammary stem cells and tumour-initiating cells. Nature 525:256–260.

https://doi.org/10.1038/nature14897
170. Rodríguez-García A, Samsó P, Fontova P, et al (2017) TGF-β1 targets Smad, p38 MAPK, and PI3K/Akt signaling pathways to induce PFKFB3 gene expression and glycolysis in glioblastoma cells. FEBS J 284:3437–3454. https://doi.org/10.1111/febs.14201
171. Masin M, Vazquez J, Rossi S, et al (2014) GLUT3 is induced during epithelial-mesenchymal transition and promotes tumor cell proliferation in non-small cell lung cancer. Cancer Metab 2:11. https://doi.org/10.1186/2049-3002-2-11
172. Liu M, Quek L-E, Sultani G, Turner N (2016) Epithelial-mesenchymal transition induction is associated with augmented glucose uptake and lactate production in pancreatic ductal adenocarcinoma. Cancer Metab 4:1–13. https://doi.org/10.1186/s40170-016-0160-x
173. Zhang Z, Li TE, Chen M, et al (2020) MFN1-dependent alteration of mitochondrial dynamics drives hepatocellular carcinoma metastasis by glucose metabolic reprogramming. Br J Cancer 122:209–220. https://doi.org/10.1038/s41416-019-0658-4
174. Cunniff B, McKenzie AJ, Heintz NH, Howe AK (2016) AMPK activity regulates trafficking of Mitochondria to the leading edge during cell migration and matrix invasion. Mol Biol Cell 27:2662–2674. https://doi.org/10.1091/mbc.E16-05-0286
175. Caino MC, Ghosh JC, Chae YC, et al (2015) PI3K therapy reprograms mitochondrial trafficking to fuel tumor cell invasion. Proc Natl Acad Sci U S A 112:8638–8643. https://doi.org/10.1073/pnas.1500722112
176. Desai SP, Bhatia SN, Toner M, Irimia D (2013) Mitochondrial localization and the persistent migration of epithelial cancer cells. Biophys J 104:2077–2088. https://doi.org/10.1016/j.bpj.2013.03.025
177. Viale A, Pettazzoni P, Lyssiotis CA, et al (2014) Oncogene ablation-resistant pancreatic cancer cells depend on mitochondrial function. Nature 514:628–632. https://doi.org/10.1038/nature13611
178. Quintana-Cabrera R, Quirin C, Glytsou C, et al (2018) The cristae modulator Optic atrophy 1 requires mitochondrial ATP synthase oligomers to safeguard mitochondrial function. Nat Commun 9:. https://doi.org/10.1038/s41467-018-05655-x
179. Cretin E, Lopes P, Vimont E, et al (2021) High-throughput screening identifies suppressors of mitochondrial fragmentation in OPA 1 fibroblasts. EMBO Mol Med 1–29. https://doi.org/10.15252/emmm.202013579
180. Frezza C, Cipolat S, Martins de Brito O, et al (2006) OPA1 Controls Apoptotic Cristae Remodeling Independently from Mitochondrial Fusion. Cell 126:177–189. https://doi.org/10.1016/j.cell.2006.06.025
181. Yamaguchi R, Lartigue L, Perkins G, et al (2008) Opa1-Mediated Cristae Opening Is Bax/Bak and BH3 Dependent, Required for Apoptosis, and Independent of Bak Oligomerization. Mol Cell 31:557–569. https://doi.org/10.1016/j.molcel.2008.07.010
182. Nagdas S, Kashatus JA, Nascimento A, et al (2019) Drp1 Promotes KRas-Driven Metabolic Changes to Drive Pancreatic Tumor Growth. Cell Rep 28:1845-1859.e5. https://doi.org/10.1016/j.celrep.2019.07.031
183. Chung KP, Huang YL, Chen YJ, et al (2021) Multi-kinase framework promotes proliferation and invasion of lung adenocarcinoma through activation of dynamin-related protein 1. Mol Oncol 15:560–578. https://doi.org/10.1002/1878-0261.12843
184. Hu M, Zhao Y, Cao Y, et al (2020) DRP1 promotes lactate utilization in KRAS-mutant non-small-cell lung cancer cells. Cancer Sci 111:3588–3599.

https://doi.org/10.1111/cas.14603
185. Rehman J, Zhang HJ, Toth PT, et al (2012) Inhibition of mitochondrial fission prevents cell cycle progression in lung cancer. FASEB J 26:2175–2186. https://doi.org/10.1096/fj.11-196543
186. Kim YY, Yun SH, Yun J (2018) Downregulation of Drp1, a fission regulator, is associated with human lung and colon cancers. Acta Biochim Biophys Sin (Shanghai) 50:209–215. https://doi.org/10.1093/abbs/gmx137
187. Yuneva MO, Fan TWM, Allen TD, et al (2012) The metabolic profile of tumors depends on both the responsible genetic lesion and tissue type. Cell Metab 15:157–170. https://doi.org/10.1016/j.cmet.2011.12.015
188. Ying H, Kimmelman AC, Lyssiotis CA, et al (2012) Oncogenic kras maintains pancreatic tumors through regulation of anabolic glucose metabolism. Cell 149:656–670. https://doi.org/10.1016/j.cell.2012.01.058
189. Reske SN, Grillenberger KG, Glatting G, et al (1997) Overexpression of glucose transporter 1 and increased FDG uptake in pancreatic carcinoma. J Nucl Med 38:1344–4348
190. Bryant KL, Mancias JD, Kimmelman AC, Der CJ (2014) KRAS: Feeding pancreatic cancer proliferation. Trends Biochem Sci 39:91–100. https://doi.org/10.1016/j.tibs.2013.12.004
191. Scafoglio C, Hirayama BA, Kepe V, et al (2015) Functional expression of sodium-glucose transporters in cancer. Proc Natl Acad Sci U S A 112:E4111–E4119. https://doi.org/10.1073/pnas.1511698112
192. Momcilovic M, Jones A, Bailey ST, et al (2019) In vivo imaging of mitochondrial membrane potential in non-small-cell lung cancer.pdf. Nature
193. Luengo A, Li Z, Gui DY, et al (2021) Increased demand for NAD+ relative to ATP drives aerobic glycolysis. Mol Cell 81:691-707.e6. https://doi.org/10.1016/j.molcel.2020.12.012
194. Zhang Z, Wakabayashi N, Wakabayashi J, et al (2011) The dynamin-related GTPase Opa1 is required for glucose-stimulated ATP production in pancreatic beta cells. Mol Biol Cell 22:2235–2245. https://doi.org/10.1091/mbc.E10-12-0933
195. Wakabayashi J, Zhang Z, Wakabayashi N, et al (2009) The dynamin-related GTPase Drp1 is required for embryonic and brain development in mice. J Cell Biol 186:805–816. https://doi.org/10.1083/jcb.200903065
196. Bankhead P, Loughrey MB, Fernández JA, et al (2017) QuPath: Open source software for digital pathology image analysis. Sci Rep 7:1–7. https://doi.org/10.1038/s41598-017-17204-5
197. Xu J (2005) Preparation, Culture, and Immortalization of Mouse Embryonic Fibroblasts. Curr Protoc Mol Biol 1–8. https://doi.org/10.1002/0471142727.mb2801s70
198. Clayton DA, Shadel GS (2014) Isolation of mitochondria from tissue culture cells. Cold Spring Harb Protoc 2014:1109–1111. https://doi.org/10.1101/pdb.prot080002
199. Beutner G, Jr GAP (2021) Native Gel Electrophoresis and Immunoblotting to Analyze Electron Transport Chain Complexes. In: Mitochondrial Medicine: Volume 2: Assessing Mitochondria. pp 103–112
200. Quiros PM, Goyal A, Jha P, Johan Auwerx. (2017) Analysis of mtDNA/nDNA ratio in mice. Curr Protoc Mouse Biol 176:139–148. https://doi.org/10.1002/cpmo.21.Analysis
201. Herkenne S, Ek O, Zamberlan M, et al (2020) Developmental and Tumor Angiogenesis Requires the Mitochondria-Shaping Protein Opa1. Cell Metab 31:987-1003.e8. https://doi.org/10.1016/j.cmet.2020.04.007

202. Eichner LJ, Brun SN, Herzig S, et al (2019) Genetic Analysis Reveals AMPK Is Required to Support Tumor Growth in Murine Kras-Dependent Lung Cancer Models. Cell Metab 29:285-302.e7. https://doi.org/10.1016/j.cmet.2018.10.005
203. Bajzikova M, Kovarova J, Coelho AR, et al (2019) Reactivation of Dihydroorotate Dehydrogenase-Driven Pyrimidine Biosynthesis Restores Tumor Growth of Respiration-Deficient Cancer Cells. Cell Metab 29:399-416.e10. https://doi.org/10.1016/j.cmet.2018.10.014
204. Martínez-Reyes I, Cardona LR, Kong H, et al (2020) Mitochondrial ubiquinol oxidation is necessary for tumour growth. Nature 585:288–292. https://doi.org/10.1038/s41586-020-2475-6
205. King MP, Attardi G (1996) [27] Isolation of human cell lines lacking mitochondrial DNA. Methods Enzymol 264:304–312. https://doi.org/10.1016/s0076-6879(96)64029-4
206. Boudreau A, Purkey HE, Hitz A, et al (2016) Metabolic plasticity underpins innate and acquired resistance to LDHA inhibition. Nat Chem Biol 12:779–786. https://doi.org/10.1038/nchembio.2143
207. Sullivan LB, Luengo A, Danai L V., et al (2018) Aspartate is an endogenous metabolic limitation for tumour growth. Nat Cell Biol 20:782–788. https://doi.org/10.1038/s41556-018-0125-0
208. Li Z, Ji BW, Dixit PD, et al (2022) Cancer cells depend on environmental lipids for proliferation when electron acceptors are limited. Nat Metab. https://doi.org/10.1038/s42255-022-00588-8
209. Cantor JR, Abu-Remaileh M, Kanarek N, et al (2017) Physiologic Medium Rewires Cellular Metabolism and Reveals Uric Acid as an Endogenous Inhibitor of UMP Synthase. Cell 169:258-272.e17. https://doi.org/10.1016/j.cell.2017.03.023
210. Kondadi AK, Anand R, Hänsch S, et al (2020) Cristae undergo continuous cycles of membrane remodelling in a MICOS -dependent manner . EMBO Rep 21:1–22. https://doi.org/10.15252/embr.201949776
211. Segawa M, Wolf DM, Hultgren NW, et al (2020) Quantification of cristae architecture reveals time-dependent characteristics of individual mitochondria. Life Sci Alliance 3:1–14. https://doi.org/10.26508/LSA.201900620
212. Lodi R, Tonon C, Valentino ML, et al (2011) Defective mitochondrial adenosine triphosphate production in skeletal muscle from patients with dominant optic atrophy due to OPA1 mutations. Arch Neurol 68:67–73. https://doi.org/10.1001/archneurol.2010.228
213. Yamada T, Murata D, Kleiner DE, et al (2022) Prevention and Regression of Megamitochondria and Steatosis by Blocking Mitochondrial Fusion in the Liver. iScience 25:103996. https://doi.org/10.1016/j.isci.2022.103996
214. Bohnert M, Zerbes RM, Davies KM, et al (2015) Central Role of Mic10 in the Mitochondrial Contact Site and Cristae Organizing System. Cell Metab 21:747–755. https://doi.org/10.1016/j.cmet.2015.04.007
215. Harner M, Körner C, Walther D, et al (2011) The mitochondrial contact site complex, a determinant of mitochondrial architecture. EMBO J 30:4356–4370. https://doi.org/10.1038/emboj.2011.379
216. Hoppins S, Collins SR, Cassidy-Stone A, et al (2011) A mitochondrial-focused genetic interaction map reveals a scaffold-like complex required for inner membrane organization in mitochondria. J Cell Biol 195:323–340. https://doi.org/10.1083/jcb.201107053
217. Varanita T, Soriano ME, Romanello V, et al (2015) The Opa1-dependent mitochondrial cristae remodeling pathway controls atrophic, apoptotic, and ischemic tissue damage. Cell Metab 21:834–844.

https://doi.org/10.1016/j.cmet.2015.05.007
218. Vempati UD, Han X, Moraes CT (2009) Lack of cytochrome c in mouse fibroblasts disrupts assembly/stability of respiratory complexes I and IV. J Biol Chem 284:4383–4391. https://doi.org/10.1074/jbc.M805972200
219. Acín-Pérez R, Bayona-Bafaluy MP, Fernández-Silva P, et al (2004) Respiratory complex III is required to maintain complex I in mammalian mitochondria. Mol Cell 13:805–815. https://doi.org/10.1016/S1097-2765(04)00124-8
220. Diaz F, Fukui H, Garcia S, Moraes CT (2006) Cytochrome c Oxidase Is Required for the Assembly/Stability of Respiratory Complex I in Mouse Fibroblasts . Mol Cell Biol 26:4872–4881. https://doi.org/10.1128/mcb.01767-05
221. Li Y, D'Aurelio M, Deng JH, et al (2007) An assembled complex IV maintains the stability and activity of complex I in mammalian mitochondria. J Biol Chem 282:17557–17562. https://doi.org/10.1074/jbc.M701056200
222. Protasoni M, Pérez-Pérez R, Lobo-Jarne T, et al (2020) Respiratory supercomplexes act as a platform for complex III -mediated maturation of human mitochondrial complexes I and IV . EMBO J 39:1–19. https://doi.org/10.15252/embj.2019102817
223. Fernandez-Vizarra E, Lo S, Sierra-magro A, et al (2022) Two independent respiratory chains adapt OXPHOS performance to glycolytic switch. Cell Metab 1–17. https://doi.org/10.1016/j.cmet.2022.09.005
224. Vercellino I, Sazanov LA (2022) The assembly, regulation and function of the mitochondrial respiratory chain. Nat Rev Mol Cell Biol 23:141–161. https://doi.org/10.1038/s41580-021-00415-0
225. Wessels HJCT, Vogel RO, Van Den Heuvel L, et al (2009) LC-MS/MS as an alternative for SDS-PAGE in blue native analysis of protein complexes. Proteomics 9:4221–4228. https://doi.org/10.1002/pmic.200900157
226. Páleníková P, Harbour ME, Prodi F, et al (2021) Duplexing complexome profiling with SILAC to study human respiratory chain assembly defects. Biochim Biophys Acta - Bioenerg 1862:. https://doi.org/10.1016/j.bbabio.2021.148395
227. Zanna C, Ghelli A, Porcelli AM, et al (2008) OPA1 mutations associated with dominant optic atrophy impair oxidative phosphorylation and mitochondrial fusion. Brain 131:352–367. https://doi.org/10.1093/brain/awm335
228. Agier V, Oliviero P, Lainé J, et al (2012) Defective mitochondrial fusion, altered respiratory function, and distorted cristae structure in skin fibroblasts with heterozygous OPA1 mutations. Biochim Biophys Acta - Mol Basis Dis 1822:1570–1580. https://doi.org/10.1016/j.bbadis.2012.07.002
229. An HJ, Cho G, Lee JO, et al (2013) Higd-1a interacts with Opa1 and is required for the morphological and functional integrity of mitochondria. Proc Natl Acad Sci U S A 110:13014–13019. https://doi.org/10.1073/pnas.1307170110
230. Stephan T, Roesch A, Riedel D, Jakobs S (2019) Live-cell STED nanoscopy of mitochondrial cristae. Sci Rep 9:1–6. https://doi.org/10.1038/s41598-019-48838-2
231. Wolf DM, Segawa M, Kondadi AK, et al (2019) Individual cristae within the same mitochondrion display different membrane potentials and are functionally independent. EMBO J 38:1–21. https://doi.org/10.15252/embj.2018101056
232. Wolf DM, Segawa M, Shirihai OS, Liesa M (2020) Method for live-cell super-resolution imaging of mitochondrial cristae and quantification of submitochondrial membrane potentials, 1st ed. Elsevier Inc.
233. Stiburek L, Cesnekova J, Kostkova O, et al (2012) YME1L controls the accumulation of respiratory chain subunits and is required for apoptotic resistance, cristae morphogenesis, and cell proliferation. Mol Biol Cell 23:1010–1023. https://doi.org/10.1091/mbc.E11-08-0674

234. MacVicar T, Ohba Y, Nolte H, et al (2019) Lipid signalling drives proteolytic rewiring of mitochondria by YME1L. Nature 575:361–365. https://doi.org/10.1038/s41586-019-1738-6
235. Mishra P, Carelli V, Manfredi G, Chan DC (2014) Proteolytic cleavage of Opa1 stimulates mitochondrial inner membrane fusion and couples fusion to oxidative phosphorylation. Cell Metab 19:630–641. https://doi.org/10.1016/j.cmet.2014.03.011
236. Head B, Griparic L, Amiri M, et al (2009) Inducible proteolytic inactivation of OPA1 mediated by the OMA1 protease in mammalian cells. J Cell Biol 187:959–966. https://doi.org/10.1083/jcb.200906083
237. Song Z, Chen H, Fiket M, et al (2007) OPA1 processing controls mitochondrial fusion and is regulated by mRNA splicing, membrane potential, and Yme1L. J Cell Biol 178:749–755. https://doi.org/10.1083/jcb.200704110
238. Wang R, Mishra P, Garbis SD, et al (2021) Identification of new OPA1 cleavage site reveals that short isoforms regulate mitochondrial fusion. Mol Biol Cell 32:157–168. https://doi.org/10.1091/MBC.E20-09-0605
239. Murata D, Yamada T, Tokuyama T, et al (2020) Mitochondrial Safeguard: a stress response that offsets extreme fusion and protects respiratory function via flickering-induced Oma1 activation. EMBO J 39:1–17. https://doi.org/10.15252/embj.2020105074
240. Oshima N, Ishida R, Kishimoto S, et al (2020) Dynamic Imaging of LDH Inhibition in Tumors Reveals Rapid In Vivo Metabolic Rewiring and Vulnerability to Combination Therapy. Cell Rep 30:1798-1810.e4. https://doi.org/10.1016/j.celrep.2020.01.039
241. Wang Y, Stancliffe E, Fowle-grider R, et al (2022) Saturation of the mitochondrial NADH shuttles drives aerobic glycolysis in proliferating cells. Mol Cell 1–14. https://doi.org/10.1016/j.molcel.2022.07.007
242. McCleland ML, Adler AS, Deming L, et al (2013) Lactate dehydrogenase B is required for the growth of KRAS-dependent lung adenocarcinomas. Clin Cancer Res 19:773–784. https://doi.org/10.1158/1078-0432.CCR-12-2638
243. Xie H, Hanai JI, Ren JG, et al (2014) Targeting lactate dehydrogenase-A inhibits tumorigenesis and tumor progression in mouse models of lung cancer and impacts tumor-initiating cells. Cell Metab 19:795–809. https://doi.org/10.1016/j.cmet.2014.03.003
244. Deng H, Gao Y, Trappetti V, et al (2022) Targeting lactate dehydrogenase B-dependent mitochondrial metabolism affects tumor initiating cells and inhibits tumorigenesis of non-small cell lung cancer by inducing mtDNA damage. Cell Mol Life Sci 79:1–23. https://doi.org/10.1007/s00018-022-04453-5
245. Faubert B, Li KY, Cai L, et al (2017) Lactate Metabolism in Human Lung Tumors. Cell 171:358-371.e9. https://doi.org/10.1016/j.cell.2017.09.019